AD-A108 390 ROCKWELL INTERNATIONAL THOUSAND OAKS CA MICROELECTR--ETC F/G 20/7
ELECTRONIC TRANSPORT IN ULTRATHIN HETEROSTRUCTURES,(U)
OCT 81 P D DAPKUS N00014-78-C-0711
UNCLASSIFIED MRDC40129 NL

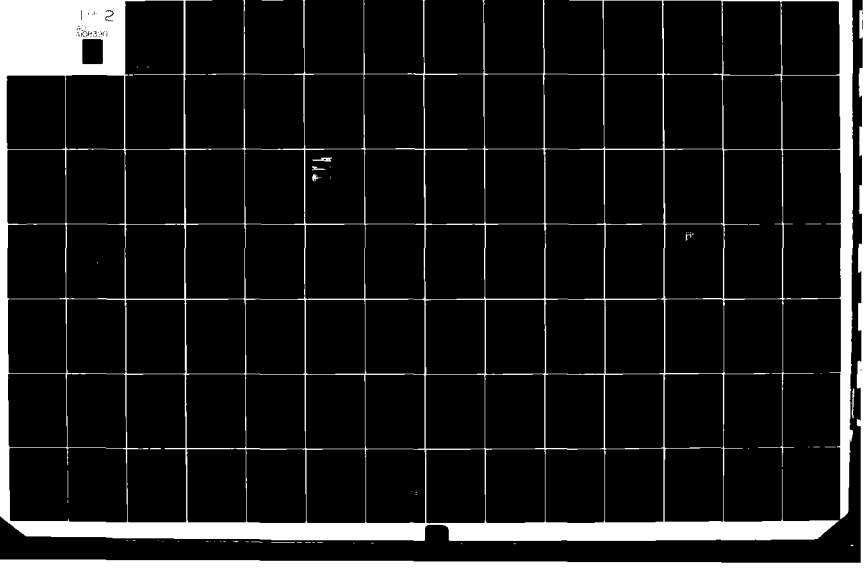

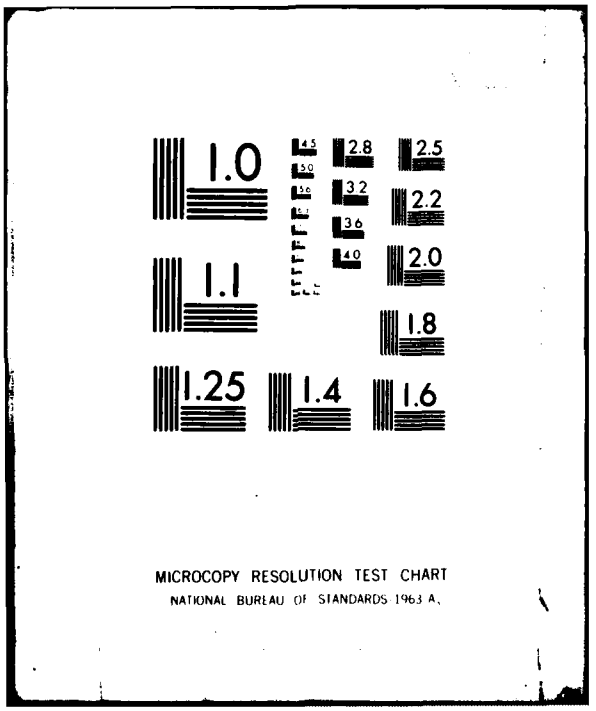
1.0
1.1
1.25
1.4
1.6
1.8
2.0
2.2
2.5
2.8
3.2
3.6
4.0
MICROCOPY RESOLUTION TEST CHART
NATIONAL BUREAU OF STANDARDS 1963 A.

(12)

2

MRDC40129

ELECTRONIC TRANSPORT IN ULTRATHIN HETEROSTRUCTURES

FINAL TECHNICAL REPORT

August 1, 1978 through July 31, 1981

Prepared for:

Electronics Division

Department of the Navy

Office of Naval Research

Arlington, VA 22217

L. R. Cooper

Prepared by:

P. D. Dapkus

Rockwell International/MRDC

1049 Camino Dos Rios

Thousand Oaks, CA 91360

Contract No. N00014-78-C-0711

Rockwell International

unclassified

SECURITY CLASSIFICATION OF THIS PAGE (When Data Entered)

REPORT DOCUMENTATION PAGE		READ INSTRUCTIONS BEFORE COMPLETING FORM
1. REPORT NUMBER	2. GOVT ACCESSION NO. AD A108 390	3. RECIPIENT'S CATALOG NUMBER
4. TITLE (and Subtitle) ELECTRONIC TRANSPORT IN ULTRATHIN HETEROSTRUCTURES		5. TYPE OF REPORT & PERIOD COVERED Final Report 08/01/78 -- 07/31/81
		6. PERFORMING ORG. REPORT NUMBER
7. AUTHOR(s) P. D. Dapkus		8. CONTRACT OR GRANT NUMBER(s) N00014-78-C-0711
9. PERFORMING ORGANIZATION NAME AND ADDRESS Rockwell International/MRDC 3370 Miraloma Avenue Anaheim, CA 92803		10. PROGRAM ELEMENT, PROJECT, TASK AREA & WORK UNIT NUMBERS
11. CONTROLLING OFFICE NAME AND ADDRESS Electronics Div., Dept. of the Navy Office of Naval Research Arlington, VA 22217		12. REPORT DATE October, 1981
		13. NUMBER OF PAGES 110
14. MONITORING AGENCY NAME & ADDRESS(if different from Controlling Office)		15. SECURITY CLASS. (of this report)
		15a. DECLASSIFICATION DOWNGRADING SCHEDULE

16. DISTRIBUTION STATEMENT (of this Report)

Approved for public release; distribution unlimited

17. DISTRIBUTION STATEMENT (of the abstract entered in Block 20, if different from Report)

18. SUPPLEMENTARY NOTES

19. KEY WORDS (Continue on reverse side if necessary and identify by block number)

Multilayer quantum well (MQW), metalorganic chemical vapor deposition (MOCVD), superlattice disorder, two-dimensional electron gas structures, quantum well heterostructures, superlattices, diffusion-enhanced disorder, transport properties, molecular beam epitaxy (MBE), photoluminescence, optical absorption, transmission electron microscopy, clusering, GaAs.

20. ABSTRACT (Continue on reverse side if necessary and identify by block number)

A detailed study of the optical and electronic transport studies of ultrathin GaAlAs/GaAs heterostructures is reported. The measurements are reported on GaAlAs multiple quantum well heterostructures (MQW) and superlattices (SL) with layer dimension ranging from 200 to 30 Å grown by metalorganic chemical vapor deposition (MOCVD). The measurements show that laser emission from these structures lie 36 meV below the absorption edge, consistent with LO phonon emission. The transport properties of modulation doped superlattices and single heterostructures demonstrate enhanced room temperature and (cont.)

DD FORM 1 JAN 73 1473 EDITION OF 1 NOV 65 IS OBSOLETE

unclassified

SECURITY CLASSIFICATION OF THIS PAGE (When Data Entered)

4112 310

20. low temperature mobility.

TABLE OF CONTENTS

APPENDICES:

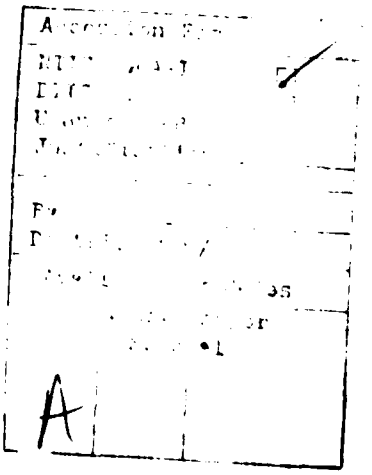

1.0 INTRODUCTION

The recent development of sophisticaed and well controlled epitaxial processes for the growth of GaAlAs and GaAs has led to the realization of heterostructure materials with unique and useful properties. The construction of single and multilayer GaAlAs/GaAs heterostructures by metalorganic chemical vapor deposition (MOCVD) and molecular beam epitaxy (MBE) has permitted the investigation of the physics of two-dimensional electron gases in a variety of conditions. Figure 1 shows two different types of heterostructures important in the study size quantization. In (a) of the figure, we illustrate a multilayer quantum well (MQW) or superlattice. This is formed by growing alternating layers of GaAs and GaAlAs each with dimensions small compared with the electron wavelength of an electron in the material. This reduced size (1 monolayer to 500 Å) results in the quantization of the energy states of the electron and a variety of effects related to that quantization. On the other hand, the material of Fig. 1(b) -- the single layer heterostructure -- owes its unique properties to details of the energy band structure of heterojunction. The discontinuity in the conduction bands results in the formation of an accumulation layer of dimension 100 Å. Thus electrons trapped in this layer behave like a two dimensional gas (2 DEG). The quantization of the electrons results in unique optical properties and electron transport properties.

The goal of this program has been to investigate these properties and to exploit them to fabricate new devices for improved electronic functions. This report describes the progress during the period September, 1980, to September, 1981.

2.0 TECHNICAL PROGRESS

A great deal of information regarding fundamental characteristics of multiple quantum well heterostructures grown by metalorganic chemical vapor deposition has been derived during this contract performance period. The following sections will describe the main points determined during the course of this study. Details of the experimental findings are found in the technical papers in the Appendix.

2.1 Scope of Investigations

The fundamental properties of multiple quantum well (MQW) heterostructures and the inherent limitations of available growth techniques in fabricating these heterostructures occupy a large portion of the efforts of this year's program. It was strongly felt that in order to be able to produce high quality electronic transport structures in MQW's grown by MOCVD as many tools as possible should be brought to bear to understand the characteristics of these structures and their inherent limitations. As a result, considerable effort in collatoration with the University of Illinois was devoted to the study of the optical properties of these quantum well structures, particularly for structures with very small well dimensions, less than 100 Å. In this region, the optical properties are extremely sensitive, not only to small changes in the well width, but also to the presence of any localized disturbance in the otherwise period MQW structure. Photoluminescence, optical absorption, and optical pumping were all used to help elucidate these fundamental limits. This work led to the observation of localized regions of

GaAs in GaAlAs barriers fabricated by MOCVD. This observation immediately raised the question as to the fundamental nature of these clusters and their relevance to other epitaxial techniques such as molecular beam epitaxy (MBE). To further varify or observe in a more direct manner the presence of these clusters, transmission electron microscopy was performed on a number of samples. These studies failed to show conclusive evidence of clustering in MOCVD grown heterostructures. The apparent clustering, however, could be avoided by the use of AlAs barriers instead of GaAlAs. An effort was directed at the growth of high quality AlAs for inclusion in these MQW structures. The successful achievement of this growth capability obviated for many device applications the relevance of clusters. However, the fundamental issue with regard to their inherent nature or their specificity to MOCVD growth remains unanswered.

A further study of the effects of thermal treatment or the inclusion of impurities into MQW's upon the structural properties of these materials was investigated by a study of thermal annealing, impurity diffusion and implantation. It was observed that both thermal annealing and diffusion of zinc into MQW structures resulted in severe intermixing of the AlAs and GaAs constituents of a periodic structure. For zinc diffusion at a level of approximately 10^{19} cm^{-3}, this intermixing was strong enough that MQW heterostructures consisting of 100 Å wells and barriers were completely intermixed to form a homogeneous alloy of GaAlAs upon zinc diffusion. Applications of this effect to monolithically integrated lasers were immediately realized and performed.

The limitations of all these effects on the transport properties of MQW modulation doped heterostructures were investigated. In contrast to the very sensitive optical effects previously mentioned, the major effects in MQW transport phenomenon was the purity of the GaAs involved in the trans port itself. Steps were taken to utilize the highest purity possible GaAs in two-dimensional electron gas structures, and this, in turn, resulted in the observation of exceedingly high enhanced mobility two-dimensional gas structures.

2.2 The Growth and Characterization of Ultrathin MQW's by MOCVD

The ultimate limit on the thickness of a layer capable of being grown by MOCVD has never been tested. During this program, we investigated the properties of multiple quantum wells with decreasing layer thicknesses, down to a layer thickness of approximately 30 Å. The purpose of these investigations was to determine when the transition width between layers grown by MOCVD became comparable to layer thickness and when other inherent crystal growth characteristics began to limit the quality of the thin layers. Furthermore, the fabrication of these thin layer MQW's allowed the investigation of optical properties of electrons confined to extremely small spatial dimensions. The results of these studies indicated that binary GaAs and AlAs layers could be grown with no apparent difficulty down to layer thicknesses as small as 30 Å. However, when GaAlAs ternary alloy layers were grown to these thicknesses, evidence was observed for the presence of Ga rich clusters in the GaAlAs alloy layer.

The presence of these clusters was inferred from the spectral emission behavior of multi-layer quantum wells with very thin GaAlAs barriers. The results from these samples indicated that in regions of the barrier GaAs rich clusters of atoms occurred that rendered the barrier useless in this spatial region. The observed effect was that multi-layer quantum wells with thin barriers instead of emitting at the energy expected for the well dimensions emitted at energies significantly lower and at energies corresponding to a well whose width was equal to two well dimensions plus one barrier dimension. This suggested that the electrons were free to pass from one well to another through a Ga rich cluster in the barrier layer. Several samples grown all in the same time period exhibited this apparently clustering behavior. However, subsequent investigation with transmission electron microscopy of samples grown under similar conditions but at a different time failed to yield any conclusive evidence for the presence of these Ga rich areas. Similarly, workers at Bell Laboratories have reported that investigation of MQW samples grown by MBE showed no evidence for clustering behavior. On the other hand, samples grown at the University of Illinois also be MBE did show evidence for these clusters.

One reaches one of two conclusions: (1) the clustering behavior that we have observed to date in photoluminescence occurs only under certain conditions of growth and is not an inherent characteristic of either MOCVD or MBE growth of thin layers or (2) the spectral characteristics observed in these very small quantum wells are being misinterpreted. With regard to the second possible explanation, we have not been able to arrive at an alternate one which explains all of the experimental data. Therefore, we are forced to conclude that the presence of clustering behavior is not an inherent feature of MOCVD growth but rather occurs under some conditions of growth possibly being nucleated by the presence of impurities in the reactor.

The problems mentioned in the previous section related to the observance of clustering behavior in ternary GaAlAs barriers of course ceases to be a problem if AlAs barriers are used in MQW structures. Extensive investigation of both the quality of AlAs grown by MOCVD as well as its inclusion in MQW structures resulted in several new observations. The first of these was that the emission of MQW heterostructures with AlAs barriers followed very closely the expected increase with decreasing well width, and for layers grown with 30 Å GaAs active regions and 30 Å barriers laser emission from MQW structures in the visible portion of the spectrum was observed. Furthermore, the width of this emission and the total spread of spectral positions seen in samples with AlAs barriers precluded the possibility of transition between the GaAs and the AlAs being greater than approximately one monolayer. Thus, the MOCVD growth technology is capable of fabricating one monolayer thick AlAs/GaAs transition regions and ultra abrupt quantum well structures.

AlAs/GaAs MQW's were compared with GaAlAs/GaAs MQW's to investigate the effect of clusters on wells with ternary GaAlAs barriers. It was observed that with AlAs barriers no evidence for emission below the expected phonon-assisted emission from the quantum well was observed. This suggests that any well characteristic which could be strongly effected by the presence of clustering in the GaAlAs barrier can be avoided by the use of AlAs barriers instead.

2.3 Phonon Effects in the Emission from MQW's

There has been a great deal of controversy over the participation of phonons in emissions from MQW's. All of the work performed on this program has clearly shown that the emission from quantum well heterostructures occurs

at multiples of 36 meV below the expected confined particle state energy. Because of the coincidence of this energy difference with the energy of a bulk phonon in GaAs, we have concluded that the emission in GaAs MQW's is phonon assisted under high levels of excitation. The mechanism appears to be one in which the relaxation of carriers from the top of the quantum well into which they are excited down to the bottom results in the emission of several LO phonons. This creates a situation in which the population of LO phonons exceeds by a great deal the thermal equilibrium population. This in turn stimulates the emission of phonons in the light emission process and results in phonon-assisted recombination.

Further evidence of phonon-assisted processes was obtained during this program year by the use of very thin MQW samples with either GaAlAs or AlAs barriers. Thin quantum wells with an average thickness on the order of 30 to 50 Å were grown to a total thickness of approximately one micron, so that a variety of studies could be performed. These included optical absorption, transmission electron microscopy, and optical photoluminescence measurements. The TEM measurements were used to measure precisely the thickness of the individual layers. The optical absorption was performed to measure the position of the confined particle states by the location of the absorption peak, and photoluminescence was performed to determine the laser emission -- all in the same samples. The results clearly indicated that the confined particle states of AlAs/GaAs superlattices occurred at the expected energies based on the thicknesses measured by transmission electron microscopy. By the same token, the laser emission from these samples occurred 36 meV in energy below the measured confined particle states of these samples. Because AlAs/GaAs samples have been shown to be free of any clustering behavior, we conclude that the 36 meV shift to lower energy

is precisely the same shift that has been observed in other samples in which the confined particle state location was calculated rather than measured experimentally. This conclusively shows that the emission in these samples is reduced in energy below the confined particle state energy by 36 meV, and the most plausible explanation is the involvement of phonons in the light emission. The properties of AlGaAs/GaAs superlattices were also measured and found to be in total agreement with the AlAs/GaAs measurements suggesting that the emission process in these two superlattices was substantially the same.

2.4 Superlattice Disorder

Attempts to fabricate diffused lasers in MQW superlattices resulted in the observation of a new and potentially very important phenomenon. It was observed that when zinc was locally diffused into a GaAlAs/GaAs superlattice total redistribution of the Ga and the Al within the diffused region occurred resulting in the formation of a homogeneous GaAlAs alloy. The composition of the alloy was determined solely by thicknesses and composition of the layers involved in the diffused region. For example, if equal layer thicknesses of GaAs and AlAs were employed, a 50% GaAlAs homogeneous alloy was formed. This phenomenon is believed to be closely related to the interdiffusion effects seen in these MQW's when they are heated to high temperatures ($\sim$ 900°C) for several hours. Under those annealing conditions, the Al and Ga completely redistribute to form a homogeneous alloy. On the other hand, the diffusion-induced redistribution occurs at relatively low temperatures ($\sim$ 500 to $\sim$ 700°C).

There are several implications of this effect. First, the formation of abrupt heterojunctions between a p^+ GaAlAs layer and another layer of different composition may be difficult to achieve because of this enhanced

diffusion. Furthermore, the utilization of this localized interdiffusion process may result in the fabrication of new types of monolithically integrated planar device structures that could greatly simplify the problem of fabricating integrated optoelectronic structures.

2.5 Transport in MQW Heterostructures in Two-Dimensional Electron Gas Structures

Detailed measurements of the transport properties of modulation doped MQW heterostructures were performed during this calendar year. It was determined that the mobility of modulation doped MQW's was substantially improved at room temperature over comparably doped bulk samples. Improvement factors of 1.5 to 2 were observed for samples with an average carrier concentration of approximately 2×10^{17}. More lightly doped samples showed virtually no increase in mobility over material doped to 2×10^{17} cm^{-3} becoming closer to the bulk samples of the same doping. At dopings above 8×10^{17}, the mobility of modulation doped samples became closer to values observed for bulk materials at the same doping.

At low temperatures, it was found that the mobility of material doped at 2×10^{17} increased drastically with temperature to a maximum value of about 12,000 to 16,000 $cm^2/Vsec$. Based on measurements of bulk GaAs, it was concluded that this mobility was being limited by the purity of the GaAs used in the MQW structures. An investigation of the low temperature mobility (μ_{77}) of bulk undoped GaAs determined that μ_{77} increases monotonically with lower growth temperature similar to results obtained in a companion study performed in a different reactor. GaAlAs of optimum quality is grown at 750°C, and due to the difficulties in cycling temperature between layer growth, it was decided to investigate the properties of two dimensional

electron gas (2 DEG) heterostructures. These structures could be grown by first growing an undoped GaAs layer at the optimum temperature for high mobility followed by the growth at 150°C of doped GaAlAs material to form the 2 DEG structure. Several of these samples were grown with and without undoped GaAlAs spacers to investigate the dependence of the low temperature mobility upon the presence of the spacer. It was determined that material with low temperature mobilities as high as 45,000 $cm^2/Vsec$ could be grown in this way provided that a spacer of 100 Å of undoped GaAlAs was included in the structure. These mobilities are somewhat lower than the highest values observed in MBE grown material. However, the mobility of MOCVD grown 2 DEG structures is still being limited we believe by the purity of the GaAs involved in the heterostructure and to a lesser extent by interface defects in the structure. Further investigation of these effects is required.

3.0 CONCLUSIONS

The studies undertaken this year represent the culmination of a three-year program in which the properties of MQW heterostructures were investigated. The materials in this study were all grown by MOCVD, and as a result this program represents a pioneering effort in the growth of ultrathin layers by this growth technique. The accomplishments of the program have been many, and a great deal of knowledge has been learned. The major conclusion reached from this year's efforts are:

1. Ultrathin layers of GaAs, AlAs, and GaAlAs of very high quality can be grown by MOCVD. Layers as thin as 30 Å can be grown by this technique.
2. In the light emission from MQW heterostructures, the light is light reduced in energy by 36 meV from the energy of the confined particle states in the well. This is believed to be due to the participation of phonon emission in the light emission process.
3. Clusters of GaAs-rich alloy sometimes occur during the growth of GaAlAs materials. It is not known whether these clusters are localized to interface regions between layers, whether they occur at the beginning of epitaxial growth alone, or whether they are nucleated by impurities in the reactor. However, they do not appear to be an inherent feature of MOCVD growth.
4. Total redistribution of Ga and Al within multi-layer structures can be effected by the diffusion of zinc and possibly other impurities in these multi-layer structures. This effect can also be achieved over the entire sample by thermal annealing. The zinc diffusion effect occurs at temperatures in the range from 500 to 700°C.

5. High quality, high mobility MQW modulation doped material and 2 DEG material can be grown by MOCVD. This opens the possibility of a production technology for ultra-high speed integrated circuits based on 2 DEG or modulation-doped material.

The conclusions reached above are based on extensive optical and electrical characterization of quantum wells grown by MOCVD. They clearly point out that the technique has a great deal of promise for a new generation of electronic and optical devices based on ultra thin quantum well dimension layers. Several problems exist which require further investigation. These include the nature and the elimination of deep traps and other impurities in GaAlAs. A detailed study of the interfaces of the redistributed effect caused by impurity diffusion in multi-layer quantum wells as well as the utilization of this effect for the fabrication of new devices.

4.0 RECOMMENDATIONS FOR FURTHER STUDY

The investigation of new structures and new materials such as MQW's and superlattices will inevitably uncover more phenomenon to study than can possibly be studied in one, two, or perhaps several programs. However, several avenues for further study are especially evident in the work performed during this calendar year. Among these are the following.

1. The investigation of the characteristics of redistributed GaAlAs/GaAs MQW heterostructures should be undertaken with the purpose of determining the electrical and the optical characteristics of this material. It provides the possibility of forming material with localized doping and/or localized variations of bandgap that are unachievable by any other technology. These investigations should include not only the diffusion of zinc to cause redistribution but also the implantation of zinc and other impurities, protons, neon, zenon, and the use of localized thermal excitation to cause the redistribution.
2. The implementation of localized redistribution of MQW material in integrated optoelectronic devices should be undertaken. These studies should include the integration of high mobility, high transconductance FET's, Gunn devices, and other electronic devices with optical devices including lasers, detectors, and modulators.
3. A detailed study of the transport properties of 2 DEG material grown by MOCVD and the application of this material to microwave and logic devices should be undertaken. This process has the virtue of being scalable to large volume and could potentially impact the fabrication of a wide variety of microwave and high speed digital devices.

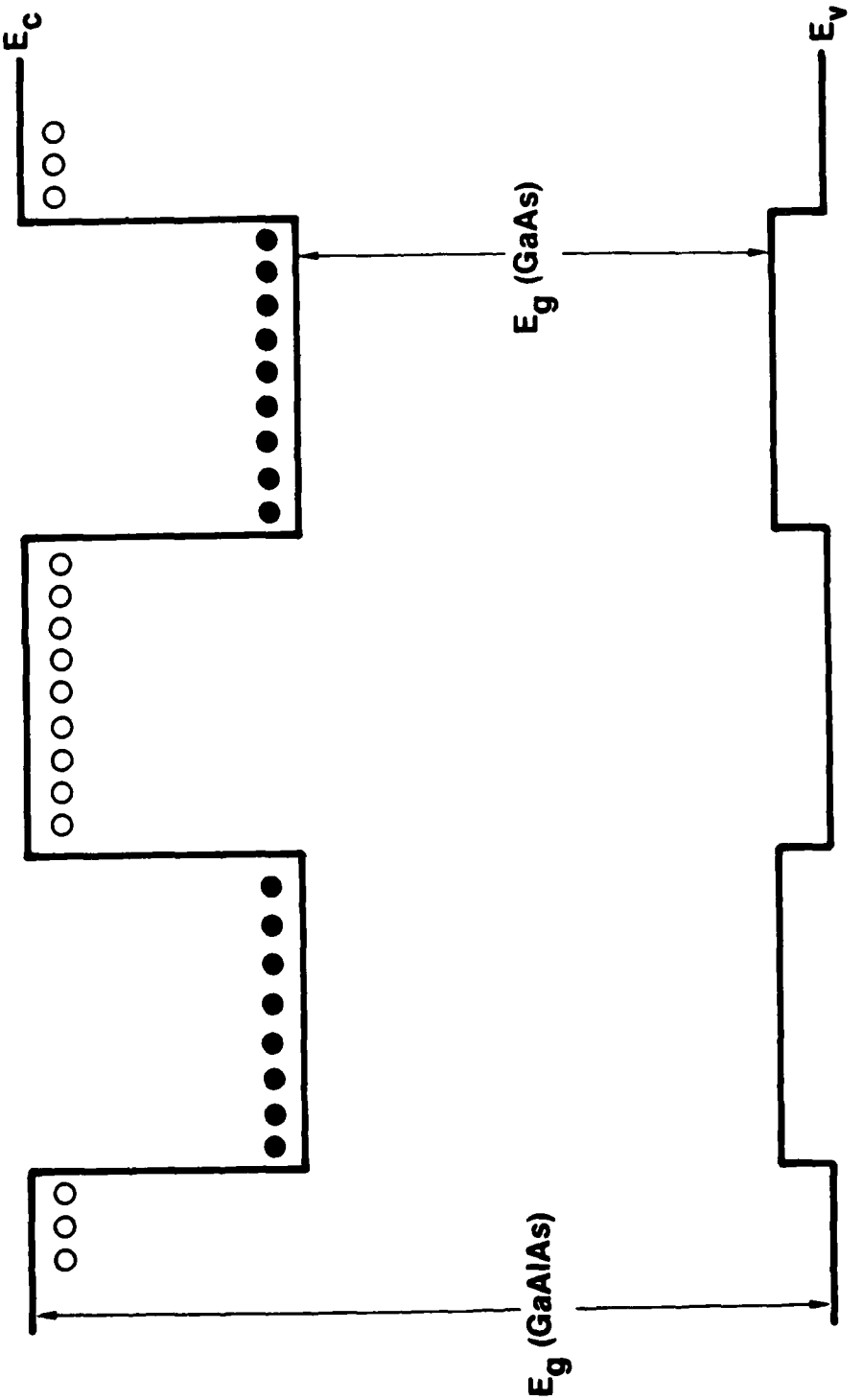

Fig. 1(a)

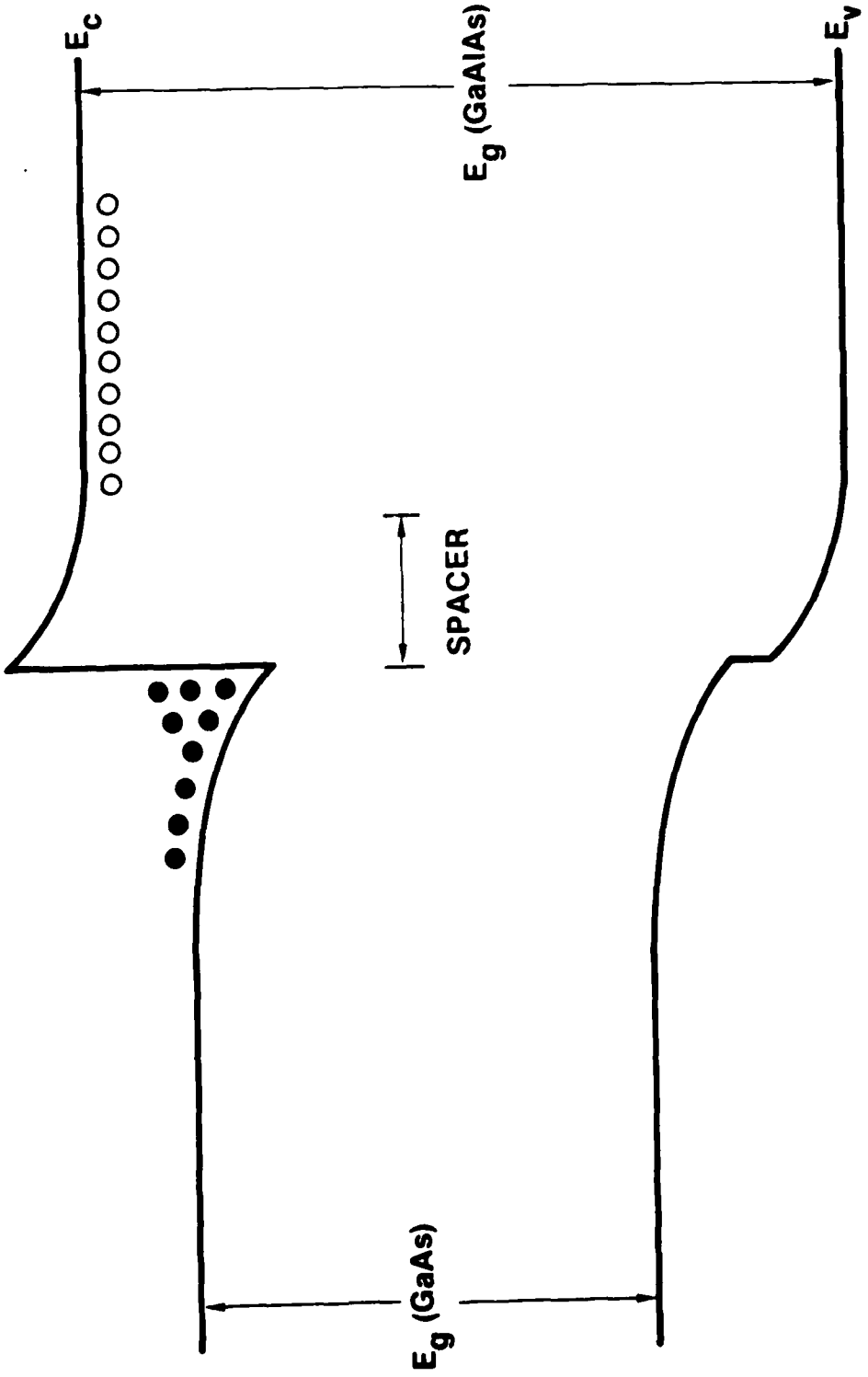

Fig. 1(b)

APPENDIX I

Clustering in MOCVD Quantum Well Heterostructures

1. Alloy Clustering in $Al_xGa_{1-x}As$-GaAs Quantum-Well Heterostructures. N. Holonyak, Jr., W. D. Laidig, B. A. Vojak, K. Hess, J. J. Coleman, P. D. Dapkus, and J. Bardeen, Phys. Rev. Lett. 45, 1703 (1980).
2. Comments, Robert C. Miller, Claude Weisbuch, and Arthur C. Gossard, Phys. Rev. Lett. 46, 1042 (1981).
3. Response, Holonyak, et al, Phys. Rev. Lett. 46, 1043 (1981).

Alloy Clustering in $Al_xGa_{1-x}As$-GaAs Quantum-Well Heterostructures

N. Holonyak, Jr., W. D. Laidig, and B. A. Vojak
Department of Electrical Engineering and Materials Research Laboratory, University of Illinois at Urbana-Champaign, Urbana, Illinois 61801

and

K. Hess
Department of Electrical Engineering and Coordinated Science Laboratory, University of Illinois at Urbana-Champaign, Urbana, Illinois 61801

and

J. J. Coleman and P. D. Dapkus
Rockwell International, Electronics Research Center, Anaheim, California 92803

and

J. Bardeen
Department of Physics, University of Illinois at Urbana-Champaign, Urbana, Illinois 61801
(Received 28 July 1980)

Data on spontaneous and stimulated emission, in the photon-energy range $E_g + 5\hbar\omega_{LO} \gtrsim \hbar\omega \gtrsim E_g$, are presented on $Al_xGa_{1-x}As$-GaAs quantum-well heterostructures with $Al_xGa_{1-x}As$ ($x \sim 0.4$–0.5) coupling barriers of size $L_B \sim 40$–70 Å and GaAs wells of size $L_z \sim 30$–40 Å. For $L_z, L_B \lesssim 50$ Å, Al-Ga disorder (clustering) in the alloy barriers is consistent with the observed spectral broadening and downward energy shift of the confined-particle transitions. A simple substitution of binary (AlAs) for ternary (AlGaAs) barriers eliminates alloy clustering and its effects, and makes unambiguous the identification of clustering in alloy barriers.

PACS numbers: 73.40.Lq, 71.50.+t, 78.45.+h

In contrast to earlier work,[1,2] stimulated emission has been observed recently at energy $5\hbar\omega_{LO}$ to $6\hbar\omega_{LO}$ below the confined-particle transitions of $Al_xGa_{1-x}As$-GaAs multiple-quantum-well heterostructures (QWH) with narrow wells ($L_z \lesssim 50$ Å) and narrow alloy barriers ($L_B \lesssim 50$ Å). An example is illustrated in Fig. 1, *a*. The lowest energies are a little above that of the GaAs energy gap, E_g. With increased pump power, stimulated emission is transferred to the neighborhood of the confined-particle states [Fig. 1, *b*]. In this paper, we show that because of disorder and clustering in the narrow ternary barriers (which can be removed by the use of binary barriers, AlAs), a continuum of states may exist in the QWH, the lowest with energies extending down to the band edge of pure GaAs. It is suggested that real phonon transitions take the electrons down to these levels, from which stimulated emission then occurs. With higher power, emission from the confined-particle states is enhanced and electrons do not have time to cascade to the lower levels.

The $Al_xGa_{1-x}As$-GaAs quantum-well heterostructures of interest here are grown by metalorganic chemical vapor deposition.[3,4] Gas flow rates and layer growth times are electronically controlled to ensure layer reproducibility. Growth rates are controllable in the range 2–50 Å/sec for GaAs and in the range 2.5–100 Å/sec for AlGaAs ($x \sim 0.40$), which makes it practical to grow layers as thin as 10 Å. The first layer grown on the {100} GaAs substrate is a GaAs buffer layer to provide a good crystallographic surface for succeeding layers. The next layer is a relatively thick (~ 1 μm) $Al_xGa_{1-x}As$ ($x \sim 0.50$) confining layer. This is followed by the QWH active region, which consists of a series of GaAs quantum wells and $Al_xGa_{1-x}As$ (or AlAs) barrier layers. The final layer is a second relatively thick (~ 0.3 μm) $Al_xGa_{1-x}As$ ($x \sim 0.50$) confining layer. All layers are undoped ($n_d - n_a \lesssim 10^{15}/cm^3$). Samples for photoluminescence experiments are prepared by polishing and selectively etching off[5] the GaAs from the substrate side. Cleaved portions (20–100 × 100–300 μm^2) of the remaining thin wafer (~ 1.3 μm thick) are imbedded for heat sinking into In under a sapphire window (77-K experiments)[6] or into annealed Cu under a diamond window (300-K experiments),[7] and are photoexcited with an Ar^+ (5145 Å) or a dye-tunable (6540-Å)

Further evidence for alloy clustering in the $Al_xGa_{1-x}As$ barriers is shown (Fig. 2) by the form of the high-level spontaneous emission spectra of a two-well, one-barrier ($x \sim 0.5$) QWH (a different QWH wafer) with all three layers ~40 Å thick. Note that in this case the barrier size is smaller (40 Å) and approaches and helps identify the average cluster size. As in Fig. 1, the confined-carrier transitions of the ideal $L_z \sim 40$ Å quantum well and also of the larger $L_z + L_B + L_z \sim 120$ Å composite quantum well are labeled in Fig. 2. The two samples (*a*, 4×10^4 W/cm², 90 $\times 360$ μm²; *b*, 10^5 W/cm², 56×195 μm²) exhibit very similar spectra as, in fact, do all of the samples from this wafer. A large peak in the range of $n' = 1'$ is observed. The emission does not drop to zero just below the $n = 1$ $e-hh$ transition, as would be expected in the ideal cluster-free limit, but extends downward in energy to nearly the location of the $n = 1$ (120) and $n' = 1'$ (120) transitions, which are near a distinct shoulder in the emission. An increase in the barrier thickness to ~70 Å results in cutoff of most of this lower energy emission.[9] As the barrier thickness L_B is decreased from ~70 Å (Ref. 9) to ~50 Å (Fig. 1) to ~40 Å (Fig. 2) and approaches the average cluster size, tunneling filaments are likely to appear in the $Al_xGa_{1-x}As$ barriers, which results in a major increase of the effective well dimension from $\sim L_z$ to $\sim L_z + L_B + L_z$. The observation of spectra such as those of Fig. 2 allow an estimate to be made of the cluster size ($\lesssim 40$ Å).

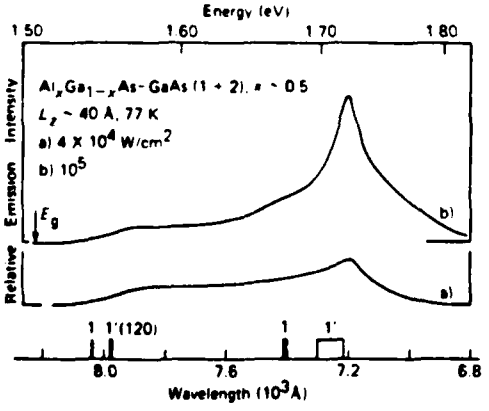

FIG. 2. Photoemission (77 K) of two QWH samples with active regions consisting of two 40-Å GaAs wells separated by one 40-Å $Al_xGa_{1-x}As$ ($x \sim 0.50$) barrier. These spectra (*a*, 4×10^4 W/cm²; *b*, 10^5 W/cm²) exhibit a peak near the $n' = 1'$ transition of a 40-Å well, with emission extending to lower energy. Note that this emission rolls off near the lowest-energy transitions of a composite-layer 120-Å well, indicated by the 1 and 1' (120) markers.

Further 300-K laser data on a 29-barrier, 30-well $L_z \sim 30$ Å, $L_B \sim 50$ Å superlattice structure (not shown) demonstrate that laser operation below E_g is also attainable. This fact, along with recent laser data on QWH's consisting of a large quantum well (or in some cases a bulk layer) coupled to a phonon-generating and -reflecting array of smaller quantum wells,[8] indicate that *virtual* phonon-assisted recombination processes with $\hbar\omega < E_g$ can occur and are not inconsistent with the present data. Alloy clustering *(in ternary barriers)*, however, allows actual states to exist between the bulk band edge and the lowest quantum states characteristic of an ideal QWH and thus permits *real* phonon processes to scatter the electrons to lower energies before recombining.

It is worth mentioning that a reinterpretation of previous investigations of disorder scattering[10-13] indicates that cluster models might have to be involved to explain successfully the experimental results for electron mobilities in III-V alloys. For example, negligible alloy scattering seems to exist[12] in $In_{1-x}Ga_xAs$ and strong alloy scattering in the quaternary system $In_{1-x}Ga_xP_{1-z}As_z$,[13] which (for the latter) cannot be explained on the basis of random-compositional-disorder models alone. In addition, these models do not take into account, in detail, the peculiarities of crystals such as $Al_xGa_{1-x}As$ or $GaAs_{1-z}P_z$ that undergo a direct-indirect transition in the range $x \approx x_c = 0.4$–0.5, nor whether such crystals are particularly prone to clustering. It is also worth mentioning that data are not presently available indicating how sensitive cluster formation is to the specific process (vapor-phase epitaxy, liquid-phase epitaxy, molecular-beam epitaxy) used to grow a III-V alloy.

In any case, the basic features of the $Al_xGa_{1-x}As$ alloy clustering described above are clear since, besides the data of Figs. 1 and 2, simple substitution of binary barriers (including very narrow barriers, ~10 Å) for the ternary barriers employed here eliminates recombination below the expected (ideal) confined-particle transitions of a QWH. These further data are shown in Fig. 3, which is for the case of a QWH with twelve GaAs wells ($L_z \sim 50$ Å) interleaved in the active region with thirteen *binary* (nonclustered) AlAs barriers ($L_B \sim 10$ Å). The laser operation of the sample (50×90 μm²) occurs exactly on the $n = 1$,

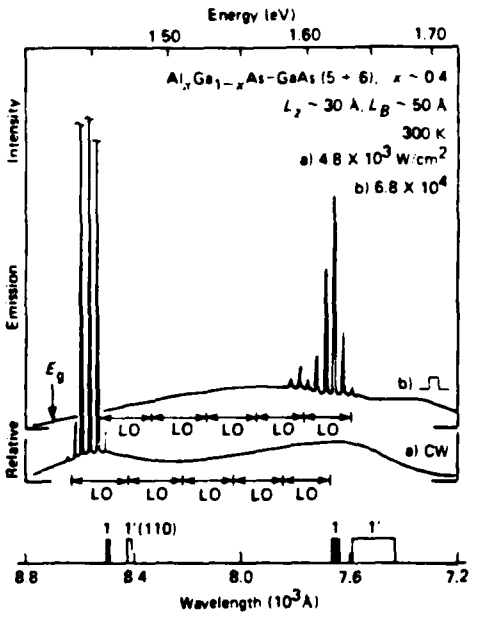

FIG. 1. Laser spectra (300 K) of a photopumped QWH grown by metalorganic chemical vapor deposition with an active region consisting of six ~30 Å GaAs wells and five ~50 Å $Al_xGa_{1-x}As$ ($x \sim 0.40$) barriers. The 1 and 1' markers indicate the allowed electron-to-heavy-hole and electron-to-light-hole transitions, respectively, for 30 Å wells separated by perfect 50-Å barriers (i.e., no alloy clustering). The 1 and 1' (110) markers indicate the lowest transitions of a 110-Å well. Typical cw laser operation (a, 4.8×10^3 W/cm^2) occurs slightly below the 1 (110) marker, while the spontaneous background extends to higher energy. Pulsed operation of a narrower sample (b, 6.8×10^4 W/cm^2) produces lasing at the expected energy of the $n = 1$ transition (30-Å well).

laser.

The 300-K laser data of Fig. 1 demonstrate the range of laser mode energies attainable from a QWH with an active region consisting of six L_z ~30 Å GaAs quantum wells coupled by five L_B ~50 Å, $Al_xGa_{1-x}As$ ($x \sim 0.4$) barrier layers. At 4.8×10^3 W/cm^2 cw excitation (*a*), a 39×110 μm^2 sample exhibits laser operation at $\lambda \sim 8560$ Å, which is in the anomalous range $\sim 5\hbar\omega_{LO}$ lower in energy than the lowest ($n = 1$) confined-carrier electron-to-heavy-hole (e–hh) or lowest ($n' = 1'$) electron-to-light-hole (e–lh) transitions of ~30 Å GaAs quantum wells coupled by ideal (microscopically uniform) ~50 Å, $Al_xGa_{1-x}As$ ($x \sim 0.4$) barriers. By exciting narrower samples at high level, we observe laser emission as high as 1.63 eV ($\lambda \sim 7600$ Å) as is shown by the 23×94 μm^2 sample of curve *b* (6.8×10^4 W/cm^2, pulsed). This high emission energy, which is expected ($L_z \sim 30$ Å), serves to identify the lowest confined-carrier transitions ($n = 1, n' = 1'$) of an ideal structure.

Alloy clustering in the $Al_xGa_{1-x}As$ barrier layers, which is a form of disorder and is inevitable, allows further interpretation of these spectra. In the extreme case of very large scale clustering, which would allow GaAs to extend across a barrier (~50 Å) and connect two or even more wells, the carrier recombination can approach E_g(GaAs) or $\lambda \sim 8707$ Å (300 K). Even for a smaller average cluster size it is possible that regions exist in the $Al_xGa_{1-x}As$ barriers where the Al concentration is nearly zero. The resulting local potential-well size is effectively increased from $L_z \sim 30$ Å to as much as $L_z + L_B + L_z \sim 110$ Å. The location (energy) of the lowest confined-carrier transitions of a ~110-Å GaAs quantum well are also labeled in Fig. 1. Note that alloy clustering in the barrier layers sufficient to create GaAs paths through the $Al_xGa_{1-x}As$ barriers is expected to have a drastic effect in broadening and lowering the energy spectrum of this quantum system. For example, the $n = 1$ confined-electron state shifts downward by ~140 meV for a size shift from L_z ~30 Å to $L_z + L_B + L_z \sim 110$ Å.

A result of this shift is that the density of states of a QWH with alloy clustering in the barriers will not exhibit an abrupt step to zero at energies below the lowest confined-particle states of an ideal structure. Instead, the density of states is expected to be small but significant below these "lowest" confined-carrier states, and then drop to zero for energies less than E_g(GaAs). Besides depending upon the barrier size L_B, the exact form of the density of states will depend on the average cluster size, the form of the cluster size distribution, and on the composition x of the $Al_xGa_{1-x}As$. Also, cluster-induced quantization in the x, y dimensions will play a role.

These additional lower-energy states are expected to play an important part in radiative emission from a QWH. The existence of small areas or patches within the active region with lower-energy states (areas that increase in number with the number of barriers) increases the probability of LO-phonon-assisted recombination processes[9] at energies $E_{1,1'} > \hbar\omega > E_g$ since virtual transitions are no longer required. Instead, real transitions in this range at multiples of $\sim\hbar\omega_{LO}$ below the $n = 1$ and $n' = 1'$ transitions of the $L_z \sim 30$ Å well are possible.

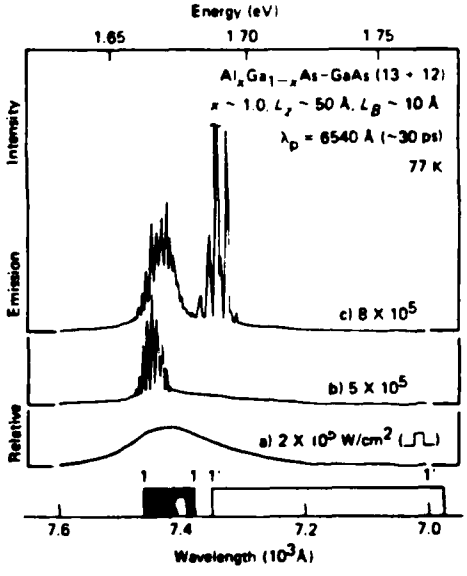

FIG. 3. Photoluminescence (laser) spectra (77 K) of a QWH sample with an all-binary (cluster-free) active region consisting of twelve ~ 50-Å GaAs wells alternating with thirteen ~ 10-Å AlAs barriers. The excitation power densities are high (~ 10^5 W/cm^2) since absorption of the incident pump beam ($\lambda_p \sim 6540$ Å) occurs only at the 50-Å GaAs wells. Spontaneous (*a*) and stimulated (*b*, *c*) emission occur only on the $n = 1$ and $n' = 1'$ transitions, and not at lower energy as in Figs. 1 and 2.

$e-hh$ and $n'=1'$, $e-lh$ "bands" with no recombination radiation between E_g ($\lambda \sim 8224$ Å) and E_1 ($\lambda \sim 7460$ Å), and with only minor spectral broadening just below E_1 as would occur for small growth fluctuations in layer size.

Finally we emphasize that the consequences of alloy clustering are very different for QWH layers and for bulk semiconductors. In a bulk III-V alloy the changes in the scattering rates (e.g., decrease in carrier mobility) due to clusters are quite small,[10] whereas in layered structures size-quantization effects can be totally destroyed. It is exactly these effects of size quantization that are probed with QWH laser emission, which is therefore a sensitive new tool to investigate clustering.

The authors are grateful to Yuri S. Moroz, R. T. Gladin, B. L. Marshall, and B. L. Payne (Urbana) for technical assistance, and to G. E. Stillman for various discussions. This work has been supported by the National Science Foundation under Grants No. DMR-79-09991 and No. DMR-77-23999 and by U. S. Navy Contract No. N00014-79-C-0768; the work has also been partially supported by the U. S. Office of Naval Research under Contract No. N00014-78-C-0711.

[1]N. Holonyak, Jr., R. M. Kolbas, R. D. Dupuis, and P. D. Dapkus, IEEE J. Quantum Electron. QE-16, 170 (1980).

[2]N. Holonyak, Jr., R. M. Kolbas, W. D. Laidig, B. A. Vojak, K. Hess, R. D. Dupuis, and P. D. Dapkus, J. Appl. Phys. 51, 1328 (1980).

[3]H. M. Manasevit, J. Electrochem. Soc. 118, 647 (1971).

[4]R. D. Dupuis and P. D. Dapkus, in *Proceedings of the Seventh International Symposium on GaAs and Related Compounds, St. Louis, 1978*, edited by C. M. Wolfe (Institute of Physics, Bristol, 1979), pp. 1–9.

[5]R. A. Logan and F. K. Reinhart, J. Appl. Phys. 44, 4172 (1973).

[6]N. Holonyak, Jr., and D. R. Scifres, Rev. Sci. Instrum. 42, 1885 (1971).

[7]N. Holonyak, Jr., R. M. Kolbas, R. D. Dupuis, and P. D. Dapkus, Appl. Phys. Lett. 33, 73 (1978).

[8]J. J. Coleman, P. D. Dapkus, B. A. Vojak, W. D. Laidig, N. Holonyak, Jr., and K. Hess, Appl. Phys. Lett. 37, 15 (1980).

[9]R. D. Dupuis, P. D. Dapkus, N. Holonyak, Jr., R. M. Kolbas, W. D. Laidig, and B. A. Vojak, Pis'ma Zh. Tekh. Fiz. 5, 132 (1979) [Sov. Tech. Phys. Lett. 5, 52 (1979)].

[10]J. W. Harrison and J. R. Hauser, Phys. Rev. B 13, 5347 (1976).

[11]M. A. Littlejohn, J. R. Hauser, T. H. Glisson, D. K. Ferry, and J. W. Harrison, Solid State Electron. 21, 107 (1978).

[12]T. P. Pearsall, R. Bisaro, P. Merenda, G. Laurencin, R. Ansel, J. C. Portal, C. Houlbert, and M. Quillec, in *Proceedings of the Seventh International Symposium on GaAs and Related Compounds, St. Louis, 1978*, edited by C. M. Wolfe (Institute of Physics, Bristol, 1979), pp. 94–102.

[13]P. D. Greene, S. A. Wheeler, A. R. Adams, A. N. El-Sabbahy, and C. N. Ahmad, Appl. Phys. Lett. 35, 78 (1979).

COMMENTS

Alloy Clustering in $Al_xGa_{1-x}As$

In the light of reported spectroscopic evidence for extensive clustering in thin $Al_xGa_{1-x}As$ barriers ($L_B \simeq 70$ Å) of GaAs quantum-well heterostructures (QWH) grown by metal-organic chemical-vapor deposition (MO-CVD),[1] plus the statement that "data are not presently available indicating how sensitive cluster formation is to the specific growth process," we have reexamined data on five samples grown by molecular-beam epitaxy (MBE) with L_B from 19 to 77 Å and remeasured two samples (one with $L_z = 54$ Å GaAs wells and $L_B = 52$ Å $Al_{0.3}Ga_{0.7}As$ barriers, the other $L_z = 188$ Å, $L_B = 19$ Å) looking specifically for the effect reported by Holonyak *et al.*, i.e., islands of GaAs in the $Al_xGa_{1-x}As$ layers. A search for peaks in the photoluminescent spectra at the expected positions for wells $2L_z + L_B$ wide[2] (the technique used by Holonyak *et al.*) and for a second set of transitions in the excitation spectra due to $2L_z + L_B$ wells (a technique not utilized by Holonyak *et al.*) failed to show any indication of wells wider than $\sim L_z$.[3]

Alloy clustering of the type reported[1] should smear the QWH interfaces. However, it has been observed that the excitation spectrum linewidth of optimally grown MBE QWH is well described by islands at the interface of about one atomic layer thick and >300 Å in lateral dimensions.[4] More recent studies indicate that the parameters of such islands are very sensitive to the growth conditions, especially to the substrate temperature T_s during growth. The island height is found to change from one monolayer at the optimum T_s to five monolayers at $T_s \pm 50$ °C.

There exists earlier *nonluminescent* evidence for very abrupt QWH interfaces in MBE material. Absorption studies by Dingle[5] point out an abruptness in the QWH interfaces of ~one monolayer. More direct structural studies of GaAs-$Al_xGa_{1-x}As$ superlattices by x-ray diffraction[6] and transmission electron microscopy[7] (TEM) have also shown sharp interfaces. In addition the TEM study showed the sensitivity of the optimal T_s to the stoichiometry of the layers, a fact which might correlate with the absence of clustering reported[1] for QWH with AlAs barriers.

In conclusion, high-quality QWH which show no spectroscopic or other evidence of clustering can be produced by MBE. The sensitivity of the QWH interface to the growth parameters might explain the extensive clustering reported,[1] but such clustering cannot be regarded as an intrinsic growth mode of these alloys.

Robert C. Miller
Claude Weisbuch
Arthur C. Gossard
Bell Laboratories
Murray Hill, New Jersey 07974

(Received 23 December 1980)
PACS numbers: 68.55.+b, 71.50.+t, 73.40.Lq, 78.55.Ds

[1]N. Holonyak, Jr., W. D. Laidig, B. A. Vojak, K. Hess, J. J. Coleman, P. D. Dapkus, and J. Bardeen, Phys. Rev. Lett. 45, 1703 (1980).

[2]Unpublished data from R. C. Miller demonstrate that quantum effects are discernible in MBE QWH for L_z up to at least 1000 Å.

[3]Some relevant data for the second sample are given in C. Weisbuch, R. C. Miller, R. Dingle, A. C. Gossard, and W. Wiegmann, Solid State Commun. 37, 219 (1981).

[4]C. Weisbuch, R. Dingle, A. C. Gossard, and W. Wiegmann, J. Vac. Sci. Technol. 17, 1128 (1980).

[5]See, for example, the detailed discussion in R. Dingle, *Festkörperprobleme*, edited by H. J. Queisser (Vieweg, Braunschweig, 1975), Vol. XV, p. 21.

[6]R. M. Fleming, D. B. McWhan, A. C. Gossard, W. Wiegmann, and R. A. Logan, J. Appl. Phys. 51, 357 (1980).

[7]P. M. Petroff, A. C. Gossard, W. Wiegmann, and A. Savage, J. Cryst. Growth 44, 5 (1978).

Holonyak *et al.* Respond: Rather than a divergence between the results obtained on quantum-well heterostructures (QWH) grown by metal-organic chemical-vapor deposition (MO-CVD) and molecular-beam epitaxy (MBE), there may actually be some convergence. In the Comment above, Miller and co-workers mention that island growth in MBE QWH's is sensitive to temperature, and becomes worse if the substrate temperature deviates $\pm 50\,^{\circ}C$ from some unspecified temperature T_s. Apparently most of the work, with no observed clustering, that these workers cite involves the use of MBE QWH crystals grown at $\leq 600\,^{\circ}C$. The best *MBE* QWH laser crystal of which we are aware, however (i.e., the only one to have operated continuously at 300 K), has been grown at $>600\,^{\circ}C$ ($\sim 650\,^{\circ}C$) and, moreover, operates (at high excitation level, $>10^3$ A/cm^2) as a laser 30–40 meV ($\sim\hbar\omega_{LO}$) below the $n=1$ electron–to–light-hole or the electron–to–heavy-hole transitions (8518 and 8567 Å; see Fig. 2 of Tsang *et al.*, Ref. 1; confined-particle transitions unmarked). This behavior agrees with the type of results we have reported for MO-CVD QWH lasers grown at 750 °C,[2,3] and can be explained by clustering.[4]

All of the work on QWH's [MBE, MO-CVD or LPE (liquid-phase epitaxy)] is sufficiently new, and totally sensitive and dependent upon the crystal-growth process and choice of experimental parameters, so that it is not established yet in any great detail what T_s and other experimental conditions are optimum for each growth process. Probably all of these crystal-growth processes will be subject to clustering for certain substrate temperatures, growth rates, and choice of crystal compositions (x in $Al_xGa_{1-x}As$). For example, more of a problem with clustering, at certain temperatures, might exist near the direct-indirect transition ($x \equiv x_c \sim 0.45$ for $Al_xGa_{1-x}As$). As we have shown,[4] however, one solution to the problem of clustering in $Al_xGa_{1-x}As$ is simply to substitute AlAs coupling and isolation barriers in $Al_xGa_{1-x}As$-GaAs QWH's. This permits also certain freedom in choice and manner of QWH crystal growth.

N. Holonyak, Jr., and W. D. Laidig
Electrical Engineering Research Laboratory and
Materials Research Laboratory
University of Illinois at Urbana–Champaign
Urbana, Illinois 61801

K. Hess
Electrical Engineering Research Laboratory and
Coordinated Science Laboratory
University of Illinois at Urbana–Champaign
Urbana, Illinois 61801

J. J. Coleman and P. D. Dapkus
Rockwell International, Electronics Research Center
Anaheim, California 92803

(Received 9 February 1981)
PACS numbers: 68.55.+b, 71.50.+t, 73.40.Lq, 78.55.Ds

[1]W. T. Tsang, C. Weisbuch, R. C. Miller, and R. Dingle, Appl. Phys. Lett. 35, 673 (1979).
[2]N. Holonyak, Jr., R. M. Kolbas, R. D. Dupuis, and P. D. Dapkus, IEEE J. Quantum Electron. 16, 170 (1980).
[3]B. A. Vojak, N. Holonyak, Jr., W. D. Laidig, K. Hess, J. J. Coleman, and P. D. Dapkus, to be published.
[4]N. Holonyak, Jr., W. D. Laidig, B. A. Vojak, K. Hess, J. J. Coleman, P. D. Dapkus, and J. Bardeen, Phys. Rev. Lett. 45, 1703 (1980).

APPENDIX II

Cluster-free AlAs/GaAs Quantum Well Heterostructures

1. Device-Quality Epitaxial AlAs by Metalorganic-Chemical Vapor Deposition, J. J. Coleman, P. D. Dapkus, N. Holonyak, Jr., and W. D. Laidig, Appl. Phys. Lett. 38, 894 (1981).
2. High-Barrier Cluster-Free $Al_xGa_{1-x}As$-AlAs-GaAs Quantum-Well Heterostructure Laser, J. J. Coleman, P. D. Dapkus, W. D. Laidig, B. A. Vojak, and N. Holonyak, Jr., Appl. Phys. Lett. 38, 63 (1981).
3. High-Energy (visible-red) Stimulated Emission in GaAs, B. A. Vojak, W. D. Laidig, N. Holonyak, Jr., and M. D. Camras, J. Appl. Phys. 52, 621 (1981).

Device-quality epitaxial AlAs by metalorganic-chemical vapor deposition

J. J. Coleman and P. D. Dapkus
Rockwell International, Electronics Research Center, Anaheim, California 92803

N. Holonyak, Jr. and W. D. Laidig
Electrical Engineering Research Laboratory and Materials Research Laboratory, University of Illinois at Urbana-Champaign Urbana, Illinois 61801

(Received 30 October 1980; accepted for publication 24 February 1981)

The growth and characterization of high-quality AlAs expitaxial layers on GaAs subtrates by metalorganic-chemical vapor deposition are described. The epitaxial layers described here are grown at intermediate temperatures (750 °C) and require no unusual reactor modifications. Comparison is made between single thick epitaxial layers and an 80-layer quantum-well heterostructure. Low-threshold photopumped laser data are presented, which indicate that the presence of AlAs in the active region of a laser (containing 80 AlAs-GaAs interfaces) does not interfere with cw room-temperature operation.

PACS numbers: 68.55. + b, 81.15.Gh, 61.10. − i

The binary III-V compound AlAs has been suggested in recent years as suitable for several device applications, particularly for various solar cell stuctures. Specifically, AlAs has been used for a wide-gap window layer on GaAs homojunction solar cells[1] and as an *n*-type layer for heterojunction solar cells on GaAs.[2] More recently, we have found that the replacement of the ternary $Ga_{1-x}Al_xAs$ with binary AlAs in the barrier layers of quantum-well heterostructures eliminates alloy clustering and its effects on carrier transport and laser emission characteristics.[3,4] AlAs has two distinct advantages in its physical nature for these and other applications. The direct band-edge energy gap of AlAs is quite large (E_Γ) ~ 3 eV,[5,6] and its lattice constant (5.6612 Å)[7] is very nearly the same as that of GaAs (5.6528 Å). AlAs presents some difficulty in handling, however, because it decomposes quite rapidly when exposed to air.[8,9] In addition, the growth of AlAs by the HCl transport method[2,10,11] requires very high temperatures (1000-1050 °C), which can lead to undesirable impurity incorporation. In this letter, we describe the growth of high-quality epitaxial AlAs by metalorganic chemical vapor deposition.[8,9] This technique allow epitaxial growth of AlAs to occur at reasonable temperatures in a system fully compatible with the growth of high-quality GaAs and $Ga_{1-x}Al_xAs$.

The AlAs epitaxial layers of this work have been grown by metalorganic-chemical vapor deposition (MO-CVD) in a vertical reactor.[8,9,12] The source materials used in the MO-CVD pyrolysis reaction are liquid trimethylaluminum (TMAl) and gaseous arsine (AsH_3) and the growth temperature is 750 °C. No intentional doping species are present, and a buffer layer of undoped GaAs (1.5 μm) is grown before any subsequent epitaxial growth. Epitaxial layers of AlAs have been grown with thicknesses in the range from less than 20 Å to greater than 1.5 μm. The substrate material in all cases is GaAs, oriented (100) ± 0.5° and doped with Si ($n \sim 2 \times 10^{18}$ cm^{-3}). In order to protect the AlAs layers from decomposition after growth, a single cap layer of undoped GaAs (50-100 Å) is grown on any exposed AlAs surface. Shown in Fig. 1 is the dependence of the AlAs growth rate (μm/min) on the flow rate (cm^3/min) of ultrapure hydrogen through the TMA1 bubbler. The growth of AlAs in this work, as in the case of MO-CVD GaAs and $Ga_{1-x}Al_xAs$, takes place under excess As conditions, and the growth rate of AlAs is linearly dependent on metal alkyl flow.

For comparison with the single (capped) epitaxial AlAs layers of this work we have prepared two additional structures. The first is an 80-layer quantum-well heterostructure (QWH) having alternating GaAs (45 Å) and AlAs (150 Å) layers. The total AlAs thickness of the QWH structure is 0.60 μm. The second additional structure is a single layer of $Ga_{1-x}Al_xAs$ ($x \sim 0.51$), which has a thickness of 0.25 μm. For the sake of accurate comparison, this structure has a final 60-Å GaAs cap layer.

An estimate of the number of dislocations at the surface of these three samples and a GaAs substrate has been made by etching the samples at room temperature in fresh AB etch.[13] Since the last grown layer (etched surface) is GaAs for all four samples, a comparison of the etch-pit densities of these samples is accurate. The region to be photographed by Nomarski interference microscopy for analysis was chosen for each sample to be average. A comparison of the sample containing a single capped AlAs layer with the GaAs substrate sample indicates that the number of dislocations evi-

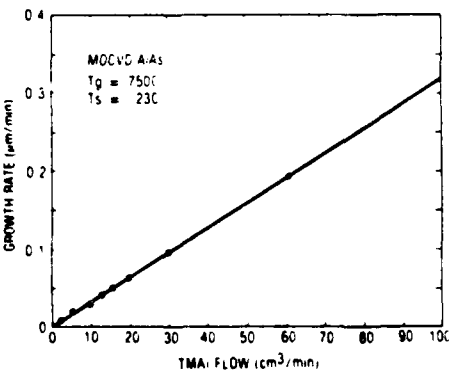

FIG. 1. Growth rate vs TMAl flow rate for MO-CVD AlAs on GaAs at 750 °C. The TMAl source temperature is 23 °C.

 0003-6951/81/110894-03$00.50

dent in the AlAs sample ($\sim 10^4$ cm^{-2}) is roughly a factor of 2 greater than in the substrate. The 80-layer QWH sample and the $Ga_{(1-x)}Al_{(x)}As$ sample have nearly the same number ($\sim 6 \times 10^3$ cm^{-2}) and this number is not much greater than in the GaAs substrate. The alloy layer has a reduced number of dislocations relative to AlAs, owing to smaller lattice constant mismatch. The 80-layer QWH is expected to have fewer dislocations than a single comparable AlAs layer, since the alternating thin layers result in reduced strain.[7,14,15] The structure appears macroscopically more nearly like $Ga_{1-x}Al_xAs$ ($x \sim 0.77$) based on the thickness ratio.

A further indication of the quality and composition of these binary AlAs layers and the AlAs-GaAs QWH is shown in Fig. 2. These are double crysal x-ray Cu-Kα (620) reflection rocking curves for the AlAs sample [Fig. 2(a)] and the 80-layer QWH sample [Fig. 2(b)]. The half-width and position of the intensity peak on the left of Fig. 2(a) relative to the GaAs substrate reference indicates high-quality AlAs. When a correction is applied[7,14,15] for the strain present in a thin epitaxial layer, the lattice mismatch between the layers corresponds to pure AlAs on GaAs.

The curve of the QWH structure [Fig. 2(b)] contains important information. The half-width of the peak is quite narrow and comparable to both the GaAs substrate reference and the AlAs single-layer peak [Fig. 2(a)]. The position of the peak corresponds to pure AlAs when the additional strain of the thinner layers is considered.[7,14,15] These and other data from layers as thin as 20 Å corroborate earlier Auger data[16] that indicate the interface width of MO-CVD grown GaAs-$Ga_{1-x}Al_xAs$ heterostructures is small. If the interface width had been much larger than expected, the structure of Fig. 2(b) would appear more nearly like a sample of $Ga_{1-x}Al_xAs$ ($x \sim 0.77$), and Fig. 2(b) would be broader and shifted considerably to the right.

In order to verify that the AlAs layers grown in this work are of sufficient quality to be usable as part of the active region of laser structures, we have examined the photopumped (Ar^+ laser) laser operation of the 80-layer quantum-well heterostructure sample described above. This sample is

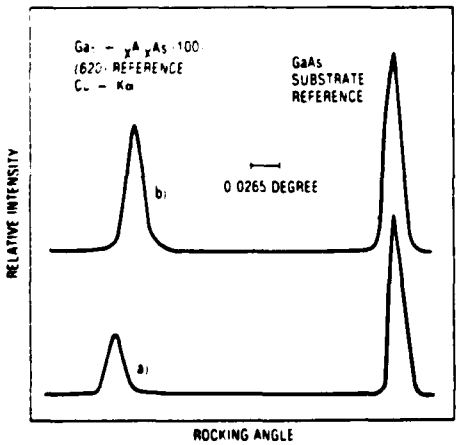

FIG. 2. Double crystal Cu-Kα x-ray (620) reflection rocking curves of (a) a single 0.75-μm-thick AlAs layer, and (b) an 80-layer AlAs (150 Å)-GaAs (45 Å) quantum-well heterostructure. The curves are aligned with respect to the GaAs substrate peak.

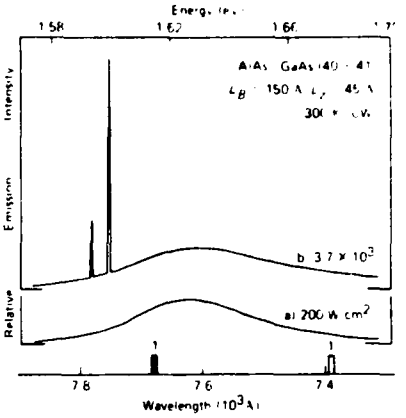

FIG. 3. Laser spectra (300 K) of a photopumped MO-CVD quantum-well heterostructure sample (15 μm wide) consisting of 41 GaAs quantum wells ($L_z \sim 45$ Å) alternating with 40 AlAs coupling barriers ($L_B \sim 150$ Å)

a bare superlattice without the thick, wide-gap confining layers characteristic of normal double-heterostructure lasers. The sample, with the substrate removed and heat sunk under diamond,[17] operates as a low-threshold, cw, 300-K laser as shown in the emission spectra of Fig. 3. At relatively low excitation power density [Fig. 3(a), 200 W/cm^2], the emission peaks near the lowest energy electron-to-heavy-hole transition ($n = 1, e \rightarrow hh$). With higher excitation [Fig. 3(b), 3.7×10^3 W/cm^2] cw, 300-K laser operation is observed at a wavelength of ~ 7750 Å. As shown by the data of Fig. 3, the presence of 80 GaAs-AlAs interfaces in this superlattice does not result in any serious losses, otherwise laser operation at low incident power densities would be impossible. Finally, comparison of these spectra with the spectra of Ref. 18 indicates that the replacement of AlAs for $Ga_{1-x}Al_xAs$ in the barrier layers of a superlattice QWH does not degrade the laser performance of the structure.

In conclusion, we have grown and characterized high-quality MO-CVD AlAs layers and AlAs-GaAs quantum-well heterostructures on GaAs substrates. The growth of these layers is possible at reasonable temperatures in a system compatible with the growtht of ternary $Ga_{1-x}Al_xAs$ and requires no extraordinary modifications to the basic reactor assembly or apparatus.[19] The quality of these layers is indicated by data which show that an 80-layer AlAs-GaAs quantum-well heterostructure (containing 80 interfaces and without thick wide-gap confining layers) operates as a low-threshold, cw, room-temperature photopumped laser.

We would like to thank D. E. Thompson, W. I. Simpson, L. A. Moudy, and R. E. Johnson for helpful discussions and technical assistance. The work of the Illinois group was supported by NSF Contract No. DMR 79-09991 and the Rockwell group was supported in part by the office of Naval Research, Contract No. N00014-78-C-0711.

[1] D. Huber and K. Bogus, *Proceedings of the* 1973 *IEEE Photovoltaic Specialists Conference* (IEEE, New York, 1974).
[2] W. D. Johnston and W. M. Callahan, Appl. Phys. Lett. **28**, 150 (1976).
[3] N. Holonyak Jr., W. D. Laidig, B. A. Vojak, K. Hess, J. J. Coleman, P. D. Dapkus, and J. Bardeen, Phys. Rev. Lett. **45**, 1703 (1980).

[4]J. J. Coleman, P. D. Dapkus, W. D. Laidig, B. A. Vojak, and N. Holonyak Jr., Appl. Phys. Lett. **38**, 63 (1981).
[5]A. Onton, Proc. 10th Int. Conf. Phys. Semiconductors Cambridge, Mass., 1970 p. 107 (unpublished).
[6]B. Monemar, Phys. Rev. B **8**, 5711 (1973).
[7]E. Estop, A. Izrael and M. Sauvage, Acta Cryst. A **32**, 627 (1976).
[8]H. T. Minden, Appl. Phys. Lett. **17**, 358 (1970).
[9]H. M. Manasevit, J. Electrochem. Soc. **118**, 647 (1971).
[10]M. Ettenberg, A. G. Sigai, A. Dreeben, and S. L. Gilbert, J. Electrochem. Soc. **118**, 1355 (1971).
[11]A. G. Sigai, M. S. Abrahams, and J. Blanc, J. Electrochem. Soc. **119**, 952 (1972).
[12]R. D. Dupuis, L. A. Moudy, and P. D. Dapkus, *Gallium Arsenide and Related Compounds* 1978 (Institute of Physics, New York, 1978, Conf. Ser. No. 45, p. 1.
[13]M. S. Abrahams and C. J. Buiocchi, J. Appl. Phys. **36**, 2855 (1965).
[14]G. A. Rozgonyi and D. C. Miller, Thin Solid Films **31**, 185 (1976).
[15]W. J. Bartels and W. Nijman, J. Cryst. Growth **44**, 518 (1978).
[16]R. D. Dupuis, P. D. Dapkus, C. M. Garner, C. Y. Su, and W. E. Spicer, Appl. Phys. Lett. **34**, 335 (1979).
[17]N. Holonyak Jr., R. M. Kolbas, R. D. Dupuis, and P. D. Dapkus, IEEE J. Quantum Electron. **QE-16**, 170 (1980).
[18]P. D. Dapkus, J. J. Coleman, W. D. Laidig, N. Holonyak, Jr., B. A. Vojak, and K. Hess, Appl. Phys. Lett. **38**, 118 (1981).
[19]G. B. Stringfellow and G. Horn, Appl. Phys. Lett. **34**, 794 (1979).

High-barrier cluster-free $Al_xGa_{1-x}As$-AlAs-GaAs quantum-well heterostructure laser

J. J. Coleman and P. D. Dapkus
Rockwell International, Electronics Research Center, Anaheim, California 92803

W. D. Laidig, B. A. Vojak, and N. Holonyak, Jr.
Department of Electrical Engineering and Materials Research Laboratory, University of Illinois at Urbana-Champaign, Urbana, Illinois 61801

(Received 8 September 1980; accepted for publication 3 October 1980)

Laser data (77 and 300 K) are presented on an $Al_xGa_{1-x}As$-AlAs-GaAs quantum-well heterostructure (QWH) grown by metalorganic-chemical vapor deposition with an active region consisting of 13 AlAs barrier layers of size $L_B \sim 10$ Å and 12 GaAs quantum wells of size $L_z \sim 50$ Å. This QWH, which is free of alloy disorder and clustering (Al-Ga clusters) in the active region, emits on the confined particle transitions and not at the lower energies characteristic of QWH's with $Al_xGa_{1-x}As$ barrier layers (and Al-Ga clusters).

PACS numbers: 42.55.Px, 81.10.Bk,

The idea of a quantum-well heterostructure (QWH) laser is to effect a basic improvement in semiconductor laser performance by confining the carriers in thin enough active layers to modify and raise the lowest carrier states, because of the confinement, to a step (electron and hole) above the band edge. In other words, a gradually increasing density of states at a bulk-crystal band edge should be converted into a sharp (rather large) step at somewhat higher energy ($> E_g$). In existing QWH lasers it is questionable if this sharp step has actually been realized. This is suggested by the fact that all present QWH lasers emit well below the lowest confined-particle states and transitions, frequently with identifiable phonon involvement. (For a review see Ref. 1.) Recent work[2] establishes a basis for this behavior: data on $Al_xGa_{1-x}As$-GaAs quantum-well heterostructures with smaller and smaller AlGaAs coupling barriers ($L_B \lesssim 50$ Å) reveal cluster-induced states extending from the expected confined-particle states to the bulk-crystal band edge E_g(GaAs). That is, Al-Ga clustering in the AlGaAs coupling and confining barriers leads to a distribution of GaAs well sizes (over a relatively large area active region) and hence broadens and smears the confined-particle states (and transitions). This behavior suggests immediately how to regain (in a QWH) a step-density-of-states and that is to remove the Al-Ga clustering from the QWH active region. This can be accomplished by replacing the AlGaAs confining and coupling barriers with AlAs as in Fig. 1. In this letter we show that the generic structure of Fig. 1 leads to an improved form of QWH laser that indeed operates, in spite of small well and barrier sizes ($L_z, L_B \lesssim 50$ Å) approaching Al-Ga cluster sizes in AlGaAs,[2] on the confined-particle transitions.

Note that no AlGaAs alloy is included in the active region of the QWH of Fig. 1. Thin AlAs buffer layers are interposed between the outside AlGaAs confining layers and the active region, and between the coupled quantum wells, in order to isolate all Al-Ga clusters from the active region (shown in Fig. 1 with 6 GaAs wells). Such a QWH can be grown by metalorganic chemical vapor deposition (MO-CVD) as has been described extensively elsewhere.[3,4] In the present work the only modification of the basic MO-CVD process is that of decreasing the GaAs growth rate to the range 2–50 Å/s and that of the $Al_xGa_{1-x}As$ (or AlAs) to 2.5–100 Å/s, so that ~10-Å-thick layers can easily be realized. A vertical (a) and a slant (b, 0.4°) cross section of such a QWH with 13 AlAs barriers ($L_B \sim 10$ Å) and 12 GaAs wells ($L_z \sim 50$ Å) are shown in Fig. 2. The active region is shown between the arrows in (a) and (b). The layers in the slant cross section of (b) (tan 0.4° ~ 1/145) appear to be wavy simply because of polishing scratches, which are obvious. It is worth mentioning that excess carriers generated in the AlGaAs confining layers (e.g., by photopumping) are collected in the active region (arrows in Fig. 1) by tunneling through the AlAs barriers and scattering to the lower energy confined-particle states.

For the experiments of interest here the substrate GaAs of the wafers is removed and cleaved rectangular samples (heat sunk in In under a sapphire window, 77-K experiments, or in annealed Cu under a diamond window, 300-K experiments) are photoexcited. This method of excitation is merely a matter of convenience, since either $Al_xGa_{1-x}As$ ($x \sim 0.5$) confining layer in Fig. 1 can be doped n type and the other p type and thus form an injection structure.

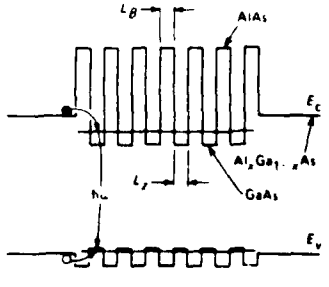

FIG. 1. Energy band diagram of an $Al_xGa_{1-x}As$-AlAs-GaAs quantum-well heterostructure laser that is free of disorder and clusters (Al-Ga clusters). The cluster-free active region consists of 7 AlAs barrier layers (size L_B) and 6 GaAs quantum wells (size L_z). Also shown are the carrier collection (via tunneling, small arrows) and the recombination transition $\hbar\omega > E_g$(GaAs) involving the lowest-energy confined-carrier electron and hole states.

 0003-6951/81/020063-03$00.50

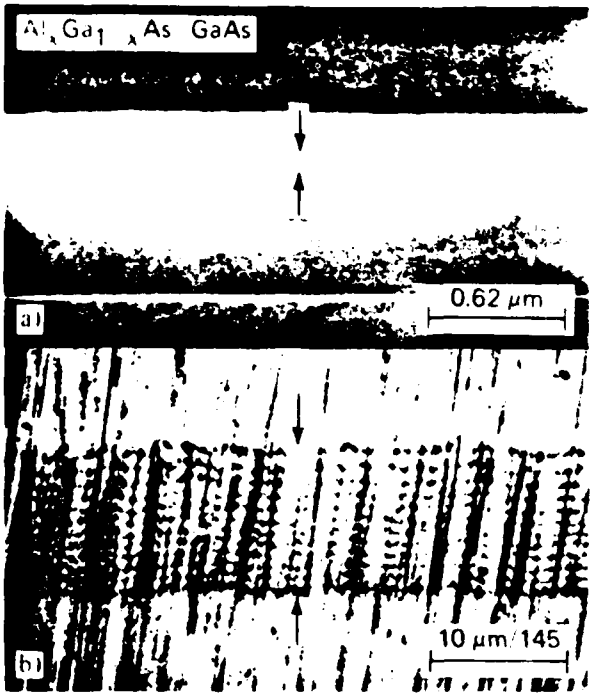

FIG. 2. Scanning photomicrographs of a cleaved and stained (a) and beveled and stained (b) $Al_xGa_{1-x}As$-AlAs-GaAs QWH (grown by MO-CVD) with a cluster-free active region. The active region, the region between the arrows, consists of 13 AlAs barriers ($L_B \sim 10$ Å) and 12 GaAs quantum wells ($L_z \sim 50$ Å). These layers are resolved in the beveled cross section (b, 0.4°).

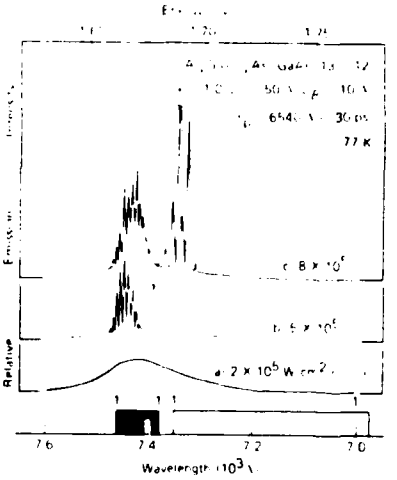

FIG. 3. Photoluminescence spectra (77 K) of a sample cleaved from the wafer of Fig. 2. The sample is photoexcited with a dye-tunable laser ($\lambda_p = 6540$ Å, ~ 30 ps pulse). At an excitation of 2×10^5 W/cm^2, the emission peaks on the lowest confined-carrier ($n = 1$) electron-to-heavy hole ($e \rightarrow hh$) transition. At higher excitation (b, 5×10^5 W/cm^2) the sample lases on the $n = 1$ ($e \rightarrow hh$) transition, $\hbar\omega \sim E_1$; at a still higher level (c, 8×10^5 W/cm^2) it lases also on the $n' = 1'$ ($e \rightarrow lh$) transitions. Note that the use of AlAs barrier layers results in laser operation on or above the confined-particle transitions ($\hbar\omega \gtrsim E_1$) and not lower as is characteristic of QWH's containing $Al_xGa_{1-x}As$ barrier layers.

Figure 3 shows the laser operation (77 K) of the QWH of Figs. 1 and 2 when pumped with a ~ 30-ps pulse at $\lambda \approx 6540$ Å from a dye-tunable laser. Note that the high pump levels are due simply to the fact that the only absorption of the excitation occurs at the quantum wells themselves (12×50 Å) and represents a very small fraction of the input power ($\alpha \sim 10^4$ cm^{-1} for GaAs). As curve (a) shows, only a small recombination-radiation tail exists below the first electron-to-heavy-hole ($n = 1$ or E_1, $e \rightarrow hh$) transition. This tail is very slight compared to the stimulated emission in the range $E_g \lesssim \hbar\omega \lesssim E_g + 5\hbar\omega_{LO} \lesssim E_1$ of the comparable QWH with AlGaAs barriers (and Al-Ga clusters) in Figs. 1 and 2 of Ref. 2. The small tail at lower energy of curve (a) in Fig. 3 is thought to be caused by slight but inevitable size variations of the GaAs wells or the AlAs coupling barriers that occur during the MO-CVD crystal growth. The important point, however, is that the laser operation occurs on the confined-particle transitions ($n = 1$ or E_1, $e \rightarrow hh$ and $n' = 1'$ or E_1', $e \rightarrow lh$) shown by curves (b) and (c), and not lower in energy—not $\hbar\omega_{LO}$ or lower.[1,2]

On other samples we have verified that if the $L_B \sim 10$-Å coupling barriers of Fig. 3 are increased in size, with the GaAs held fixed in size at $L_z \sim 50$ Å, the $n = 1$ ($e \rightarrow hh$) band (Fig. 3) contracts a little, and the $n' = 1'$ ($e \rightarrow lh$) band contracts much more (but remains fixed in center position) and shifts the $n' = 1'$ ($e \rightarrow lh$) recombination to considerably higher energy than shown in Fig. 3. In either case (larger or smaller L_B) the laser operation occurs on the confined-particle transitions, not lower in energy.

At higher temperature (Fig. 4, cw 300 K) the laser operation (5145-Å photoexcitation) occurs also on the confined-particle transitions, but because the $n = 1$ ($e \rightarrow hh$) and $n' = 1'$ ($e \rightarrow lh$) bands are so close ($\delta E < 10$ meV $< kT$), it is not possible to observe laser operation separately on the $n = 1$ or $n' = 1'$ band. Note that the 300 K continuous (cw) laser operation of Fig. 4 is not particularly high in threshold ($< 4.7 \times 10^3$ W/cm^2 or 1.9×10^3 A/cm^2) when it is realized that the laser operation is 155 meV above E_g (GaAs) and the sample is only 15 μm wide ($\alpha_{loss} \sim 780$ cm^{-1}).

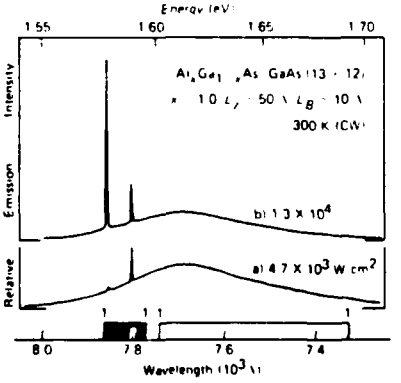

FIG. 4. Continuous room-temperature laser operation of a photopumped sample cleaved (15×223 μm) from the wafer of Figs. 2 and 3. Laser operation is observed at $\hbar\omega \sim E_1$ (a, 4.7×10^3 W/cm^2; b, 1.3×10^4 W/cm^2). Just as demonstrated in Fig. 3 (77 K), no laser emission (300 K) is observed at $\hbar\omega < E_1$ in the case of a cluster-free (no Al-Ga clusters) QWH, i.e., one with all binary layers in the active region.

The results presented above, along with the data of Ref. 2, show that an improved form of QWH can be realized that is free of alloy disorder and clustering and that operates as a laser *on* (not below) the confined-particle transitions.

We thank J. Bardeen, K. Hess, and G. E. Stillman for helpful conversations, and Yuri S. Moroz, R. T. Gladin, B. L. Marshall, and B. L. Payne (Urbana) for technical assistance. The work of the Rockwell group has been partially supported by the Office of Naval Research, Contract No. N00014-78-C-0711, and that of the Illinois group by NSF, Grant Nos. DMR 79-09991 and DMR 77-23999.

[1] N. Holonyak, Jr., R. M. Kolbas, R. D. Dupuis, and P. D. Dapkus, IEEE J. Quantum Electron **QE-16**, 170 (1980).
[2] N. Holonyak, Jr., W. D. Laidig, B. A. Vojak, K. Hess, J. J. Coleman, P. D. Dapkus, and J. Bardeen (unpublished).
[3] H. M. Manasevit, J. Electrochem. Soc. **118**, 647 (1971).
[4] R. D. Dupuis and P. D. Dapkus in *7th International Symposium on GaAs and Related Compounds, St. Louis*, 1978, edited by C. M. Wolfe (Institute of Physics, London, 1979), pp. 1–9.

High-energy (visible-red) stimulated emission in GaAs

B. A. Vojak, W. D. Laidig, N. Holonyak, Jr., and M. D. Camras
Department of Electrical Engineering and Materials Research Laboratory, University of Illinois at Urbana-Champaign, Urbana, Illinois 61801

J. J. Coleman and P. D. Dapkus
Rockwell International, Electronics Research Center, Anaheim, California 92803

(Received 26 September 1980; accepted for publication 23 October 1980)

The high-energy (visible-red) photpumped laser operation (6345 Å at 77 K, 6785 Å at 300 K) of $Al_xGa_{1-x}As$-AlAs-GaAs quantum-well heterostructures (QWH) grown by metalorganic chemical vapor deposition (MO-CVD) is described. The QWH active regions are alloy-free and consist of GaAs quantum wells and AlAs barrier layers. The effect of the AlAs barrier-layer thickness on the energy banding of the confined-carrier states and transitions is demonstrated. The laser operation of the coupled GaAs quantum wells is observed as high as 400–445 meV above the bulk-GaAs band edge, which agrees with the calculated locations ($L_z \sim 30$ Å) of the lowest ($n = 1$) electron, heavy-hole, and light-hole confined-particle states or energy bands.

PACS numbers: 42.55.Px, 78.55.Ds, 81.15.Gh, 78.45. + h

I. INTRODUCTION

Although most current interest in semiconductor lasers is concerned with longer-wavelength fiber-optic sources, e.g., $Al_xGa_{1-x}As$-GaAs or InP-$In_{1-x}Ga_xP_{1-z}As_z$ double heterostructures, there is ample reason (such as photocopying or video-disk recording) for interest in visible-spectrum heterostructure lasers. The latter, however, are in a more primitive state of development because of various difficulties in working with high-gap III–V alloys. (See Ref. 1 for a discussion.) In the case of high-gap $In_{1-x}Ga_xP_{1-z}As_z$, the substrates employed [commercial GaAsP LED (light-emitting diode) substrates] are not lattice matched throughout and are of relatively poor quality. For the case of high-gap $Al_xGa_{1-x}As$ there is, in the direct-gap alloy range ($x < x_c \sim 0.45$), an obvious limit to the heterobarrier height or energy-gap discontinuity between the active region and the confining layers. Also, in the high-gap energy range (i.e., for $E_g \gtrsim 1.8$ eV or within ~ 250 meV of x_c in $Al_{1-x}Ga_xAs$), there is some question whether alloy disorder and clustering is more extreme and a source of difficulty.[2]

A possible answer to the problem of constructing a visible-spectrum semiconductor laser is to employ a GaAs quantum-well active region. For example, single GaAs quantum wells ($L_z \sim 200$ Å) have operated as photopumped lasers, at 77 K, as high in energy as 1.77 (Fig. 10 of Ref. 3) to 1.80 eV (Fig. 1 of Ref. 4). Unfortunately these quantum-well heterostructures (QWH's) are relatively inefficient laser sources because of their broad spontaneous spectra and thus wasted electron-hole recombination. If an attempt is made to effect an improvement in $Al_xGa_{1-x}As$-GaAs QWH's by shifting the $n = 1$ states (electrons, heavy holes, light holes) to higher energies by reducing the GaAs quantum-well sizes to $L_z < 50$ Å, multiple wells must be employed to collect the injected carriers[3] and to yield a sufficiently large active region but, unfortunately, lower-energy ($\hbar\omega \sim E_g$) recombination and a broad recombination-radiation spectrum are still observed.[3] We have shown that this behavior is a consequence of alloy clustering in the $Al_xGa_{1-x}As$ coupling barriers that are used in $Al_xGa_{1-x}As$-GaAs QWH's.[2] This compromised behavior of a QWH laser can be eliminated by utilizing AlAs barriers (with clearly no disorder or clustering) as demonstrated in Ref. 5. Then it is indeed possible to use small quantum-well size ($L_z < 50$ Å) to generate high-energy recombination. This can be done, moreover, in an active region consisting of only binary layers (AlAs and GaAs) and thus with no III–V alloy problems. In this paper we demonstrate that the laser operation of GaAs quantum wells can be achieved on a relatively narrow recombination-radiation spectrum and be at least as high in energy as 1.83 eV (6785 Å) at 300 K and 1.95 eV (6345 Å) at 77 K, which, remarkably, is 400–445 meV above E_g (GaAs) and in an energy range comparable (and competitive) with III–V alloys.

II. ALLOY-FREE AlAs-GaAs ACTIVE REGION

The diagram of Fig. 1 illustrates a simplified model of the conduction and valence bands of a QWH free of III–V alloy disorder and clustering in the active region.[2,5] The active region consists of several thin GaAs wells ($L_z \lesssim 50$ Å) alternating with thin AlAs barrier layers ($L_B \lesssim 50$ Å). On both sides of the active region are thicker (0.3–1.0 μm) $Al_xGa_{1-x}As$ ($x \sim 0.5$) confining layers. These confining layers provide a thick layer for efficient absorption of a laser excitation beam in the case of photopumping, or can be doped n type and p type for current injection. The electrons and holes generated in the confining layers (photopumped sample) diffuse to the active region, where they tunnel and scatter to the lower-energy quantum-well states and recombine (arrows in Fig. 1).

For design and experimental reasons it is important to know the location of the lowest-energy ($n = 1$) electron e, heavy-hole hh, and light-hole lh states or bands of the improved (prototype) QWH of Fig. 1. These states can be determined by solving Schrödinger's equation (for electrons, heavy holes, and light holes) in each layer and by, as usual, matching the solutions across the boundaries. This proce-

 0021-8979/81/020621-06$01.10

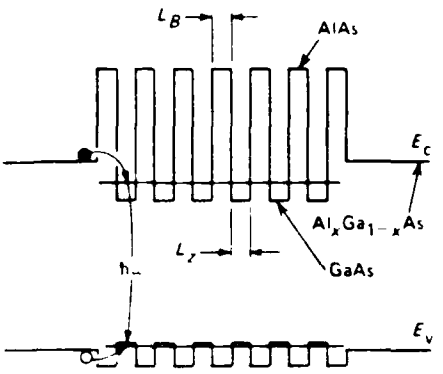

FIG. 1. Schematic diagram of the conduction and valence bands of an Al$_x$Ga$_{1-x}$As-AlAs-GaAs QWH with an alloy-free active region. The GaAs wells of width L_z are bounded on both sides by AlAs coupling barriers of width L_B. These thin layers of GaAs and AlAs, which compose the active region of the QWH, are sandwiched between thicker (0.3–1.0 μm) confining layers of Al$_x$Ga$_{1-x}$As. Electrons and holes generated in the Al$_x$Ga$_{1-x}$As diffuse to the active region where they tunnel and scatter to lower-energy states and then recombine, emitting photons of energy $\hbar\omega$.

dure is practical for a small number ($\lesssim 6$) of quantum wells and can be conveniently programmed on a small laboratory computer (HP 9825). For QWH's with only a few wells, the exact number of wells and the composition of the Al$_x$Ga$_{1-x}$As confining layers have a pronounced effect on the allowed energy states. Beyond ~6 wells, however, the allowed energy states begin to form energy bands, and a Kronig-Penney[6] analysis serves as a useful approximation for calculating the lowest ($n = 1$) electron, heavy-hole, and light-hole energy bands. Although these calculations are not exact, they provide a useful guide for choosing layer thickness corresponding to the desired ($n = 1$) e, hh, lh energies.

The $n = 1$ energy bands (Fig. 2) are calculated (via an HP 9825 computer) as a function of well size L_z for an infinite series of GaAs wells and with the AlAs barriers chosen here to be $L_B = 20$ Å. The Kronig-Penney analysis leads to the familiar expression

$$1 \geq |[(\alpha^2-\beta^2)/2\alpha\beta] \times \sinh(\alpha L_B)\sin(\beta L_z) + \cosh(\alpha L_B)\cos(\beta L_z)|, \quad (1)$$

where

$$\alpha \equiv 2m_1^*(V-E)^{1/2}/\hbar, \quad (2)$$

and

$$\beta \equiv (2m_2^*E)^{1/2}/\hbar. \quad (3)$$

Equation (1) can be solved for the allowed energies E of electrons in the conduction band and holes in the valence band.

In the present work E is the electron energy above the GaAs conduction band edge or the hole energy below the valence band edge (the 0 boundary in Fig. 2). The electron effective mass in the AlAs barriers, m_1^*, is taken to be 0.15 m_0, where m_0 is the free-electron mass. The electron effective mass in GaAs, m_2^*, is calculated as a function of energy from[7]

$$m_2^* = [0.0665 + 0.0436E + 0.236E^2 - 0.147E^3]m_0, \quad (4)$$

where E is in meV. Equation (4) is employed to take into account, as a first-order approximation, the nonparabolic nature of the Γ minimum and the variation of the electron effective mass with E ($E \lesssim 300$ meV). The conduction-band discontinuity or barrier height V is taken to be

$$V = 0.85[E_\Gamma(0,T) - E_\Gamma(1,T)], \quad (5)$$

where the energy of the Γ minimum in Al$_x$Ga$_{1-x}$As as a function of both crystal composition x and temperature T is given by[7]

$$E_\Gamma(x,T) = 1.519 + 1.247x - 5.405\times10^{-4}T^2/(T+204), \quad x < 0.45 \quad (6a)$$

$$= 1.519 + 1.247x + 1.147(x-0.45)^2 - 5.405\times10^{-4}T^2/(T+204), \quad x > 0.45 \quad (6b)$$

The effective masses used for the heavy holes are $m_1^* = 0.75m_0$ (AlAs) and $m_2^* = 0.45m_0$ (GaAs). For light holes, $m_1^* = 0.15m_0$ (AlAs) and $m_2^* = 0.087m_0$ (GaAs). The valence-band discontinuity, in agreement with Eq. (5), is taken to be

$$V = 0.15[E_\Gamma(0,T) - E_\Gamma(1,T)], \quad (7)$$

where $E_\Gamma(x,T)$ is calculated from Eqs. (6a) and (6b).

The electron and heavy-hole energy bands calculated from the above expressions and shown in Fig. 2 are relatively narrow in comparison to the light-hole energy band because of the low effective mass of the light holes and because of the rather small band-edge discontinuity in the valence band. As expected, for barrier widths L_B smaller than 20 Å, the energy bands tend to broaden equally above and below the band centers. Also, for $L_B > 20$ Å the bands contract to smaller widths. These effects are demonstrated in Sec. IV (Fig. 3).

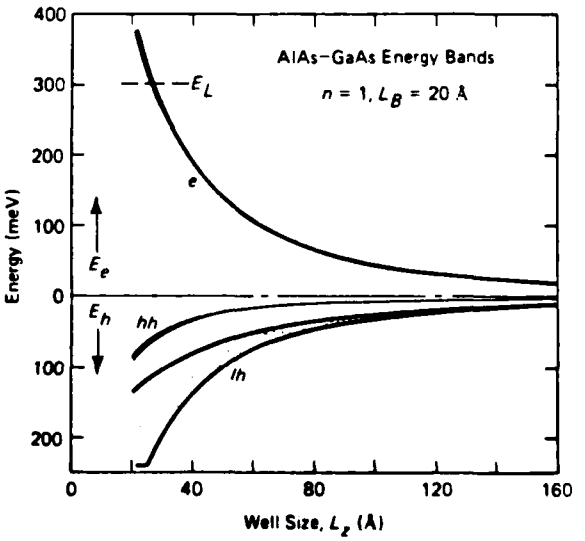

FIG. 2. Lowest ($n = 1$) confined-particle energy bands for electrons e, heavy holes hh, and light holes lh as a function of well size L_z for GaAs wells coupled by AlAs barriers of thickness $L_B = 20$ Å as shown in Fig. 1. The dashed line $E_L \sim 300$ meV indicates the position in the GaAs conduction band of the L indirect minima. A common zero reference is used for quantum-well electrons (increasing energy upward) and for holes (increasing energy downward).

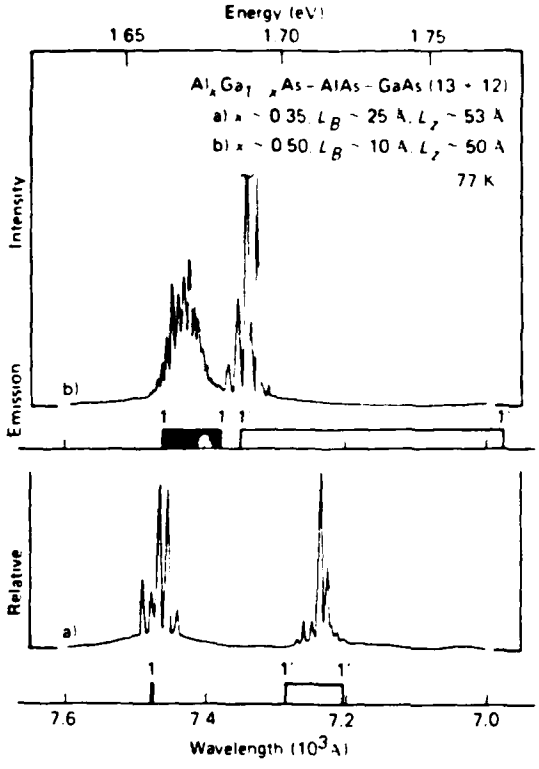

FIG 3. Photoluminescence spectra (77 K) of two quantum-well heterostructures (QWH) with active regions consisting of 13 AlAs barriers L_B and 12 GaAs quantum wells L_z (a, $L_z \sim 53$ Å; b, $L_z \sim 50$ Å). The fundamental difference between these wafers is the size of the AlAs barriers (a, $L_B \sim 25$ Å, 8×10^4 W/cm^2, $\lambda_p \sim 5145$ Å; b, $L_B \sim 10$ Å, 8×10^4 W/cm^2, $\lambda_p \sim 6540$ Å). As the barrier thickness is decreased from $L_B \sim 25$ Å to $L_B \sim 10$ Å, the laser operation shifts to lower energy as the transitions broaden (increased coupling). The dark and light bars on the horizontal axis mark the calculated electron-to-heavy-hole ($e \rightarrow hh$, $n = 1$) and electron-to-light-hole ($e \rightarrow lh$, $n' = 1'$) transitions (see text).

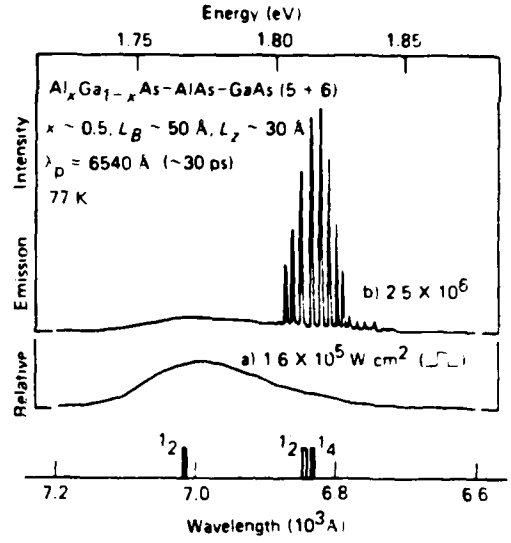

FIG 4. Emission spectra (77 K) of a QWH consisting of six 30-Å GaAs wells coupled by five 50-Å AlAs barriers. The alloy-free active region is sandwiched between confining layers of $Al_xGa_{1-x}As$ ($x \sim 0.5$). A rectangular sample ($50 \times 230\ \mu m^2$) is photopumped below the confining-layer absorption with a mode-locked dye laser ($\lambda_p \sim 6405$ Å, ~30-ps pulse) and, because of the low absorption, requires high excitation levels.

Notice that for $L_z \leq 25$ Å ($L_B = 20$ Å) the light-hole band extends downward to the "top" of the potential well (~235 meV), which is the upper limit for the hole energy bands. This is the basis for the small horizontal line on the *lh* band at $L_z \leq 25$ Å (Fig. 2). In the same size range the electron band *e* extends to ≳ 300 meV above the bulk-crystal conduction band edge and is somewhere near the GaAs *L* indirect band edge.[8] This is shown in Fig. 2 by the E_L horizontal marker. It is clear from Fig. 2 that the size limit that leads to the maximum realizable $n = 1$ electron and hole energies [and maximum recombination radiation energy, $\hbar\omega = E_g + E_e + E_{lh}$ (or E_{hh})] is $L_z = 25$–30 Å. As described in the following, we are close to these limits in the work reported here.

III. SAMPLE PREPARATION AND EXCITATION

The $Al_xGa_{1-x}As$-AlAs-GaAs QWH's of interest in this work have been grown by the metalorganic-chemical-vapor-deposition (MO-CVD) process, which is described extensively elsewhere.[9,10] QWH wafers are grown on {100} GaAs substrates. The first layer is a ~1-μm-thick GaAs buffer layer to provide a good crystallographic surface for the succeeding layers. This is followed by a ~1-μm-thick $Al_xGa_{1-x}As$ confining layer, next the all-binary QWH active region, and finally a second $Al_xGa_{1-x}As$ confining layer that is ~0.3-μm thick. Two of the wafers (data of Fig. 3) contain active regions of the form of Fig. 1 and consist of 13 AlAs barrier layers and 12 GaAs quantum wells. Although the GaAs well sizes differ slightly and the $Al_xGa_{1-x}As$ confining-layer compositions *x* are not the same, the fundamental difference between these wafers is their AlAs barrier-lay-

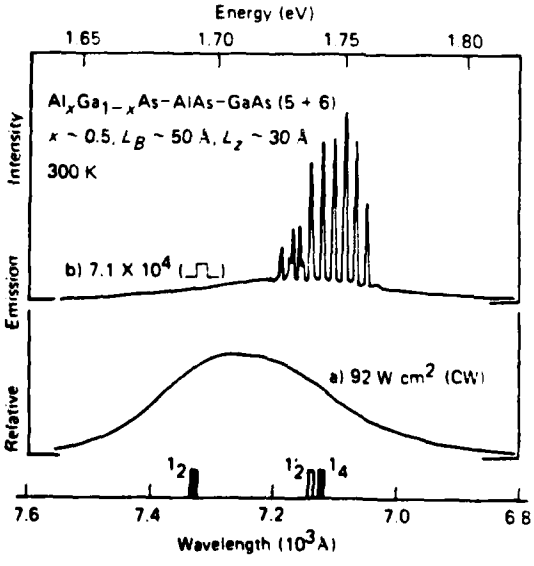

FIG 5. Room-temperature emission spectra of a sample ($35 \times 40\ \mu m^2$) taken from the same QWH described in Fig. 4. The sample is photopumped with an Ar^+ laser ($\lambda_p \sim 5145$ Å, ~20-nsec pulse) and shows that the 300-K behavior is consistent with that at 77 K (Fig. 4).

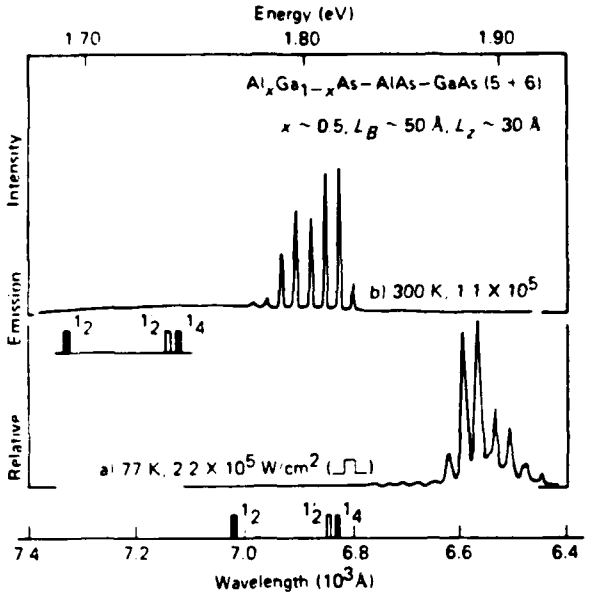

FIG. 6. Visible-spectrum stimulated emission obtained by photopumping ($\lambda_p \sim 5145$ Å) samples from the QWH of Figs. 4 and 5. Curve a (2.2×10^5 W/cm^2) shows the laser operation at 77 K of a narrow sample (20 μm); laser modes extend to wavelengths as short as 6440 Å (other samples to 6345 Å). At room temperature, curve b (1.1×10^5 W/cm^2), laser modes of another 20-μm-wide sample extend from 7000 to 6800 Å (other samples to 6785 Å).

er thicknesses: (a) $L_B \sim 25$ Å and (b) $L_B \sim 10$ Å. For the wafer providing most of the high-energy data of this paper (Figs. 4–6), the active region consists of 6 $L_z \sim 30$-Å GaAs quantum wells and 5 $L_B \sim 50$-Å AlAs coupling barrier layers. In contrast to the work of Ref. 5 and the QWH wafer of Fig. 3, no AlAs barrier layers are used to separate the $Al_xGa_{1-x}As$ ($x \sim 0.5$) confining layers from the two outermost GaAs quantum wells of the active region. All of the layers are undoped ($n_d - n_a \lesssim 10^{15}/cm^3$).

Photopumping with an Ar^+ laser ($\lambda \sim 5145$ Å) or a dye-tunable laser ($\lambda_p \sim 6540$ Å) is employed. In the case of the latter, significant absorption occurs only at the GaAs quantum wells; thus the excitation levels necessary to attain laser threshold are typically quite high as compared to the power densities necessary when using an Ar^+ laser.

Photoluminescence samples are prepared by first polishing the wafer from the substrate side and then selectively etching off the GaAs substrate and buffer layers. The remaining ~ 1.3-μm-thick wafer is then cleaved into rectangles (20–100×50–$300\ \mu m^2$) which are heat sunk in In under a sapphire window for 77-K operation or in annealed Cu under a diamond window for 300-K operation.

IV. PHOTOLUMINESCENCE DATA

The effect of the AlAs barrier-layer thickness on QWH emission spectra is shown by the photopumped-laser spectra (77 K) of Fig. 3. The two curves of Figs. 3(a) and 3(b) correspond to two QWH wafers, each with 12 GaAs quantum wells of almost the same size ($L_z \sim 50$ Å). The laser spectrum of (a) (8×10^4 W/cm^2) is from a sample with thicker AlAs barriers ($L_B \sim 25$ Å), while that of (b) (8×10^5 W/cm^2, $\lambda_p \sim 6540$ Å, only the quantum wells excited) is from a sample with thinner AlAs barriers ($L_B \sim 10$ Å). This difference in well coupling is reflected (Fig. 3) in the energy spread, curve *a* narrower and curve *b* broader, of the $n = 1$ electron-to-heavy-hole ($e \rightarrow hh$) and $n' = 1'$ electron-to-light-hole ($e \rightarrow lh$) transitions. The laser operation in both cases occurs at the lower-energy end of the $n = 1$ ($e \rightarrow hh$) and $n' = 1'$ ($e \rightarrow lh$) bands, as is evident in Fig. 3. These data make clear the important effect of decrease in size of L_B.

Typical 77-K photoluminescence spectra of a sample cleaved from the six-well wafer described above are shown in Fig. 4. Because of the form of the QWH active region, the confined-carrier states and thus the transitions are slightly modified from those typical of wafers[5] of the form of Fig. 1. The potential barrier formed by a ~ 50-Å-thick AlAs layer has a relatively large effect in localizing carriers in the GaAs layers. Because of this, the confined carriers in the two outermost GaAs quantum wells are in asymmetric potential wells with a lower-energy $Al_xGa_{1-x}As (x \sim 0.5)$ barrier on one side and a higher-energy AlAs barrier on the other; the confined carriers in each of the remaining four GaAs quantum wells are in a symmetric potential formed by two higher-energy AlAs barriers. Therefore, two of the lowest-energy confined-carrier states (there are six $n = 1$ confined-carrier states for a six-well QWH) are nearly degenerate and characteristic of the outermost GaAs layers. These states are somewhat lower in energy than the remaining four nearly degenerate states characteristic of the four inner GaAs wells. The energy of these states is approximated rather well by Fig. 2. The resulting recombination transitions corresponding to these states are labeled in Fig. 4 as 1_2 for the two lower-energy $e \rightarrow hh$ transitions, 1_4 for the four higher-energy $e \rightarrow hh$ transitions, and $1_2'$ for the two lower-energy $e \rightarrow lh$ transitions. The other four $e \rightarrow lh$ transitions are not allowed, since only the first two light-hole states are bound in the well. (Note that the locations of these transitions in Fig. 4 have been determined by accurate calculations, as described above, and have not been simply estimated from Fig. 2.)

The emission spectra (77 K) of Fig. 4, as in the case of Fig. 3(b), are obtained by photoexciting a QWH sample with a dye-tunable laser (~ 30-psec pulse width). The energy gap of the $Al_xGa_{1-x}As (x \sim 0.5)$ confining layers is $E_g \sim 2.07$ eV while the pump-beam photon energy ($\lambda_p \sim 6540$ Å) is $\hbar\omega_p \sim 1.90$ eV, or ~ 170 meV (~ 25 kT) lower in energy. Thus as already mentioned, the excitation occurs only at the GaAs wells and is quite high. At a photoexcitation level of 1.6×10^5 W/cm^2 (curve a), the spontaneous-emission spectrum of this sample peaks very near the $n = 1_2$ $e \rightarrow hh$ transition and exhibits a high-energy tail in the range of the $n' = 1_2'$ $e \rightarrow lh$ and $n = 1_4$ $e \rightarrow hh$ transitions. Upon increase in excitation level to 2.5×10^6 W/cm^2 (curve b), laser operation occurs in the energy range of the $n' = 1_2'$ $e \rightarrow lh$ and $n = 1_4$ $e \rightarrow hh$ transitions. Note, however, that a small spontaneous emission peak still exists near $n = 1_2$ but not lower in energy as in QWH's with disordered ternary coupling barriers.[2]

This QWH exhibits similar behavior at 300 K. Figure 5 shows the room-temperature emission spectra of another

sample cleaved from the same wafer described in Fig. 4. With low-level cw excitation using an Ar^+ laser pump (curve a, 92 W/cm^2), spontaneous emission occurs, as expected and described above, in the energy range of the confined-carrier transitions and not at lower energy. When excited with a cavity-dumped Ar^+ laser (7.1×10^4 W/cm^2, curve b), the same sample lases near the $n' = 1_2$ $e\rightarrow lh$ and $n = 1_4 e\rightarrow hh$ transitions.

The emission spectra of Figs. 4 and 5 are typical of average-size photoluminescence samples (sample width $\gtrsim 40$ μm). An important feature of both Figs. 4 and 5 (77 and 300 K) is that the spontaneous-emission spectra peak near the $n = 1_2$ transitions, while laser operation occurs near the $n' = 1_2$ and $n = 1_4$ transitions. These higher-energy confined-carrier transitions represent a larger density of states and thus are expected to have more gain than the $n = 1_2$ $e\rightarrow hh$ transitions. From the data of Figs. 4 and 5, it appears that bandfilling to a higher density of states for laser operation to occur is nescessary in a structure of this type. This may simply be a consequence of the small active volume of GaAs (6×30 Å $= 180$ Å).

By selectively exciting very narrow samples (sample widths ~20 μm), with correspondingly high cavity end losses, we can force laser operation to still higher energies than those shown in Figs. 4 and 5. This is demonstrated by the 77 and 300 K laser spectra of Fig. 6. At 77 K (curve a, 2.2×10^5 W/cm^2), a 20 μm-wide samples, when pulse-excited with a cavity-dumped Ar^+ laser, exhibits laser modes peaked near ~6570 Å with a high-energy mode at ~6440 Å. The highest-energy laser mode observed from a sample from this wafer (data not shown) is at 6345 Å, or 445 meV above the bulk-GaAs band gap and ~150 meV higher than the previously reported highest-energy laser operation of GaAs.[8] Of more practical importance, very high-energy stimulated emission in an AlAs-GaAs QWH also occurs at 300 K. Room-temperature laser operation (curve b, 1.1×10^5 W/cm^2, sample width ~20 μm) is peaked at 6850 Å with a high-energy mode at 6800 Å. Laser modes as short in wavelength as 6785 Å, or ~400 meV higher in energy than the 300 K bulk-GaAs energy gap, have also been observed (data not shown). These data indicate that with proper design of the QWH active region, room-temperature laser operation at least approaching, if not surpassing, ~6800 Å is possible in $Al_xGa_{1-x}As$-AlAs-GaAs QWH's of the type shown in Fig. 1.

V. DISCUSSION AND CONCLUSIONS

Through the use of AlAs instead of $Al_xGa_{1-x}As$ ($x<1$) coupling barriers in QWH's the problem of alloy clustering, and thus the existence of confined-carrier states and transitions at lower energies and of broader linewidth than expected, has been eliminated. The behavior demonstrated in Figs. 3 and 4 of Ref. 5 and Figs. 4, 5, and 6 of this work indicates that relatively narrow-linewidth, high-energy ($E_g + 150$ meV $\lesssim \hbar\omega \lesssim E_g + 445$ meV) stimulated emission from GaAs is possible. The usefulness of $Al_xGa_{1-x}As$-AlAs-GaAs QWH's as visible-spectrum lasers depends upon, among other factors such as efficiency and reliability, how high in energy laser operation can occur.

Of the various processes that place an upper energy limit on the laser operation of GaAs, one of the most fundamental is the transfer of electrons from the direct Γ minimum to the indirect L minima. The energy difference of these minima has been measured to be $E_L - E_\Gamma = 330 \pm 40$ in bulk GaAs[8] and $E_L - E_\Gamma \sim 295$–310 meV in an $L_z \sim 100$-Å-thick GaAs QWH.[7,11] Therefore, unless size-quantization effects force electron states in the L minima to higher energy, which is possible, only ~300 meV of the GaAs emission energy can be attributed to high-energy electrons. Thus as shown in Fig. 2, the well size must be kept in the range $L_z \gtrsim 25$ Å in order to keep the $n = 1$ electron state (or band) at lower energy than the bulk-GaAs L minima.

Another important limitation is that of how much of the emission energy can be attributed to holes and valence-band effects. Since the excess carriers enter the QWH-active region from the $Al_xGa_{1-x}As$ ($x<1$) confining layers, the largest fraction of the GaAs photon energy that comes from high-energy holes (assuming no k selection rule) is that associated with the valence-band discontinuity between the $Al_xGa_{1-x}As$ ($x<1$) confining layers and the GaAs quantum wells. The total energy-gap discontinuity is given by

$$\Delta E_g = E_g(\text{AlGaAs}) - E_g(\text{GaAs}) = \Delta E_v + \Delta E_c, \quad (8)$$

where ΔE_v and ΔE_c are the valence-band and conduction-band discontinuities, respectively. Using $\Delta E_v = 0.15\Delta E_g$ and assuming $x = 0.5$ $Al_xGa_{1-x}As$ confining layers leads to $\Delta E_v \sim 90$ meV. Therefore, even though Fig. 2 shows hole energy states in the range $0 < E_h \lesssim 235$ meV, if a finite AlAs-GaAs QWH is located between $Al_xGa_{1-x}As$ ($x\sim0.5$) confining layers, only $\Delta E_v \sim 90$ meV of this ~235 meV range can contribute to the GaAs quantum-well recombination-radiation energy. If x is increased to make ΔE_g and thus ΔE_v greater ($\Delta E_v \simeq 0.15\Delta E_g$), or if $\Delta E_v/\Delta E_g > 0.15$ (or even if $\Delta E_v/\Delta E_g$ is a function of x), then still more of the GaAs quantum-well recombination energy may be attributed to the hole energy.

By considering electron transfer from the Γ to the L minima and the valence-band discontinuity (for $x\sim0.5$ in this case) as the two limiting factors of high-energy stimulated emission in GaAs, we estimate a maximum recombination-radiation energy of $\hbar\omega \sim E_g(\text{GaAs}) + \Delta E_v + (E_L - E_\Gamma) \sim E_g(\text{GaAs}) + 390$ meV. The high-energy modes observed in this work at $\hbar\omega \sim E_g(\text{GaAs}) + 400$ meV at 300 K and $\hbar\omega \sim E_g(\text{GaAs}) + 445$ meV at 77 K are most likely near or at the high-energy limit of laser operation of any AlAs-GaAs QWH with $Al_xGa_{1-x}As$ ($x\sim0.5$) confining layers unless size-quantization effects substantially increase the ground-state energy of the L minima electrons, or unless ΔE_v is larger than ~90 meV ($x\sim0.5$). Still higher-energy laser operation might be attainable if the Al composition in the confining layers is increased to $x > 0.5$, resulting in $\Delta E_v > 90$ meV. It should be mentioned that in the present work we have tried to establish if GaAs, in the form of a quantum well, is capable of visible-red laser emission, and whether this can be accomplished in an alloy-free QWH with an AlAs-GaAs-active region that is free of disorder or clustering as a source of spectral broadening. This has been ac-

complished, and it is clear that, at 300 K, GaAs is capable of stimulated emission at wavelengths as short at 7000–6800 Å. We have not constructed an optimum practical structure (in terms of design, doping profile, freedom from defects, etc.) in the present work, but from this and related work[5] have reason to believe that the type of QWH described here (Fig. 1) will eventually operate as a laser continuously at room temperature in the visible-red.

ACKNOWLEDGMENTS

The authors are grateful to J. Bardeen, K. Hess, and G. E. Stillman for helpful discussions, and to Yuri S. Moroz, R. T. Gladin, B. L. Marshall, and B. L. Payne (Urbana) for technical assistance. The work of the Illinois group has been supported by NSF Grants DMR 79-09991 and DMR 77-23999, the work of the Rockwell group has been partially supported by the Office of Naval Research, Contract N00014-78-C-0711.

[1] S. W. Kirchoefer, E. A. Rezek, B. A. Vojak, N. Holonyak, Jr., D. Finn, D. L. Keune, and J. A. Rossi, IEEE J. Quantum Electron QE-16, 198(
[2] N. Holonyak, Jr., W. D. Laidig, B. A. Vojak, K. Hess, J. J. Coleman, P. D. Dapkus, and J. Bardeen, Phys. Rev. Lett. 45, 1703 (1980).
[3] N. Holonyak, Jr., R. M. Kolbas, R. D. Dupuis, and P. D. Dapkus, IEEE J. Quantum Electron QE-16, 170 (1980).
[4] R. D. Dupuis, P. D. Dapkus, R. M. Kolbas, N. Holonyak, Jr., and H. Shichijo, Appl. Phys. Lett. 33, 596 (1978).
[5] J. J. Coleman, P. D. Dapkus, W. D. Laidig, B. A. Vojak, and N. Holonyak, Jr., Appl. Phys. Lett. 38, 63 (1981).
[6] R. de L. Kronig and W. G. Penney, Proc. Roy. Soc. (London) A130, 499 (1930).
[7] R. M. Kolbas, Ph. D. dissertation, Urbana, IL, 1979 (unpublished).
[8] D. E. Aspnes and M. Cardona, Phys. Rev. B 17, 741 (1978).
[9] H. M. Manasevit, J. Electrochem. Soc. 118, 647 (1971).
[10] R. D. Dupuis and P. D. Dapkus, in *Seventh International Symposium on GaAs and Related Compounds, St. Louis*, 1978, edited by C. M. Wolfe (Institute of Physics, London, 1979), pp. 1–9.
[11] R. D. Dupuis, P. D. Dapkus, R. M. Kolbas, and N. Holonyak, Jr., Solid State Commun. 27, 531 (1978).

APPENDIX III

Phonon-Assisted Emission from Quantum Wells

1. Phonon Contribution to Metalorganic Chemical Vapor Deposited $Al_xGa_{1-x}As$-GaAs Quantum-Well Heterostructure Laser Operation, B. A. Vojak, N. Holonyak, Jr., W. D. Laidig, K. Hess, J. J. Coleman, and P. D. Dapkus, J. Appl. Phys. 52, 959 (1981).
2. Quenching of Stimulated Phonon Emission in $Al_xGa_{1-x}As$-GaAs Quantum-Well Heterostructures, W. D. Laidig, N. Holonyak, Jr., M. D. Camras, B. A. Vojak, K. Hess, J. J. Coleman, and P. D. Dapkus, Solid State Commun. 38, 301 (1981).
3. Absorption, Stimulated Emission, and Clustering in AlAs-$Al_xGa_{1-x}As$-GaAs Superlattices, J. J. Coleman, P. D. Dapkus, M. D. Camras, N. Holonyak, Jr., W. D. Laidig, T. S. Low, M. S. Burroughs, and K. Hess, to be published in J. Appl. Phys.
4. Absorption and Stimulated Emission in an AlAs-GaAs Superlattice, J. J. Coleman, P. D. Dapkus, D. R. Clarke, M. D. Camras, and N. Holonyak, Jr., to be published in J. Appl. Phys.

Phonon contribution to metalorganic chemical vapor deposited $Al_xGa_{1-x}As$-GaAs quantum-well heterostructure laser operation

B. A. Vojak, N. Holonyak, Jr., and W. D. Laidig
Department of Electrical Engineering and Materials Research Laboratory, University of Illinois at Urbana-Champaign, Urbana, Illinois 61801

K. Hess
Department of Electrical Engineering and Coordinated Science Laboratory, University of Illinois at Urbana-Champaign, Urbana, Illinois 61801

J. J. Coleman and P. D. Dapkus
Rockwell International, Electronics Research Center, Anaheim, California 92803

(Received 16 July 1980; accepted for publication 29 October 1980)

A series of experiments have been conducted to determine the extent of longitudinal optical (LO) phonon contribution to quantum-well-heterostructure (QWH) laser operation. Extensive data are presented on metalorganic chemical vapor deposited (MO-CVD) $Al_xGa_{1-x}As$-GaAs QWH's with active regions consisting of larger quantum wells, or in some cases bulk layers ($L_z > 500$ Å), coupled to phonon-generating and -reflecting arrays of coupled smaller quantum wells. Because of the electronic and vibrational coupling of the single larger layer to the array, the spontaneous emission and laser emission from these structures differ from that of QWH's containing either a single well or a multilayer of uniform well thickness. In fact, phonon sideband laser operation of the larger GaAs layer can be induced at $\hbar\omega \sim E_g - \hbar\omega_{LO}$ (undoped layers, $n_d - n_a \lesssim 10^{15}$ /cm^3). An increase in either the thermal or nonthermal phonon occupation number is shown to cause phonon sideband laser operation in a QWH. A guide to the design of the multilayer array also is presented.

PACS numbers: 78.50.Ge, 78.45.+h, 63.20.-e, 81.15.Gh

I. INTRODUCTION

Until quite recently, the design of III-V semiconductor lasers has involved the optimization of carrier, current, and electromagnetic field confinement in some form of stripe-configuration double-heterostructure laser. As the carriers are better confined, however, so also to some extent are the longitudinal optical (LO) phonons that are emitted during the process of carrier energy relaxation from the wider-energy-gap confining layers (injecting layers) to the narrower-gap active region. The role that phonons might play in double-heterojunction (DH) and quantum-well-heterostructure (QWH) lasers has been poorly understood in spite of the fact that large phonon densities are likely to exist in the active region at threshold, which is typically high ($J \sim 10^3$ A/cm^2). For example, in an $Al_xGa_{1-x}As$-GaAs ($x \sim 0.4$, $T = 300$ K) DH laser approximately $[E_g(\text{AlGaAs}) - E_g(\text{GaAs})]/\hbar\omega_{LO} = (1.923\text{-}1.424)/0.036 \simeq 14$ LO phonons are emitted for each electron-hole pair injected into the active region. That LO phonons do modify laser action has been shown in the phonon-sideband operation of AlGaAs-GaAs,[1,2] InGaPAs-InP[3,4] and InGaPAs-GaAsP,[5] quantum-well heterostructures. All of these are III-V semiconductor compounds in which, unlike II-VI compounds, phonon participation in laser operation has not previously been identified. This has been more or less expected because the electron-LO phonon coupling is inherently relatively weak in comparison with II-VI compounds.

The relevant recombination and LO phonon scattering processes for undoped GaAs in the bulk and quantum-well cases are illustrated in the density of states versus energy diagram of Fig. 1. As electronic carriers are confined to a thin-lower-energy-gap semiconductor layer between two wider-gap layers, the single-particle energy spectrum takes on a particle-in-a-box character in the dimension in which

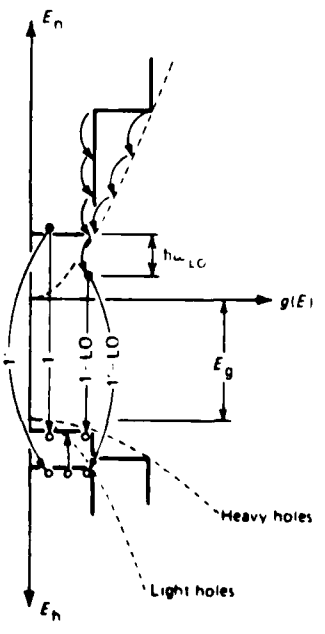

FIG. 1. Density of states diagrams for electrons, heavy holes, and light holes. The step-like cumulative density of states $g(E)$ characteristic of quantum-well heterostructures is contrasted with the density of states of bulk material (dashed curves). The smaller curved arrows indicate electron energy loss (in units of $\hbar\omega_{LO}$) via electron-LO-phonon scattering. The arrows labeled 1 and 1' represent the recombination of an electron in the $n = 1$ confined-particle state with a heavy hole ($n = 1$) and a light hole ($n = 1$), respectively. Light-to heavy-hole relaxation is indicated by the small upward arrow.

 0021-8979/81/020959-10$01.10

the layer is constricted (e.g., for GaAs $L_z < 500$ Å), and results in a number of quasi-two-dimensional subbands each of which has a constant density of states.[6] The cumulative densities of states for electrons and for light and heavy holes in the quantum-well regime is steplike as shown in Fig. 1, with each step occurring at the energy of the one-dimensional confined-carrier energy. In the bulk limit, the usual parabolic density of states exists (dashed). The curved arrows on the conduction-band densities of states represent LO-phonon emission by thermalizing electrons while the 1, 1', 1-LO, 1'-LO arrows illustrate the various low-energy confined-carrier radiative recombination transitions in QWH lasers (1 is $n = 1$ electron to heavy-hole, 1' is $n' = 1'$ electron to light-hole, and 1-LO and 1'-LO are phonon sidebands of the 1 and 1' transitions). Also shown is the light- to heavy-hole relaxation.

The form of the density of states is fundamental to the process of LO-phonon emission and absorption in polar optical scattering and is so important that, in the two-dimensional limit, the basic electron–LO-phonon interaction is actually slightly enhanced over the bulk case,[7] making stimulated phonon emission more of a possibility.[2] Because of this, the nonthermal LO-phonon occupation number is expected to be greatly increased in QWH lasers.[8] These phonons, however, are extremely difficult to detect. Earlier work[8] indicates that multiple thin-layer ($L_z \lesssim 80$ Å) structures, in contrast to single ($L_z \lesssim 500$ Å) quantum wells, are very efficient in carrier collection and thermalization, and operate readily on LO-phonon sidebands. A valid verification of the role of *LO phonons in a QWH* is, therefore, the artificial inducing of phonon-sideband laser operation in a larger quantum well ($L_z \sim 200$-500 Å) or bulk layer by a phonon-generating and -reflecting array of small ($L_z \sim 50$-80 Å) quantum wells. Also, the identification of phonon-sideband laser operation of a thicker layer ($L_z \gtrsim 200$ Å) is easier because of the advantage that the lowest-energy confined-carrier transitions converge to E_g as L_z increases, the uncertainty in determining L_z and the confined-carrier transitions is thus decreased.

The purpose of the present work is to determine the extent to which LO phonons affect the laser operation (77–300 K) of both QWH and DH $Al_xGa_{1-x}As$-GaAs semiconductor lasers. Phonons generated in a thin multiple QWH array are used to induce phonon-sideband emission in a larger, coupled, "phonon-detector" GaAs layer. The extensive data presented on QWH's of various well thicknesses show that $Al_xGa_{1-x}As$-GaAs heterostructure lasers can be designed which take advantage of the LO phonons that are inherently generated in these structures.

II. CRYSTAL PREPARATION AND EXCITATION

The $Al_xGa_{1-x}As$-GaAs samples of interest here are grown by metalorganic chemical vapor deposition (MO-CVD), which has been described extensively elsewhere.[9,10] The wafers, grown at 750 °C on {100} GaAs substrates at a calibrated growth rate of $\sim 0.25\,\mu$m/min (or slower), consist of a ~ 1-μm-thick GaAs buffer layer to provide a good crystallographic surface for the succeeding layers, followed by a ~ 1-μm $Al_xGa_{1-x}As$ ($x \sim 0.36$) confining layer, then the QWH active region, and finally a second ~ 0.3-μm $Al_xGa_{1-x}As$ ($x \sim 0.36$) confining layer. All layers are *undoped* ($n_a - n_d \lesssim 10^{15}$ cm^{-3}).

Six different QWH active regions composed of thin-layer phonon-generating arrays coupled to larger GaAs quantum wells ($L_z \lesssim 500$ Å) or standard DH active layers (500 Å $\lesssim L_z \lesssim 2000$ Å) are employed. They are (i) a single $L_{z1} \sim 200$-Å GaAs well and seven $L_{z2} \sim 50$-Å GaAs wells with all of the wells coupled by seven ~50-Å-thick $Al_xGa_{1-x}As$ ($x \sim 0.32$) barriers [structure denoted as (1–7) 200 – 50 Å],[11] (ii) a structure identical to (i) with the exception that the thicker GaAs layer is changed to $L_{z1} \sim 500$ Å [(1–7) 500 – 50 Å], (iii) a structure identical to (i) with the exception that the largest GaAs well is increased in size to $L_{z1} \sim 1500$ Å [(1–7) 1500 – 50 Å], (iv) a structure similar to (i) with $L_{z1} \sim 160$ Å, $L_{z2} \sim 80$ Å and with ~80-Å-thick $Al_xGa_{1-x}As$ ($x \sim 0.32$) coupling barriers [(1–7) 160 – 80 Å], (v) a phonon-generating array of seven $L_{z2} \sim 50$-Å GaAs wells on either side of an $L_z \sim 500$-Å GaAs layer all of which are coupled by fourteen ~50-Å-thick

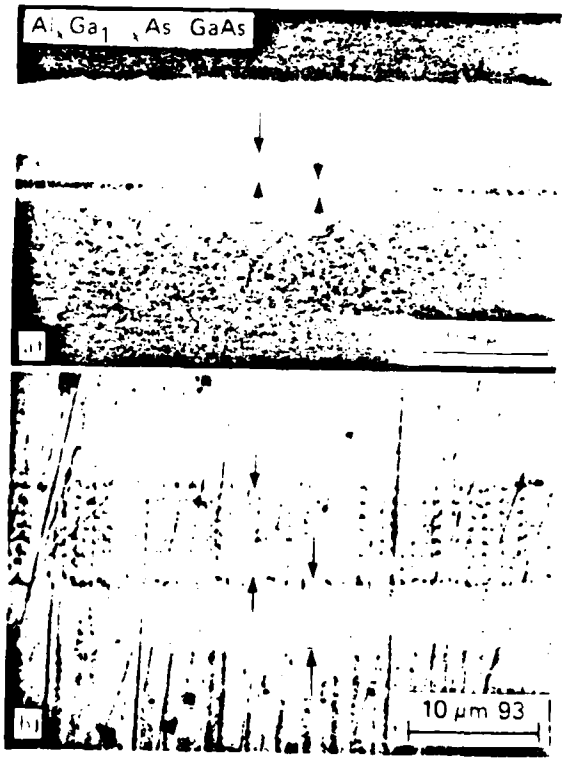

FIG. 2. Scanning-electron microscope photographs of a multiple-quantum-well heterostructure grown by MO-CVD with an active region consisting of seven 50-Å GaAs wells and one 500-Å GaAs well coupled by seven 50-Å $Al_xGa_{1-x}As$ ($x \simeq 0.32$) barriers. The cleaved and stained cross section a shows the 500-Å GaAs layer (right-hand arrows), the left-hand arrows indicate the array of seven 50-Å layers, which cannot be individually resolved. Photograph b) shows a shallow-angle beveled and stained cross section of the same QWH. The shallow-angle bevel and stain causes the layers to appear enlarged (by a factor of 93 for this cross section), allowing the array of seven 50-Å wells and seven 50-Å barriers to be resolved (left-hand arrows).

$Al_xGa_{1-x}As$ ($x \sim 0.32$) barriers [(7–1–7)50-500-50 Å], and (vi) two $L_{z1} \sim 120$-Å GaAs wells with one located on either side of an array of six $L_{z2} \sim 80$-Å GaAs wells with all of the GaAs layers coupled by seven ~ 80-Å-thick $Al_xGa_{1-x}As$ ($x \sim 0.32$) barrier layers [(1–6–1)120-80-120 Å]. In addition to the undoped wafers described above, four "degenerate" case multilayer structures in which all wells and barriers are the same thickness are used for comparison. These contain undoped active regions which include (a) six $L_z \sim 50$-Å GaAs wells coupled by five ~ 50-Å $Al_xGa_{1-x}As$ ($x \sim 0.30$) barriers [(5 + 6) 50 Å or simply (6) 50 Å],[12] (b) four $L_z \sim 80$-Å GaAs layers coupled by three ~ 80-Å $Al_xGa_{1-x}As$ ($x \sim 0.35$) barriers [(3 + 4) 80 Å or (4) 80 Å],[13] (c) six $L_z \sim 80$-Å-thick GaAs layers coupled by five ~ 80-Å $Al_xGa_{1-x}As$ ($x \sim 0.30$) barriers with one p-type and one n-type confining layer and a p-type GaAs contact layer to form a p-n junction QWH diode [(5 + 6) 80 Å or (6) 80 Å], and (d) six $L_z \sim 120$-Å GaAs wells coupled by five ~ 120-Å $Al_xGa_{1-x}As$ ($x \sim 0.27$) barriers [(5 + 6) 120 Å or (6) 120 Å].[14]

Layer thicknesses of the QWH samples are estimated by SEM microphotographs taken on cleaved cross sections or on bevel cross sections ($\sim 1°$ angle).[15] Both of these forms of measurement agree with the growth rate calibration on thicker layers and with sputter-Auger measurements.[16] The bevel angle, and thus also the magnification factor, is precisely determined using a SLOAN DEKTAK surface profilometer. Examples of a SEM microphotograph (a) on a cleaved and (b) on a beveled and stained cross section of the (1–7) 500-50 Å structure [ii] are shown in Fig. 2. Starting from the bottom of photomicrograph (a) is the ~ 1.0-μm $Al_xGa_{1-x}As$ ($x \sim 0.36$) confining layer. Next, between the right-hand pair of head-to-head arrows is the $L_{z1} \sim 500$-Å GaAs layer. This is then followed by the seven $L_{z2} \sim 50$-Å GaAs wells coupled by the ~ 50-Å-thick $Al_xGa_{1-x}As$ (~ 0.32) barriers, all of which are between the left-hand pair of head-to-head arrows. The individual ~ 50-Å-thick layers in (a) are not resolvable. Finally, the uppermost portion is the second ~ 0.3-μm $Al_xGa_{1-x}As$ ($x \sim 0.36$) confining layer. Note that the "large" GaAs layer is indeed ~ 500 Å thick, while the net thickness of the multilayer region is $(7 + 7) \times 50$ Å $= 700$ Å. The (b) part of Fig. 2 is a SEM photomicrograph of a beveled ($\sim 0.62°$, $\sim 93\times$ magnification) and stained portion of the same (1–7) 500-50-Å wafer as that of (a). Here the individual ~ 50-Å-thick layers, which comprise the multilayer phonon-generating array between the left-hand head-to-head arrows, are resolved as is also the ~ 500-Å (L_{z1}) GaAs layer between the right-hand head-to-head arrows. The apparent layer nonuniformity and unevenness are due to scratches inherent in the bevel technique and in no way imply poor crystal quality.[17]

In order to study small samples with large Fabry-Perot cavity end losses, and undoped samples to avoid the confusion of recombination radiation involving impurities, photopumping is used for sample excitation. The data presented here are obtained using an Ar^+ laser ($\lambda \sim 5145$ Å) which can be operated either cavity-dumped or cw. Sample preparation[18] consists of first mechanically polishing the wafer from the substrate side down to a thickness of ~ 50 μm and then selectively etching off[18] the remaining GaAs substrate and buffer layer. The resulting thin (~ 1.4-μm-thick) wafer is then cleaved into rectangular samples ~ 10–100 μm wide by ~ 100–300 μm long which are imbedded into In under a sapphire window for 77 K operation[19] or into annealed Cu under diamond for 300 K operation.[20] Typically, a circular spot of Ar^+ laser light comparable in diameter to the sample width is used to excite electron-hole pairs in the $Al_xGa_{1-x}As$ confining layers. Since $\alpha L_z \ll 1$, most of the carriers are generated in the confining layers. The carriers diffuse to the active region where they thermalize by emitting LO phonons and then recombine. The one (5 + 6) 80-Å structure that is grown sandwiched between n- and p-type confining layers has been both fabricated into simple stripe-geometry laser diodes and has been processed into a photoluminescence sample by selectively etching off the GaAs substrate and contact layers.

III. EXPERIMENTAL DATA

The emission spectra of a large quantum well ($L_{z1} \gtrsim 200$Å) coupled to an array of small wells ($L_{z2} \lesssim 80$ Å) dif-

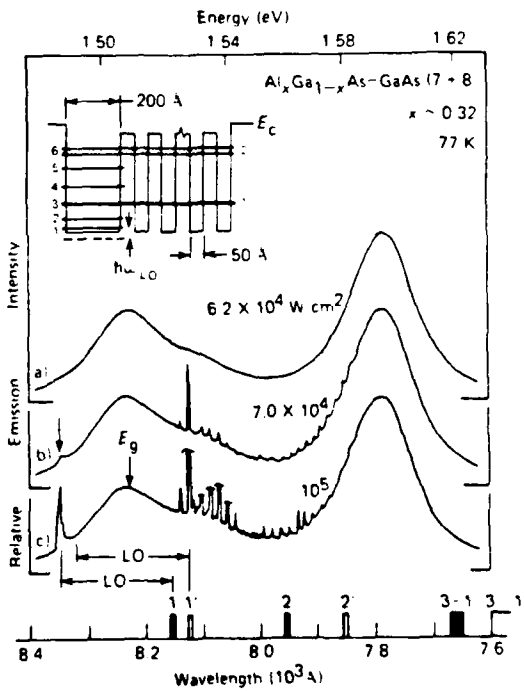

FIG. 3. Pulsed photoluminescence spectra (77 K) of a sample (55×488 μm^2) cleaved from a heterostructure similar to that shown in Fig. 2 but with a 200-Å GaAs layer in place of the 500-Å layer. A one-dimensional model of the conduction band and the allowed electron energy levels are indicated by the inset. The heavy and light bars on the horizontal axis mark the transition energies for electrons to recombine with heavy holes ($e \rightarrow hh$, n confined-particle transitions) or with light holes ($e \rightarrow lh$, n' confined-particle transitions) respectively. The spontaneous spectrum shows the emission just below lasing threshold [a], 6.2×10^4 W/cm^2]. At slightly higher excitation power [b], 7.0×10^4 W/cm^2] the main laser mode occurs on the $n' = 1'$ transition with the simultaneous occurrence of a small spectral bump at energy $\hbar\omega_{LO}$ below the $n = 1$ transition. At higher power [c], 10^5 W/cm^2] the small bump develops into a well-defined laser mode.

fer markedly from those of a single large well ($L_z \gtrsim 200$ Å), or from a degenerate multilayer structure ($L_z \lesssim 80$ Å) in which all the quantum wells are the same thickness. The proximity ($\lesssim 80$ Å) of a larger well to an array (see the inset of Fig. 3) is very important in the electronic and vibrational coupling of the two systems. Both electrons, which have a significant tunneling probability for an ~ 80-Å-thick ~ 400-meV rectangular barrier, and LO phonons, with a 100–500-Å mean free path, are likely to be shared in the whole system and affect the recombination and inelastic scattering processes. For example, LO phonons generated in the small-well arrays of these heterostructures influence the recombination in the larger layers.

Typical emission spectra (77 K) of a photopumped, rectangular sample from the (1–7) 200-50-Å wafer (i) are shown in Fig. 3. The form of the conduction-band edge in the vicinity of the active region is illustrated in the inset. The horizontal lines indicate the electron eigenenergies of this one-dimensional potential. These lines are sketched to correspond to the spatial extent of the wavefunctions. The numbers 1–6 on the left side of the lines and the 1 and 2 on the right side denote those states of the system which arise because of the $L_{z1} \sim 200$-Å-thick well and the $L_{z2} \sim 50$-Å multilayer, respectively. While this numbering scheme is not strictly correct for the complete coupled quantum system, it is very useful since some eigenfunctions are more localized in the $L_{z1} \sim 200$-Å well and others are more localized in the $L_{z2} \sim 50$-Å multilayer. Note that this localization should not restrict the motion of the electrons since the very-small-layer dimensions easily allow electron tunneling between the multilayer and the larger GaAs layer.

The (1–7) 200-50-Å sample, when pulse excited (6.2×10^4 W/cm^2) partially across its width, exhibits the high-level spontaneous emission spectrum, Fig. 3(a). Spontaneous emission peaks are observed at slightly lower energies than the first electron–to–heavy-hole $n = 1$ confined-carrier transitions of both the multilayer array and the larger quantum well. With an increase in pump power to 7×10^4 W/cm^2, Fig. 3(b), a laser mode appears abruptly near the first electron–to–light-hole $n' = 1'$ transition of the $L_{z1} \sim 200$-Å GaAs well, and *simultaneously* a small bump emerges $\sim \hbar\omega_{LO}$ lower in energy than the $n = 1$ $L_{z1} \sim 200$-Å confined-carrier transition. Upon further excitation [(c), 10^5 W/cm^2], this bump also lases although it is still much lower in intensity than the higher-energy confined-carrier stimulated emission. The location in energy and the unique manner of turn-on of the bump with the laser line are interpreted as evidence for stimulated phonon emission.

The emission spectrum (77 K) of a second sample from the (1–7) 200 – 50-Å wafer is shown in Fig. 4. At low-level cw excitation [curve (a), 250 W/cm^2] the spontaneous emission peaks at very nearly the same energies as the sample of Fig. 3. For pulsed excitation, however, laser operation is observed [curve (b), 5×10^4 W/cm^2] both on a phonon sideband of the lowest-confined-carrier transitions and also near the $n = 2$ transition of the $L_{z1} \sim 200$-Å well. Note that with this sample and excitation geometry the phonon-sideband laser modes can be made to dominate the emission spectrum as opposed to the relatively weak modes at that energy shown in Fig. 3. That this effect is primarily due to the excitation geometry can be seen by comparing the spectrum of Fig. 4 with that of Fig. 3(b) of Ref. 8. Both spectra are from the same cleaved sample (28×244 μm^2) and are excited to the same level (5×10^4 W/cm^2). However, the pump beam is at a slightly different location of the sample in the two cases, this results in the relative emission intensities of the phonon sideband and the higher-energy laser modes to be different.

As mentioned earlier, this type of emission spectrum, i.e., with stimulated emission occurring $\sim \hbar\omega_{LO}$ lower in energy than the lowest-confined-carrier transition, is not similar to that of a single ~ 200-Å-thick well. Depending on sample and pump beam geometry and also the excitation power, laser action has occurred over a very broad energy range in a single $L_z \sim 200$-Å QWH (see Fig. 10 of Ref. 6). However, it has not been observed as low in energy as $\sim \hbar\omega_{LO}$ below the lowest ($n = 1$, $n' = 1'$) confined-carrier transitions. A direct comparison of pulse-excited room-temperature laser operation of a single $L_z \sim 200$-Å QWH and the (1–7) 200-50-Å QWH (i) of Figs. 3 and 4 is shown in Fig. 5. At 2.8×10^4 W/cm^2 the single well structure, curve (a), exhibits considerable bandfilling[6,21] because of its very small active region thickness and relative inability to collect and thermalize hot electrons from the confining layers.[6,22] Upon coupling of a phonon-generating and reflecting array of smaller $L_{z2} \sim 50$-Å GaAs layers to a single $L_{z1} \sim 200$-Å-thick GaAs well, we observe [curve (b), 7×10^4 W/cm^2] that the carrier collection, thermalization, and bandfilling problems are drastically reduced. Most of the carriers are collected by and scatter to lower energy in the multilayer portion (64% of the GaAs

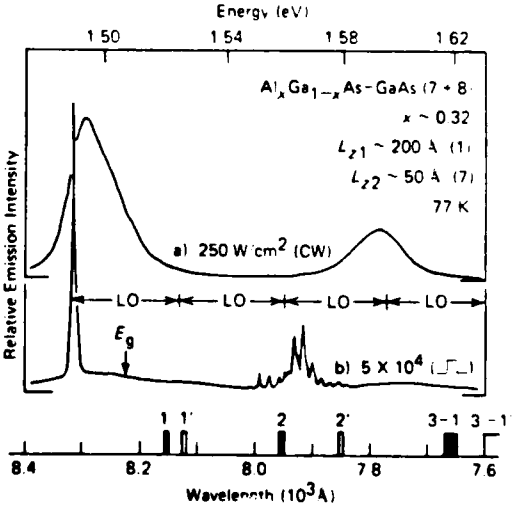

FIG. 4. Spectra (77 K) of a photopumped sample (28×244 μm^2) cleaved from the same wafer as that of Fig. 3. Low-level cw excitation [a), 250 W/cm^2] produces a peak at energy $\hbar\omega_{LO}$ below the $n' = 1'$ transitions of the 200-Å well and another peak ($\lambda \sim 7800$ Å) approximately an LO-phonon below the $n' = 1'$ transitions of the 50-Å wells. (The $n = 1$ transitions of the 50-Å well are degenerate with the $n = 3$ transition of the 200-Å well, see inset of Fig. 3.) Pulsed excitation [b), 5×10^4 W/cm^2] results in laser operation an LO phonon below the $n = 1$ transitions of the 200-Å well. Smaller laser modes also appear near the $n = 2$ transitions of the 200-Å well.

in the active region is in the multilayer array) of the heterostructure. In the process, LO phonons are emitted and carriers either recombine or scatter to still lower energy in the larger well and recombine. For the samples of Figs. 3, 4, and 5(b) (7×10^4 W/cm^2), a sizable portion of the carriers scatter to the lowest-energy confined-carrier states before recombining radiatively, including at energy $\hbar\omega_{LO}$ below the $n = 1$ or 1′ transitions. Although other excitation geometries modify the emission spectra of a (1–7) 200-50-Å QWH, these data demonstrate that this design of the active region enables recombination to be observed at lower energies than for the case of a single $L_z \sim 200$-Å-thick well, or even an $L_z \sim 50$-Å multilayer array, and that LO-phonon effects therefore play a considerable role in the operation of this form of QWH.

A further interesting feature of the (1–7) 200-50-Å QWH is the presence of emission and laser modes in the range between the lowest-energy confined-carrier transitions of the system and the phonon sidebands. This is demonstrated clearly in the 77 K photoluminescence spectra of Fig. 6. As with the spontaneous emission data of Figs. 3, curve (a), and 4, curve (a), the CW emission at low level [Fig. 6 curve (a), 10 W/cm^2] of this wafer peaks at slightly lower energies than the $n = 1$ confined-carrier transitions of the $L_{z1} \sim 200$-Å well. In addition, in the case of this sample a shoulder in the emission is observed ~ 20 meV lower in energy than the $n = 1$ transition of the $L_{z1} \sim 200$-Å well. At

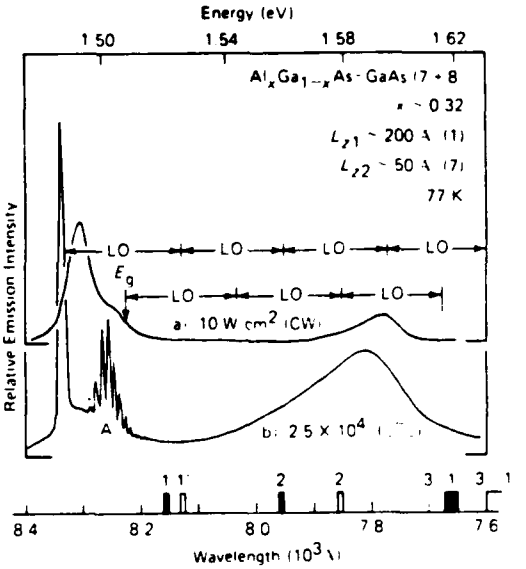

FIG. 6. Photoemission (77 K) of a sample ($94 \times 234\ \mu m^2$) cleaved from the same wafer described in Fig. 3. Besides the low-level (250 W/cm^2) spontaneous peaks of Fig. 4, the low-level spectrum a) (10 W/cm^2) exhibits a shoulder approximately 20 meV below the $n = 1$ transition, corresponding to the expected binding energy of a two-dimensional exciton in GaAs. At higher power [b), 2.5×10^4 W/cm^2] a well-defined group of laser modes labeled A, 20 meV below the $n = 1$ marker, appears as well as laser operation one phonon below the $n' = 1'$ transition.

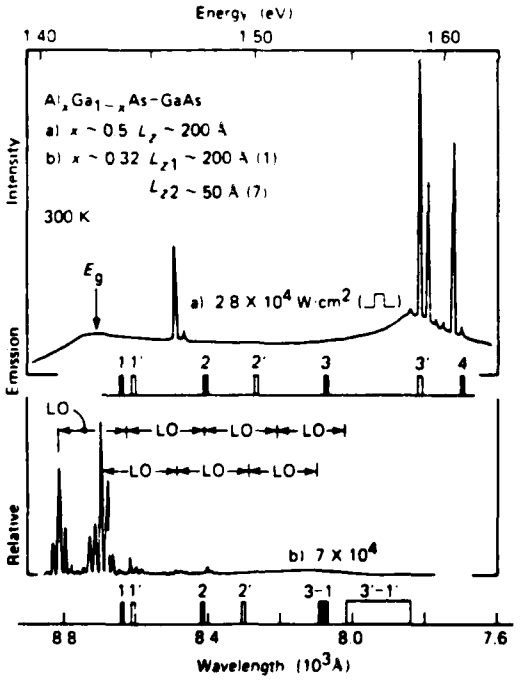

FIG. 5. Comparison of the pulsed photoemission (300 K) of a rectangular sample ($47 \times 234\ \mu m^2$) cleaved from a single 200-Å QWH with a rectangular sample ($62 \times 226\ \mu m^2$) cleaved from the same QWH wafer as the samples of Figs. 3 and 4. The high energy emission a) of a single 200-Å QWH (2.8×10^4 W/cm^2) is cut off by the 7-well ($L_{z2} \sim 50$ Å) array of b) (7×10^4 W/cm^2).

higher pulsed photoexcitation [curve (c), 2.5×10^4 W/cm^2], *laser operation* is observed both on a phonon-sideband of the $n' = 1'$ transition and also ~ 20 meV below the $n = 1$ transition, labeled A. The location of A is in excellent agreement with the energy expected of a two-dimensional exciton involving a heavy hole.

The binding energy of a two-dimensional exciton is $4\times$ larger than for the three-dimensional limit.[23,24] This results in two-dimensional-exciton binding energies of ~ 20 meV for the electron–heavy-hole exciton and ~ 13 meV for the electron–light-hole exciton.[25] The $4\times$ increase over the three-dimensional case is expected in the limit of two-dimensional confinement and will be reduced to $1\times$ as the layer thickness is increased to the bulk limit. For layer thicknesses less than the bulk-exciton diameter (~ 240 Å *e-hh*, ~ 340 Å *e-lh*), the factor of $4\times$ continues to agree well with photoluminescence data; this is in contrast to earlier absorption measurements (on crystals grown by MBE) that indicate an enhancement of only $\sim 2\times$ in the exciton binding energy for $L_z < 100$ Å.[26] The data of Fig. 6 and other low-level cw and laser data[25] on rectangular cleaved samples indicate that the two-dimensional exciton can be involved in recombination in these quantum-well heterostructures.

In order to determine how closely the low-energy phonon-sideband laser modes observed in the data from the (1–7) 200-50-Å QWH (Figs. 3–6) are related to the confined-carrier transitions, a number of samples with a thicker GaAs layer substituted in place of the "large" $L_{z1} \sim 200$-Å well have been employed. As the layer size L_{z1} is increased, the

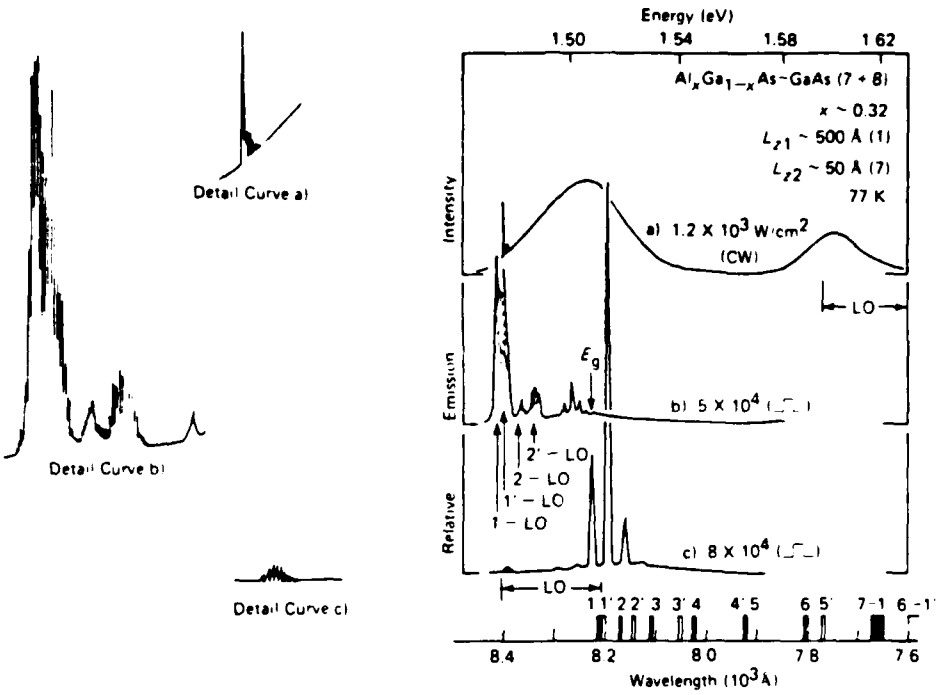

FIG. 7. Induced phonon-assisted recombination (77 K) of the QWH shown in the cross section of Fig. 2 cw emission from a photopumped rectangular sample ($59 \times 254\ \mu m^2$) peaks near the $n' = 1'$ transitions of the 50-Å wells ($\lambda \sim 7800$ Å) and slightly below the $n = 1$ transition of the the 500 Å well [(a), 1.2×10^3 W/cm^2]. At higher excitation [(b), 5×10^4 W/cm^2] laser operation occurs *one phonon* (ω_{LO}) below the confined-particle transitions 1, 1', 2, 2', 3, and 3'. A narrower sample ($23 \times 211\ \mu m^2$) lases across the sample on the lowest transitions [(c), 8×10^4 W/cm^2] with some end-to-end closely spaced modes apparent one phonon below the $n' = 1'$ transition.

behavior of the larger well shifts more toward bulk GaAs; the confined-carrier states then become very closely spaced and the $n = 1$ transition is very nearly degenerate with E_g. The uncertainty in assigning an edge or origin for phonon-sideband laser operation is thus greatly decreased. This is the case for $L_{z1} \sim 500$ Å.

An example of the emission spectra (77 K) of the (1–7) 500-50-Å QWH sample (ii) is shown in Fig. 7. The cw spectrum [curve (a), 1.2×10^3 W/cm^2] exhibits laser operation on a phonon sideband of the $n' = 1'$ transition of the 500-Å quantum well. Spontaneous emission peaks as seen in Figs. 3, 5, and 6 are also observed. At a pulsed excitation of 5×10^4 W/cm^2, curve (b), the same sample lases strongly in the range of the phonon sidebands of the $n = 1$, 1', 2, 2', 3, and 3' transitions of the $L_{z1} \sim 500$-Å layer. A narrower sample [curve (c), 8×10^4 W/cm^2], with higher cavity losses, is used to force laser operation up in energy to the lowest confined-carrier transitions to enable their identification.

A design modification on the (1–7) 500-50-Å QWH is achieved by introducing a second phonon-generating and -reflecting array of seven $L_{z2} \sim 50$-Å quantum wells on the other side of the $L_{z1} \sim 500$-Å-thick GaAs layer. The result is a (7–1–7) 50-500-50-Å structure in which $\sim 58\%$ of the GaAs in the active region is in the small-well array portion. Any reflection of LO phonons by the twin 50 Å-well arrays should tend to localize the LO phonons in the vicinity of the $L_{z1} \sim 500$-Å-thicker layer and strongly affect the recombination radiation spectrum. Typical pulsed room-temperature photoluminescence spectra are shown in Fig. 8. The bars numbered 1–5 are the locations of the five lowest-energy electron-to-heavy-hole transitions of the 500-Å quantum well. At 10^4 W/cm^2, curve a), laser threshold occurs $\sim \hbar\omega_{LO}$ lower in energy than the $n = 1$ transition. Slight ringing is also observed in the energy range of the $n = 2$ transition. An increase in excitation level to 2×10^4 W/cm^2, curve b), results in intense laser operation on the phonon sideband of the lowest confined-particle transitions and also weaker laser modes between the $n = 1$ and $n = 4$ transitions. Note that the data of Figs. 7 and 8 exhibit laser operation $\sim \hbar\omega_{LO}$ lower in energy than the lowest-energy laser emission expected due to band-to-band recombination in bulk, undoped GaAs. This emission occurs at a transition energy in which no states exist in these structures. As mentioned earlier, both of these samples are undoped ($n_d - n_a \lesssim 10^{15}$ cm^{-3}). Therefore this laser operation is not impurity related, since $\gtrsim 10^{17}$ cm^{-3} impurities are necessary for GaAs to lase on a band-to-impurity transition.[27] The emission spectra of Figs. 7 and 8 establish that phonon-sideband laser operation can be achieved in a GaAs laser of nearly bulk dimensions (~ 500 Å) that is sandwiched between $Al_xGa_{1-x}As$ confining layers.

Further increase in the size of the larger GaAs well in these coupled array heterostructures begins to decrease the effectiveness of the laser operation of the larger layer. For these heterostructures (inset of Fig. 3), as the single larger well (L_{z1}) is increased in size from 200 to 500 to 1500 Å, the GaAs fraction in the active region represented by the $L_{z2} \sim 50$-Å seven-well array decreases from 0.64 to 0.41 to 0.19. Assuming that this is roughly the percent of injected electrons that thermalize in the small-well array section, we expect the number of LO phonons generated by the seven well $L_{z2} \sim 50$-Å array to decrease rapidly with increasing L_{z1}. Note that the fraction of electrons that recombine in the array is expected to be even less than the above estimate since carriers can tunnel into the larger GaAs layer and scatter to

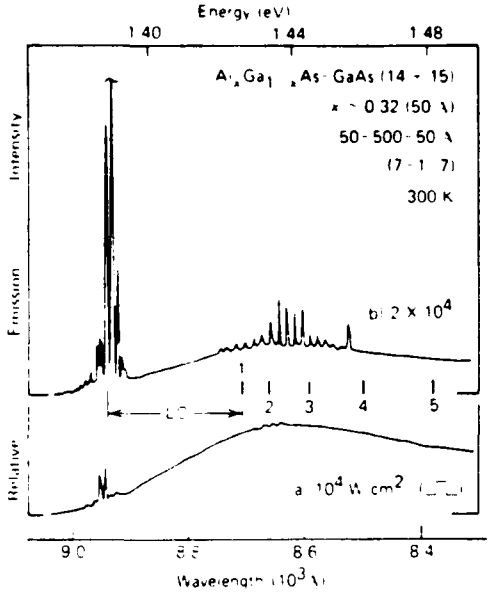

FIG. 8. Pulsed room-temperature laser operation of a rectangular (68 × 234 μm^2) QWH sample with an active region consisting of a 500-Å GaAs well sandwiched between two arrays of seven 50-Å GaAs wells all of which are coupled by 50-Å $Al_xGa_{1-x}As$ ($x \simeq 0.32$) barriers. At 10^4 W/cm^2 all spontaneous emission is peaked in the range of the lowest transitions of the 500-Å well ($n = 1$-4) with laser modes developing one phonon below the $n = 1$ transition located almost at E_g. At 2×10^4 W/cm^2, b) the laser operation is well developed one phonon below the $n = 1$ transition (or E_g), and weaker laser emission is observed between the $n = 1$ and $n = 4$ transitions of the 500-Å well.

still lower energy before recombining. Therefore, in spite of the fact that the small-well array contributes some recombination radiation, which can serve as a reference, this radiation is relatively weak and has little effect on the lasing behavior of the larger GaAs layer for $L_{z1} < 500$ Å.

Pulsed room-temperature laser operation of the (1–7) 1500-50-Å QWH sample (iii) is shown in Fig. 9. Since the single $L_{z1} \sim 1500$-Å-GaAs layer (coupled to the L_{z2} 50-Å array) is definitely in the bulk limit, only the GaAs energy gap E_g is used as a reference for emission originating in the thick layer. The 1 and 1′ bars near 8000 Å in Fig. 9 denote the energies of the first electron–to–light- and –to–heavy-hole transitions for carriers localized in the $L_{z2} \sim 50$ Å seven-well multilayer. One interesting feature of the data in Fig. 9 is the relatively weak spontaneous emission peak located $\sim \hbar\omega_{LO}$ lower in energy than the $L_{z2} \sim 50$-Å multilayer transitions $n = 1$ and $n' = 1'$. This emission is weak because of the small fraction (0.19) of the active region GaAs that is contributed by the 50-Å array. The most important feature of this sample is that it too lases at energies below E_g, as far below as $\sim \hbar\omega_{LO}$. At 77 K this heterostructure lases[28] at E_g and also exhibits the higher-energy spontaneous reference peak of Fig. 9. This peak, however, is not shifted below the $L_{z2} \sim 50$-Å $n = 1$ transition as it is at 300 K, but rather occurs very nearly on the $n = 1$ transition. That both the multilayer array and the larger-layer emission shift down in energy relative to their band-to-band transitions as the lattice temperature is increased indicates that the thermal LO-phonon occupation number is increased enough to cause both transitions to operate on phonon sidebands. A further experiment on a DH wafer with $L_z \sim 600$ Å (all layers undoped, $n_d - n_a \lesssim 10^{15}$ cm^{-3}) has exhibited a similar temperture dependence.[28] Therefore laser operation at $\hbar\omega \sim E_g - \hbar\omega_{LO}$ in a DH is considered as originating in phonon-assisted recombination. The thermal phonons present due to the lattice temperature (300 K) plus the nonthermal LO phonons generated during carrier relaxation are sufficient to produce phonon-sideband laser operation at the high injection levels characteristic of DH laser operation.

While the data of Fig. 9 indicate that phonon-sideband laser operation can be induced by changing the thermal LO-phonon occupation number, the spectra of Fig. 10 demonstrate that a similar result can be achieved by increasing the nonthermal phonon occupation number. The cw room-temperature laser spectra of Fig. 10 have both been obtained on samples from an $L_z \sim 80$–Å six-well, five-barrier ($x \sim 0.30$) QWH. This undoped multiple quantum-well active region (n_d-$n_a \lesssim 10^{15}$ cm^{-3}) is imbedded in an $Al_xGa_{1-x}As$ ($x \sim 0.4$) p-n junction. The (a) spectrum is from a portion of the wafer processed into simple stripe geometry diodes. In contrast, the (b) spectrum is from a smaller portion of the wafer from which both the n-type GaAs substrate and also the $p+$ GaAs contact layers have been removed. Note that the diode, 10(a), operates on the phonon-sideband of the $n' = 1'$ transition, while the photoexcited sample operates at

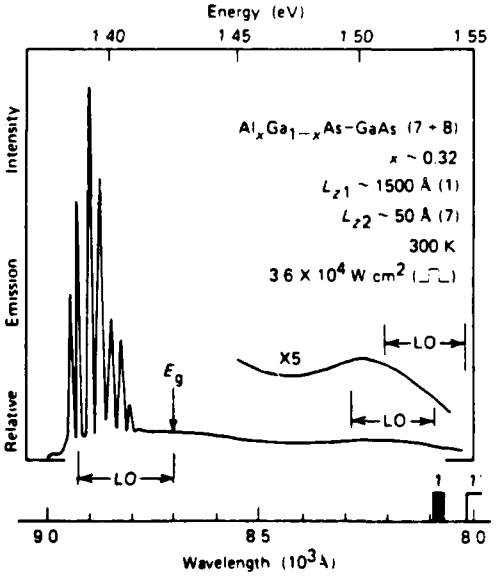

FIG. 9. Pulsed room-temperature photoemission (3.6×10^4 W/cm^2) of a sample (43×94 μm^2) whose active region consists of a 1500-Å layer of GaAs (bulk dimensions) coupled to an array of seven 50-Å GaAs wells. The coupling barriers are 50-Å $Al_xGa_{1-x}As$ ($x \simeq 0.32$). A reference spontaneous spectral bump occurs between the 1-LO and 1′-LO transitions of the 50-Å array, and the sample lases in the range $\hbar\omega_{LO}$ below the energy gap of bulk material, indicating (from the 50-Å-array reference) that phonon-assisted recombination contributes to emission in heterostructures with layers as thick as 1500 Å.

much lower energy, $\sim 2x\hbar\omega_{LO}$ below the $n = 1$ transition. The important difference between the diode and the photoluminescence sample, other than the method of excitation, is the optical cavity size. The diode is 223 μm long, while the photoexcited sample is 22 μm in width and has nearly ten times larger cavity end loss than the diode. Two factors enter into the laser operation of very narrow samples: (1) bandfilling tends to increase the lasing energy, and (2) the increased density of electron-hole-pairs necessary to attain laser threshold gives rise to an increase in the nonthermal LO phonon occupation number and increases the probability of phonon-asssisted laser operation, thus decreasing the lasing energy. In order to achieve laser threshold [10(a), $\sim 2.4\times10^3$ A/cm^2; 10(b), $\sim 7.9\times10^3$ A/cm^2 equivalent current density], the narrow photoexcited sample must be driven to more than three times the power density necessary for laser operation of the diode. Therefore in this sample the larger nonthermal phonon occupation number made possible by the higher laser threshold density induces lower-energy phonon-assisted laser operation.

While the data of Figs. 3–10 have focused on the *laser* behavior of QWH's, the low-level spontaneous emission spectra of these samples also provide insight into the QWH behavior. Typical 77 K spontaneous emission spectra for six

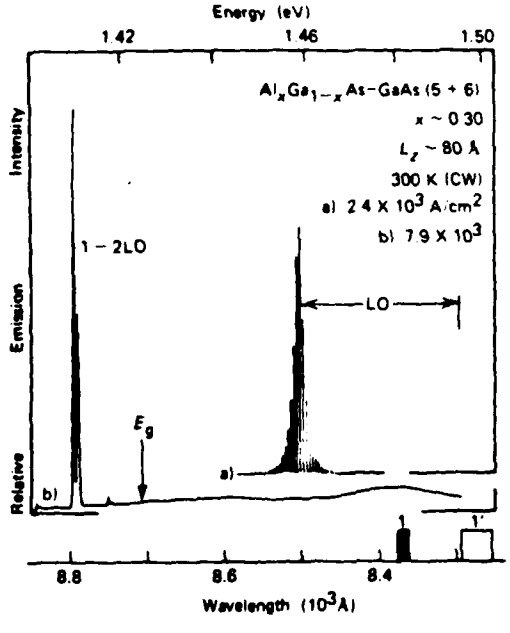

FIG. 10. Comparison of cw room-temperature laser operation of a diode and a photoexcited sample from the same QWH material. The active region consisting of six 80-Å GaAs quantum wells separated by five 80-Å $Al_xGa_{1-x}As$ ($x \simeq 0.30$) barriers is undoped ($n_a - n_d < 10^{15}$ cm^{-3}) and is sandwiched between an n- and p-type confining layer of $Al_xGa_{1-x}As$ ($x \simeq 0.40$). The diode [a), 2.4×10^3 A/cm^2] lases $\hbar\omega_{LO}$ below the $n' = 1'$ transition, while the photopumped sample [b), 7.9×10^3 A/cm^2], with the substrate and contact layers removed, lases at energy $2\hbar\omega_{LO}$ below the $n = 1$ transition (1–2LO transition). Note also the spontaneous bump near the $n = 1$ transition on the photopumped emission spectrum.

various QWH's are shown in Fig. 11. Curves (a), (b), and (c) are from the quantum-well structures consisting of a large GaAs quantum well [or wells as in (c)] coupled to a phonon-generating and -reflecting array of thinner GaAs layers. The remaining three spectra are from degenerate-case structures of uniform layer thickness [curve (d), six wells + five barriers, $L_z \sim 120$ Å; curve (e) four wells + three barriers, $L_z \sim 80$ Å; curve (f), six wells + five barriers, $L_z \sim 50$ Å] and serve as comparisons for the emission from the first three QWH's. The confined-carrier transitions are labeled for each spectrum, as are phonon spacings, and the two-dimensional exciton transitions relative to $n = 1$ (A) and to $n' = 1'$ (B).

A noticeable feature of these spectra is that the samples containing GaAs layers of different sizes (L_{z1} and L_{z2}) exhibit two emission peaks, one related to each well size, while the degenerate case samples [curves (d), (e), (f)] each have one dominant peak. Only in the case of the six-well (6) 50-Å degenerate structure, curve (f) is the spontaneous peak lower ($2x\hbar\omega_{LO}$) in energy than the lowest confined-carrier transition ($\lambda \sim 7600$ Å). This behavior is possibly due to the better phonon confinement that is believed to exist in a 50-Å-layer QWH as discussed below. It is interesting to compare this emission [(f), six-well, $L_z \sim 50$ Å] with that of the (1–7) 200-50-Å structure, curve (a), which also contains a 50-Å multilayer array. Note that the spontaneous emission from the multilayer array portion of curve (a), $\lambda \sim 7800$ Å, is not as low in energy as that from the degenerate case curve (f), $\lambda \sim 8000$ Å, indicating that the carriers in the (1–7) structure are more likely to scatter to the 200 Å well than recombine on a sideband $2x\hbar\omega_{LO}$ lower in energy than the 50-Å $n = 1$ transitions.

An important feature of these spectra is that the existence of two peaks in the (1–7) and (1–6–1) QWH's are likely (because of spectral broadening) to lead to relatively inefficient laser operation of these structures. The broadening of the emission into two peaks is due to the spatial separation of the electron-hole pairs in the QWH (in L_{z1} and in nL_{z2}). This broadened emission implies both a spatial and an energetic line broadening (an inhomogeneous line). As the L_{z1} and L_{z2} GaAs layer sizes are chosen to approach the same thickness [(a) to (b) to (c)], the broadening in the emission is decreased until finally the degenerate case [($L_{z1} = L_{z2} = L_z$; (d), (e), and (f)] results. Thus while the case of nondegenerate structures can be designed to demonstrate LO-phonon effects and are interesting light emitters, their usefulness as efficient lasers is questionable because the emission linewidth is artificially broadened.

IV. DISCUSSION

A complete theoretical description of the effects described above is difficult for several reasons. For example, not much is known about the mean free path of phonons under the condition of high excitation,[29] or about multiphonon emission, or in general about indirect optical transitions in a direct semiconductor. Usually it is agreed that indirect transitions, i.e., transitions involving phonons and photons, are negligible in direct materials if the electron-phonon coupling constant is small as it is in GaAs.[30] This

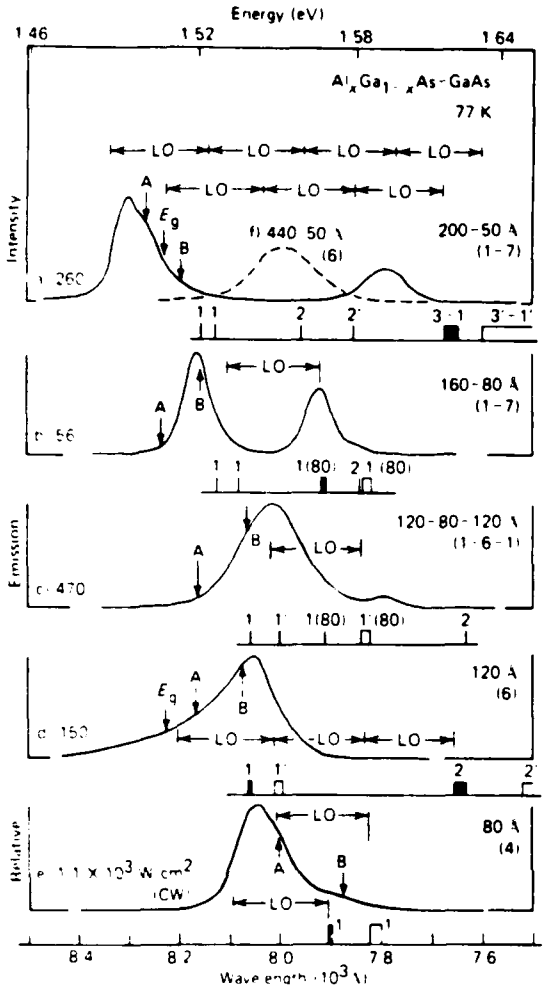

FIG. 11. Photopumped spontaneous emission spectra (cw, 77 K) of six different multiple-quantum-well heterostructures. The arrows marked A are located 20 meV below the $n = 1$ electron–to–heavy-hole transitions, corresponding to the estimated binding energy of a two-dimensional electron–heavy-hole exciton. Similarly, the arrows marked B are located 13 meV below the $n = 1$ electron–to–light-hole transitions, corresponding to the estimated binding energy of a two-dimensional electron–light-hole exciton. The confined-particle-transition markers for each heterostructure are located beneath each spectrum, the active-layer structure is designated to the right of each spectrum. For example, spectrum a) (260 W/cm^2) is from a heterostructure with an active region consisting of one 200-Å GaAs well and seven 50-Å GaAs wells, all of which are coupled by 50-Å $Al_xGa_{1-x}As$ barriers.

argument does not hold for high excitation levels since the average phonon occupation number which appears in the matrix elements for indirect transitions increases rapidly, resulting in a high "effective" electron-phonon interaction.

This should be generally true and the effect should give important contributions to the optical constants under high excitation conditions, for example, as encountered in the parallel case of laser annealing. Before describing our choice of sample geometries to enhance the phonon effects, we would like to emphasize that previous studies have shown that size-quantization effects tend to favor a nonthermal phonon occupation. This occurs because of the two-dimensional density of states,[2] a slight increase in the electron-phonon coupling constant,[7] and the high-power densities "compressed" into a relatively small volume[2,6,28] (the QWH active region). Below we describe the criteria that have guided the choice of the sample geometry.

In spite of the fact that not much is known about phonon-phonon interactions, the phonon mean free path at high excitation levels, and the direction of maximum emission intensity, we assume that layers with dimensions of a multiple of the phonon wavelength at the maximum phonon intensity would reflect and confine most. The wavelength of maximum intensity of phonons emitted perpendicular to the layers can be determined in the following way: Previous calculations[8] show that the emission probability for phonons (perpendicular to the layers) is a monotonically decreasing function of q if free-carrier screening is not taken into account. A two-dimensional analysis shows that all wavelengths longer than $2a_B^* \simeq 160$ Å are effectively screened, where a_B^* is the effective Bohr radius. Therefore we expect a maximum in the phonon intensity at wavelengths near $2a_B^*$. The emission probability parallel to the layers (again for quasi-two-dimensional electrons) shows two distinct peaks.[8] The peak at the longer wavelength is again almost certainly screened. The peak at the shorter wavelength occurs as given in Ref. 8 at

$$q = 2.52\times10^{-6}\,m^{1/2}[1+(1-1/m)^{1/2}]\,\mathrm{cm}^{-1}. \quad (1)$$

Here we have used the material constants of GaAs. The integer m corresponds to the energy $m\hbar\omega_{LO}$ above the bottom of the quantum-well subband from where the electron cascades downward in thermalizing. Using the above expression, we obtain as a typical wavelength and thus layer or well size the values shown in Table I. These values have been used as guidelines in the choice of sample dimensions.

V. CONCLUSIONS

A series of experiments have been described above to determine the extent of LO-phonon contribution to metalorganic chemical vapor deposited $Al_xGa_{1-x}As$-GaAs quantum-well-heterostructure (QWH) laser operation. The undoped photoluminescence structures studied have active regions consisting of a large GaAs quantum well (L_{z1}), or in some cases a bulk layer ($L_{z1} > 500$ Å), coupled to a small-well (L_{z2}) multilayer array. Phonons generated during carrier

TABLE I. Phonon wavelengths at which the emission probability parallel to QWH layers exhibits a short wavelength peak (Eq. 1). (Owing to screening, longer wavelength peaks are not included. The $m = 1$ $\lambda \sim 250$-Å phonon is also expected to be screened while the rest are not.)

m	$\lambda = 2\pi/q$ (Å)
1	250
2	103
3	79
4	67
5	58
6	53
7	49
8	45
9	42
10	40

thermalization in the multilayer array have been shown to induce phonon-sideband laser operation of the larger GaAs layer. In undoped structures with the large-well dimension $L_{z1} \sim 500$Å, the phonon-sideband emission is in the range $\hbar\omega \sim E_g - \hbar\omega_{LO}$; that is, the emission is $\sim \hbar\omega_{LO}$ lower in energy than the lowest transition allowed in bulk (undoped) GaAs. Phonon-sideband laser operation has been shown to be induced by an increase in either the thermal or the nonthermal LO-phonon occupation number. In fact, the increase in the thermal phonon occupation number at 300 K over that at 77 K has been shown to result in phonon-sideband laser operation of a bulk GaAs active layer in the size range of standard double heterojunctions ($L_{z1} \sim 1500$ Å). While these heterostructures, which contain a large quantum well coupled to a thin multilayer array, are useful in understanding phonon-sideband laser operation, they are not likely to be the most efficient lasers because of the artificially created line broadening resulting from two different quantum-well sizes. The MO-CVD QWH wafers used in this work have been designed to optimize the auxiliary phonon-generating and -reflecting arrays coupled to the larger GaAs quantum-well active layers. The optimization has been accomplished by choosing the array layer size equal to the wavelengths of the phonons with maximum emission probability.

ACKNOWLEDGMENTS

The authors are grateful to Yuri S. Moroz, R.T. Gladin, B. L. Marshall, and B. L. Payne (Urbana) for technical assistance, and to G. E. Stillman for helpful discussions. The work of the Illinois group has been supported by NSF Grants DMR 79-09991 and DMR-77-23999 and Navy Contract N00014-79–C-0768; the work of the Rockwell group has been partially supported by the Office of Naval Research, Contract N00014-78-C-0711.

[1] N Holonyak, Jr., R. M. Kolbas, W. D. Laidig, M. Altarelli, R. D. Dupuis, and P. D. Dapkus, Appl. Phys. Lett. **36**, 502 (1979).
[2] N. Holonyak, Jr., R. M. Kolbas, W. D. Laidig, B. A. Vojak, K. Hess, R. D. Dupuis, and P. D. Dapkus, J. Appl. Phys. **51**, 1328 (1980).
[3] E. A. Rezek, R. Chin, N. Holonyak, Jr., S. W. Kirchoefer, and R. M. Kolbas, Appl. Phys. Lett. **35**, 45 (1979).
[4] E. A. Rezek, R. Chin, N. Holonyak, Jr., S. W. Kirchoefer, and R. M. Kolbas, J. Electron. Mater. **9**, 1 (1980).
[5] R. Chin, N. Holonyak, Jr., and B. A. Vojak, J. Appl. Phys. **51**, 4017 (1980).
[6] N. Holonyak, Jr., R. M. Kolbas, R. D. Dupuis, and P. D. Dapkus, IEEE J. Quantum Electron. **QE-16**, 170 (1980).
[7] K. Hess, Appl. Phys. Lett. **35**, 484 (1979).
[8] K. Hess, N. Holonyak, Jr., W. D. Laidig, B. A. Vojak, J. J. Coleman, and P. D. Dapkus, Solid State Commun. **34**, 749 (1980).
[9] H. Manasevit, J. Electrochem. Soc. **118**, 647 (1971).
[10] R. D. Dupuis and P. D. Dapkus, *Seventh International Symposium on GaAs and Related Compounds, St. Louis*, 1978, edited by C. M. Wolfe (Institute of Physics, London, 1979), pp. 1–9.
[11] J. J. Coleman, P. D. Dapkus, B. A. Vojak, W. D. Laidig, N. Holonyak, Jr., and K. Hess, Appl. Phys. Lett. **37**, 15 (1980).
[12] R. M. Kolbas, N. Holonyak, Jr., B. A. Vojak, K. Hess, M. Altarelli, R. D. Dupuis, and P. D. Dapkus, Solid State Commun. **31**, 1033 (1979).
[13] N. Holonyak, Jr., R. M. Kolbas, W. D. Laidig, B. A. Vojak, R. D. Dupuis, and P. D. Dapkus, Appl. Phys. Lett. **33**, 737 (1978).
[14] B. A. Vojak, N. Holonyak, Jr., R. Chin, E. A. Rezek, R. D. Dupuis, and P. D. Dapkus, J. Appl. Phys. **50**, 5835 (1979).
[15] N. Holonyak, Jr., B. A. Vojak, R. M. Kolbas, R. D. Dupuis, and P. D. Dapkus, Solid State Electron. **22**, 431 (1979).
[16] R. D. Dupuis, P. D. Dapkus, C. M. Garner, C. Y. Su, and W. E. Spicer, Appl. Phys. Lett. **34**, 335 (1979).
[17] E. A. Rezek, N. Holonyak, Jr., B. A. Vojak, and H. Shichijo, J. Appl. Phys. **49**, 69 (1978).
[18] R. A. Logan and F. K. Reinhart, J. Appl. Phys. **44**, 4172 (1973).
[19] N. Holonyak, Jr. and D. R. Scifres, Rev. Sci. Instrum. **42**, 1885 (1971).
[20] N. Holonyak, Jr., R. M. Kolbas, R. D. Dupuis, and P. D. Dapkus, Appl. Phys. Lett. **33**, 73 (1978).
[21] N. Holonyak, Jr., R. M. Kolbas, E. A. Rezek, R. Chin, R. D. Dupuis, and P. D. Dapkus, J. Appl. Phys. **49**, 5392 (1978).
[22] H. Shichijo, R. M. Kolbas, N. Holonyak, Jr., R. D. Dupuis, and P. D. Dapkus, Solid State Commun. **27**, 1029 (1978).
[23] A. Shinada and S. Sugano, J. Phys. Soc. Jp. **21**, 1936 (1966).
[24] A. M. Kazaryan and E. M. Kazaryan, Fiz. Tekh. Poluprov. **11**, 1383 (1977) [Sov. Phys. Semicond. **11**, 813 (1977)].
[25] B. A. Vojak, N. Holonyak, Jr., W. D. Laidig, K. Hess, J. J. Coleman, and P. D. Dapkus, Solid State Commun. **35**, 477 (1980).
[26] R. Dingle, in *Festkorperprobleme, Advances in Solid State Physcis*, Vol. XV, edited by H. J. Queisser (Pergamon/Vieweg, Braunschweig, 1975), pp. 21–48.
[27] J. A. Rossi, N. Holonyak, Jr., P. D. Dapkus, J. B. McNeely, and F. V. Williams, Appl. Phys. Lett. **15**, 109 (1969).
[28] N. Holonyak, Jr., B. A. Vojak, W. D. Laidig, K. Hess, J. J. Coleman, and P. D. Dapkus, Appl. Phys. Lett. **37**, 136 (1980).
[29] J. Shah, Solid State Electron. **31**, 43 (1978).
[30] H. B. Bebb and E. W. Williams, in *Semiconductors and Semimetals* edited by R. K. Willardson and A. C. Beer (Academic Pr., New York, 1972), Vol. 8, pp. 321-392.

Solid State Communications, Vol. 38, pp. 301–304.
Pergamon Press Ltd. 1981. Printed in Great Britain.

0038–1098/81/160301–04$02.00/0

QUENCHING OF STIMULATED PHONON EMISSION IN $Al_xGa_{1-x}As$–GaAs QUANTUM-WELL HETEROSTRUCTURES

W.D. Laidig, N. Holonyak, Jr., M.D. Camras and B.A. Vojak

Department of Electrical Engineering and Materials Research Laboratory, University of Illinois at Urbana-Champaign, Urbana, IL 61801, U.S.A.

K. Hess

Department of Electrical Engineering and Coordinated Science Laboratory, University of Illinois at Urbana-Champaign, Urbana, IL 61801, U.S.A.

and

J.J. Coleman and P.D. Dapkus

Rockwell International, Electronics Research Center, Anaheim, CA 92803, U.S.A.

(*Received* 3 *November* 1980 *by J. Tauc*)

Data are presented on MO–CVD $Al_xGa_{1-x}As$–GaAs multiple quantum-well heterostructures (QWH's) consisting of a large GaAs well (500 Å) coupled to one or two arrays of smaller wells (50 Å) that act, when photopumped, as phonon sources and resonators. These data show that the induced phonon-sideband laser operation of the larger well is quenched when the phonon-generating array, but not the larger well, is destroyed by thermal annealing. An estimate of the electron–phonon coupling coefficient for indirect optical transitions is presented, indicating enhanced coupling with increased phonon density and establishing a basis for *stimulated* phonon emission in QWH's.

PHONONS, JUST AS PHOTONS, are bosons and have a basis to be involved in stimulated emission. For LO phonons in GaAs (or $Al_xGa_{1-x}As$) it is not a straightforward matter, however, to observe *stimulated* phonon emission ($\hbar\omega_{LO} \sim 36$ meV). In earlier work [1, 2] we have pointed out that an $Al_xGa_{1-x}As$–GaAs multiple quantum-well heterostructure (QWH) can form a phonon resonator, and thus assist stimulated phonon emission. Such a resonator consisting of an array of 7 $L_{z1} \sim 50$ Å GaAs quantum wells coupled by 6 $L_B \sim 50$ Å $Al_xGa_{1-x}As$ barriers has been coupled with one more barrier ($L_B \sim 50$ Å) to a single larger GaAs "detector"-well ($L_{z2} \sim 200$ or 500 Å) and, when photopumped, has been used to induce phonon-sideband laser operation one phonon ($\hbar\omega_{LO}$) below the confined-carrier transitions of the larger GaAs quantum well(s) [3–5]. In this paper we show that the phonon-generating small-well array can be "destroyed" (Q spoiled), and the induced phonon-sideband laser operation of the larger well, which remains intact, is quenched. The induced phonon-sideband laser operation that occurs when the quasi-two-dimensional (as-grown) layered structure is preserved is consistent with an estimate, described here, showing that the effective electron–phonon coupling constant for indirect (intraband) optical transitions is enhanced at higher phonon occupancy, N_Q. These results confirm that *stimulated* phonon emission is supported by a multiple quantum-well resonator.

The quantum-well heterostructures of this work have been grown (750°C) by metalorganic chemical vapor deposition (MO–CVD) as described extensively elsewhere [6, 7]. In the present work some of the samples of [3] are employed; also another complementary set of samples is used consisting of two 7-well ($L_{z1} \sim 50$ Å) resonators coupled (by $L_B \sim 50$ Å barriers) onto either side of an $L_{z2} \sim 500$ Å GaAs "detector" well. Rectangular samples from both wafers are heat sunk in In under sapphire windows and are photodumped with an Ar^+ laser (5145 Å).

The bevel cross-section [8], at the shallow angle 0.41°, of Fig. 1(a) shows (arrows) the small-well resonator section of the as-grown wafer of [3]. The larger well ($L_{z2} \sim 500$ Å) is obvious below the small-well resonator. It is identified in (c) by the arrows. The resonator, which photopumped is a phonon source [3], constitutes 58% of the heterostructure active region and, because of its thin layer size ($L_{z1} \sim 50$ Å, $L_B \sim 50$ Å), can be destroyed by thermal annealing without damaging the larger well. Bevel cross-section (b), which is at a

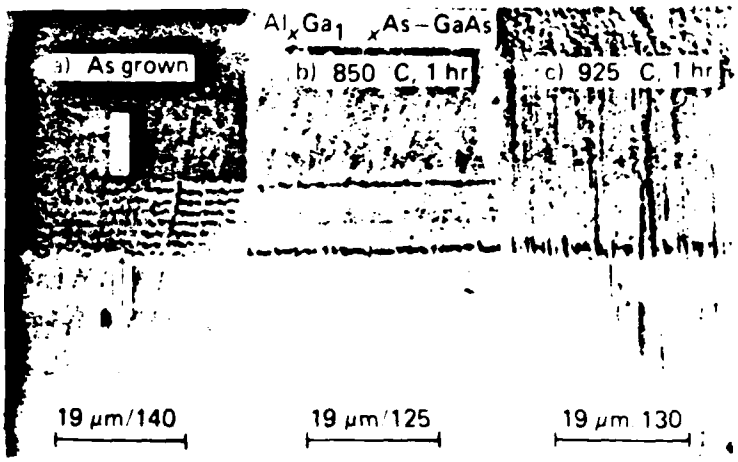

Fig. 1. Beveled and stained cross sections of an MO–CVD multiple quantum-well heterostructure (QWH). The bevel angle ($\theta \leq 0.5°$) is slightly different for each cross section, resulting in the scale factors 140, 125 and 130. Cross section (a) shows the as-grown active region with seven 50 Å GaAs wells (arrows) and one 500 Å GaAs well coupled by seven 50 Å $Al_xGa_{1-x}As$ ($x \sim 0.4$) barriers. The array of 50 Å wells (a) are smeared after annealing for 1 hr at 850°C (b), and are no long visible after 1 hr at 950°C (c). The 500 Å well, however, can still be seen and is marked by the arrows in (c).

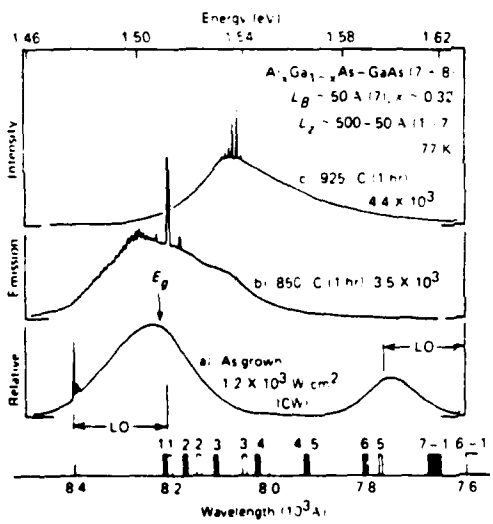

Fig. 2. CW emission spectra (77 K) of photopumped samples (Ar^+, 5145 Å) from the QWH of Fig. 1. The dark and light markers on the horizontal axis correspond to $e \rightarrow hh$ (n) and $e \rightarrow lh$ (n') transitions. Luminescence from the as-grown QWH (a) peaks one phonon below the lowest states of the 50 Å wells (~ 7750 Å) and more strongly below and near E_g with, moreover, laser operation one phonon below E_g. After sample annealing 1 hr at 850°C (b) luminescence from the 50 Å wells disappears, and laser operation near threshold moves up to E_g. The emission and laser operation moves to still higher energy (c) after sample annealing at 925°C for 1 hr.

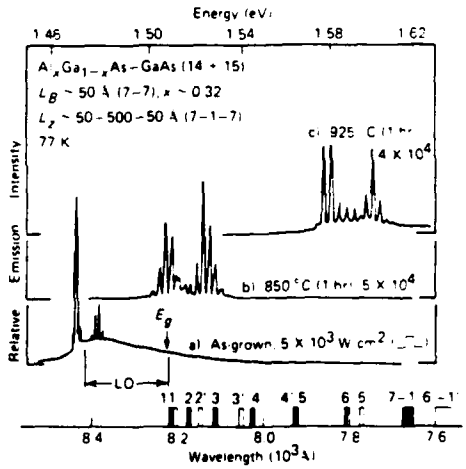

Fig. 3. Laser operation (pulsed, 77 K) of a QWH similar to that of Figs. 1 and 2, but with seven 50 Å wells and seven 50 Å barriers on both sides of the 500 Å well. The as-grown sample (a) lases strongly one phonon below E_g; after sample annealing for 1 hr at 850°C and smearing of the small wells (b) laser emission is cut off below E_g and shifts to the lowest transitions ($L_{1,1'} \sim E_g$) of the 500 Å GaAs well. After sample annealing of 1 hr at 925°C (c), stimulated emission shifts to still higher energy (see text).

slightly larger angle (0.46°) than (a), shows that after thermal annealing for 1 hr at 850°C the small quantum wells are still apparent but smeared and fainter; after 1 hr at 925°C (cross-section (c), 0.44°) the interdiffusion

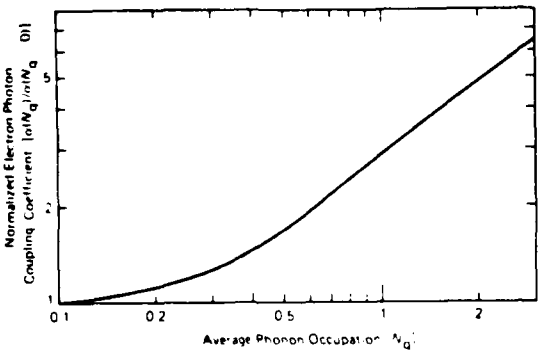

Fig. 4. Calculated electron–phonon coupling coefficient, $\alpha(N_q)$, normalized to $\alpha(N_q = 0)$. The coupling between electrons and longitudinal optical (LO) phonons of wavevector q increases by a factor ~ 6 when the average phonon occupation number, N_q, is increased from 0.1 to 3.

of Al and Ga (over a distance of ~ 50 Å) is sufficiently complete [9] so that the ~ 700 Å small-well section vanishes, and the phonon-resonator Q is spoiled.

Note that the large well of Fig. 1 (identified by arrows in (c)) is basically intact after thermal annealing and, in fact, still functions as a photopumped laser. This is shown by the data (77 K) of Fig. 2 and by the data of Fig. 3, which are for a structure like that of Figs. 1 and 2 but with a 7-well resonator coupled to either side of the large GaAs well. Note that in both cases induced phonon-sideband laser operation [3] of the larger well is clear in the case of the as-grown wafers (Figs. 2(a) and 3(a)). This is shown by the LO markers that extend from ~ $E_g - \hbar\omega_{LO}$ to ~ E_g, which is where, because of the large well size (500 Å), the lowest electron-to-heavy-hole ($e \rightarrow hh$, n) and electron-to-light-hole ($e \rightarrow lh$, n') transitions asymptote ($E_{1,1'} \sim E_g$). For both wafers the first stage of annealing (850°C, 1 hr) causes the laser operation to shift to $\hbar\omega \sim E_g$ from $\hbar\omega \sim E_g - \hbar\omega_{LO}$. Also, it is important to note in Fig. 2(b), compared to Fig. 2(a), that recombination radiation one phonon below the $n = 1, n' = 1'$ transitions (7750 Å) of the small-well resonator (labeled 7-1 and 6'-1') vanishes. It is clear that the small-well section after annealing no longer serves as before as a phonon source and resonator. As a consequence the laser operation of the big well receives slight if any auxiliary stimulation and loses its phonon sideband at $E_g - \hbar\omega_{LO}$.

It is evident from curves (c) of Figs. 2 and 3 that thermal annealing of the wafers at 925°C for 1 hr not only totally destroys the small-well phonon resonators (Fig. 1(c)) but also shrinks the larger (~ 500 Å) GaAs quantum well, shifts it somewhat towards $Al_xGa_{1-x}As$, and moves the recombination radiation well above E_g(GaAs). No sign of phonon-sideband laser operation ($\hbar\omega \sim E_g - \hbar\omega_{LO}$) is evident after thermal annealing of the samples at 850 and 925°C for 1 hr.

The data above make clear that phonon-sideband laser operation of QWH's relies upon a strong component of phonon generation, not to mention stimulated phonon emission which makes possible laser operation of a large well at $E_g - \hbar\omega_{LO}$ (Figs. 2(a) and 3(a)). Relative to this point, an interesting question is that of whether in a quasi-two-dimensional structure the basic electron–phonon interaction is enhanced, particularly at higher phonon occupancy, N_q. The second order perturbation theory necessary to calculate the phonon-assisted (indirect) transitions [10] has been reviewed in detail [11] and can be extended. Analogous to previous caculations [12] we introduce a damping factor and calculate in the weak coupling limit. The electron–phonon interaction is treated for the case of a quasi-two-dimensional system (size quantization). In addition to the weak coupling approximation, two other major approximations have been made: (i) we assume that the value of the one-electron wavevector is small (electrons close to Γ), which is justified for emission below the lowest confined-particle states, and (ii) we assume the phonon occupation N_q to be independent of q. As discussed elsewhere [4], this is a rather poor approximation but the inclusion of q dependence does not influence the result substantially. In many practical cases the phonons due to stimulated emission have relatively small q values [4] so that real phonon absorption cannot occur for electrons near Γ. In Fig. 4 we plot, as a result of these calculations, the relative electron–phonon coupling constant $\alpha(N_q)$ normalized to $\alpha(N_q = 0)$. It can be seen that for easily obtainable values of N_q [1, 2] the coupling is enhanced by almost an order of magnitude. This means that the weak polar coupling of GaAs is enhanced by an order of magnitude at higher phonon occupancy. In other words, GaAs quantum wells behave, at the high pumping intensities characteristic of this work (and of double heterostructure laser operation) [13], in a manner similar to strongly coupled II–VI compounds.

It is clear that a basis exists for the type of laser operation ($\hbar\omega \sim E_g$(GaAs)–$\hbar\omega_{LO}$) shown in Figs. 2(a) and 3(a). To conclude, we have not attempted to determine the Q of the phonon resonator sections of the QWH's described here because near the Bragg condition the exact value of reflectivity (and Q) is hard to calculate for a real structure. Nevertheless, it is apparent from the thermal annealing results described above that the only basic modification to our as-grown QWH samples is the spoiling of their small-well array sections and their ability to act as phonon Bragg reflectors – and thus as strong auxiliary phonon sources for large-well induced phonon-sideband laser operation.

Acknowledgements – The authors wish to thank G.E. Stillman for various discussions, and Y.S. Moroz, B.L. Marshall, R.T. Gladin and B.L. Payne (Urbana) for technical assistance. The work of the Illinois group has been supported by NSF Grants DMR 79-09991 and DMR 77-23999, and Navy Contract N00014-76-C-0708; the work of the Rockwell group has been partially supported by the Office of Naval Research, Contract N00014-78-C-0711.

REFERENCES

1. R.M. Kolbas, N. Holonyak, Jr., B.A. Vojak, K. Hess, M. Altarelli, R.D. Dupuis & P.D. Dapkus, *Solid State Commun.* **31**, 1033 (1979).
2. N. Holonyak, Jr., R.M. Kolbas, W.D. Laidig, B.A. Vojak, K. Hess, R.D. Dupuis & P.D. Dapkus, *J. Appl. Phys.* **51**, 1328 (1980).
3. J.J. Coleman, P.D. Dapkus, B.A. Vojak, W.D. Laidig, N. Holonyak, Jr. & K. Hess, *Appl. Phys. Lett.* **37**, 15 (1980).
4. K. Hess, N. Holonyak, Jr., W.D. Laidig, B.A. Vojak, J.J. Coleman & P.D. Dapkus, *Solid State Commun.* **34**, 749 (1980).
5. B.A. Vojak, N. Holonyak, Jr., W.D. Laidig, K. Hess, J.J. Coleman & P.D. Dapkus, *J. Appl. Phys.* **52**, to be published.
6. H.M. Manasevit, *J. Electrochem. Soc.* **118**, 647 (1971).
7. R.D. Dupuis & P.D. Dapkus, *7th Int. Symp. on GaAs and Related Compounds*, (Edited by C.M. Wolfe), pp. 1–9. St. Louis Institute of Physics, London, (1979).
8. N. Holonyak, Jr., B.A. Vojak, R.M. Kolbas, R.D. Dupuis & P.D. Dapkus, *Solid-State Electronics* **33**, 431 (1979).
9. L.L. Chang & A. Koma, *Appl. Phys. Lett.* **29**, 138 (1976).
10. L.H. Hall, J. Bardeen & F.J. Blatt, *Phys. Rev.* **95**, 559 (1954).
11. H.B. Bebb & E.W. Williams, *Photoluminescence I. Theory* (Edited by R.K. Williardson and A.C. Beer), *Semiconductors and Semimetals*, Vol. 8, pp. 181–320. Academic Press, New York (1972).
12. B. Segall & G.D. Mahan, *Phys. Rev.* **171**, 935 (1968).
13. N. Holonyak, Jr., B.A. Vojak, W.D. Laidig, K. Hess, J.J. Coleman & P.D. Dapkus, *Appl. Phys. Lett.* **37**, 136 (1980).

Tech. Dig. Dec 81 accepted
cc
EC

ABSORPTION, STIMULATED EMISSION, AND CLUSTERING IN AlAs-$Al_xGa_{1-x}As$-GaAs SUPERLATTICES

J.J. Coleman and P.D. Dapkus

Rockwell International, Electronics Research Center

Anaheim, California 92803

M.D. Camras, N. Holonyak, Jr., W.D. Laidig, and T.S. Low

Electrical Engineering Research Laboratory and Materials Research Laboratory

University of Illinois at Urbana-Champaign, Urbana, Illinois 61801

M.S. Burroughs* and K. Hess

Electrical Engineering Research Laboratory and Coordinated Science Laboratory

University of Illinois at Urbana-Champaign, Urbana, Illinois 61801

ABSTRACT

Absorption and photoluminescence data are presented on two AlAs-$Al_xGa_{1-x}As$-GaAs superlattices (SL's) grown by metalorganic chemical vapor deposition (MO-CVD). One SL is an 80-period all-binary structure with AlAs barriers and GaAs wells. The other SL consists of 121 periods of $Al_xGa_{1-x}As$ (x ~ 0.5) barriers and GaAs wells. The effects of clustering in the alloy-barrier SL lead to a spectral shift to lower energy that can be characterized by an effective well size L_z' larger than the intended well size of L_z ~ 80 Å. Absorption data and low-level photoluminescence data on both SL's correspond closely to the calculated confined-particle transitions. At high excitation levels, however, stimulated emission, including cw 300-K laser operation, occurs ~ $\hbar\omega_{LO}$ below the lowest (n=1) confined-particle transitions.

* Also with Western Electric (Reading, PA).

I. INTRODUCTION

Quantum-well heterostructure (QWH) lasers are interesting, first, for various fundamental reasons (see Ref.1 for a review) and, second, because they offer, beyond ordinary double heterostructure (DH) lasers,[2] the practical prospect of improved room temperature continuous (cw 300 K) operation, e.g., lesser temperature sensitivity (T_o as high as 437°C)[3] as well as improved dynamic properties.[4] In a number of papers[1,5-10] dealing with this form of laser, specifically papers dealing with $Al_xGa_{1-x}As$-GaAs QWH's grown by metalorganic chemical vapor deposition (MO-CVD), we have reported that phonon participation in the laser operation is a major effect. Others,[11] working with QWH's grown by molecular beam epitaxy (MBE), question the importance of phonon participation in this form of laser. The further criticism has been offered[12] that the confined-particle state identification in the case of MO-CVD crystals has not been confirmed by absorption measurements. This comment is not well founded in view of the fact that the typical MO-CVD $Al_xGa_{1-x}As$-GaAs QWH laser structure has a total thickness of GaAs in the quantum-well active region of <u>less</u> than 1000 Å. Bulk-crystal GaAs or direct-gap $Al_xGa_{1-x}As$ absorption coefficients, however, are of the order of $\alpha \sim 10^4$ cm^{-1} (or $1/\alpha \sim 1$ μm), so that a typical $Al_xGa_{1-x}As$-GaAs QWH laser has an insufficient total thickness of GaAs in the active region (i.e., $\sim 1/\alpha$) for a meaningful low-level absorption measurement.

Recently an exception to these arguments, a special form of QWH laser, has been introduced. The exception is an MO-CVD $Al_xGa_{1-x}As$-GaAs[13]

or AlAs-GaAs[14] superlattice (SL) laser. This is a remarkable form of heterostructure, because without confining layers (a bare SL) and even with as many as >200 interfaces (over 100 periods), it is capable of cw 300 K laser operation. It is clear that in this case it is possible to "stack" enough coupled GaAs quantum wells to give the effect (magnitude) of the usual bulk-crystal absorption. Then absorption measurements, which can be compared with photoemission measurements, become practical. In this paper we present such absorption measurements on an MO-CVD $Al_xGa_{1-x}As$-GaAs and an all-binary AlAs-GaAs superlattice, and compare these measurements with low-level and high-level photoemission data. The same SL samples used for absorption measurements can be photopumped and, in fact, exhibit stimulated emission shifted to lower energy below the confined-particle absorption edge by typically the phonon energy - $\hbar\omega_{LO}$. Also, for the case of SL's with $Al_xGa_{1-x}As$ coupling barriers, an overall energy shift in absorption and emission is observed that can be accounted for by alloy clustering.[15] Presumably these effects have not been observed on some MBE samples (see Refs.16 and 17 for a discussion), but in recent stimulated emission measurements on comparable MO-CVD[15,18] and MBE[19,20] $Al_xGa_{1-x}As$-GaAs QWH laser samples we find similar clustering behavior, and thus expect alloy clustering owing to the random Al-Ga arrangement in $Al_xGa_{1-x}As$ to be generally important.

II. CRYSTAL AND SAMPLE PREPARATION

The crystals employed in the present work have been grown by the basic MO-CVD process described extensively elsewhere.[21,22] Of special interest is the fact that the computer-controlled MO-CVD crystal-growth

process has been used successfully to grow high quality all-binary AlAs-GaAs QWH's[18,23] and SL's.[14,18,24] Two different MO-CVD SL's are used in the present work: The first is an 80-period all-binary AlAs-GaAs SL with L_B(AlAs) ~ 25 Å and L_z(GaAs) ~ 75 Å. The SL period of L_B+L_z ~ 100 Å agrees both with the MO-CVD crystal-growth-apparatus calibration and with a shallow-angle slant cross section of the wafer.[25] The second wafer is a 121-period $Al_xGa_{1-x}As$-GaAs (x ~ 0.5) SL with the MO-CVD crystal-growth apparatus set to give the dimensions L_B(AlGaAs) ~ 80 Å and L_z(GaAs) ~ 80 Å. This agrees with the shallow-angle (0.38°) slant cross section of Fig.1 (150x vertical magnification, no horizontal magnification)[25] and a measured period of L_B+L_z ~ 160 Å. (The shallow angle, and thus magnification, are measured by "dragging" the stylus of a Sloan profilometer along the wafer surface and down the polished incline.)

Reference 18 gives a more extensive summary of all the methods of confirming the sizes L_B, L_z and the period L_B+L_z of a QWH or SL. As already mentioned, in the present work absorption measurements are part of this process. For both absorption and photoemission experiments, the GaAs substrate on the as-grown MO-CVD wafers (the region below the lower arrow of Fig.1) is removed partly by polishing and then completely by selective etching.[26] Generally, rectangular cleaved samples (as narrow even as ~ 10 μm) are compressed and heat sunk in In under sapphire windows for 77 K and in annealed Cu under diamond windows for pulsed and cw 300 K photoexcitation (Ar^+ laser, λ ~ 5145 Å). For absorption measurements (with a Cary 14RI), and for direct comparison stimulated emission measurements, bare SL samples

(0.8 μm or 1.9 μm thick) of size ≥2500 μm x ≥2500 μm are attached with a thin layer of vacuum grease to a sapphire window that is itself heat sunk over a 2000-μm diameter hole in a Cu plate.

III. AlAs-GaAs SUPERLATTICE

From other work on all-binary MO-CVD AlAs-GaAs QWH's and SL's, we know that it is possible to restrict quantum-well size fluctuations, δL_z, to the range of a monolayer (2.83 Å).[18] An all-binary AlAs-GaAs SL turns out then to be an important special case that should make possible an accurate size-fit (L_B, L_z) to absorption data. These data, with an excellent size-fit to the L_z ~ 75-Å, L_B ~ 25-Å SL mentioned above, are shown by the absorption curves (a) [77 K] and (b) [4.2 K] of Fig.2. Note that, except for a small shift, there is little difference between the 77-K curve of (a) and the 4.2-K curve of (b). The two main lower-energy absorption peaks are separated by the expected n=1 electron-to-heavy-hole (e→hh) and n'=1' electron-to-light-hole (e→lh) confined-particle transitions. (See Ref.23 for typical calculations of these transitions.) Note that these two transitions are expected to involve quasi-two-dimensional excitons,[27,28] and because of the heavy-hole, light-hole mass difference might differ in their downward shift from the confined-particle transitions. These effects are ignored here. It is possible also that broken selection rules are at issue.[29] These also are ignored.

Of particular interest in Fig.2 are the photoemission curves (c) and (d), which are for the <u>same</u> large-area sample as the absorption curves (a) and (b). At low-level [(c), 70 W/cm^2], the spontaneous emission lies very

close to the n=1 e→hh and n'=1' e→lh confined-particle transitions either as calculated or as set by the absorption measurements. When the photopumping is increased to high level (> 10^3 W/cm^2), then as shown by curve (d) [10^5 W/cm^2] the emission narrows (modes appear but are not resolvable on the scale of Fig.2) and <u>shifts</u> by the phonon energy $\hbar\omega_{LO}$ - 36 meV below the n=1 e→hh confined-particle transitions. The LO markers in the figure set a natural energy scale and serve as references. Clearly this behavior agrees with past work.[1,5-10] Curve (d) [10^5 W/cm^2] shows for another sample, a rectangular sample measuring 63 μm x 330 μm, that this behavior is indeed quite general.

Figure 3 shows that the 77-K behavior of the all-binary AlAs-GaAs SL of Fig.2 is basically unchanged at 300 K. The absorption curve (a) shifts as expected to lower energy by $E_g(77)-E_g(300)$ - 85 meV. Also a lower energy shoulder develops on the higher energy n'=1' e→lh peak. This may be related to the lower reduced mass of the e-lh exciton, its larger effective radius, and perhaps more complicated behavior in the quasi-two-dimensional SL structure at higher lattice temperature. Also, broken selection rules may be important.[29]

Curve (b) [140 W/cm^2] of Fig.3 shows the low-level cw 300-K photoemission of a 63 μm x 190 μm rectangular sample. This spontaneous emission is located essentially right on the n=1 e→hh and the n'=1' e→lh transitions. More interesting is the cw 300-K laser operation of the 30 μm x 170 μm sample of curve (c). This laser emission agrees with that of Fig.2 and occurs - $\hbar\omega_{LO}$ below the n=1 e→hh confined-particle transitions. This behavior is general and agrees with past work.[1]

IV. $Al_xGa_{1-x}As$-GaAs SUPERLATTICE

In most respects the behavior of the 121-period MO-CVD $Al_xGa_{1-x}As$-GaAs SL described in Sec.II is similar to that of the 80-period AlAs-GaAs SL of Figs.2 and 3. The absorption and the emission behavior at 77 K are shown in Fig.4. Although this 121-period alloy-barrier SL was grown, and was measured (Fig.1), to have sizes $L_B \sim 80$ Å and $L_z \sim 80$ Å, this GaAs well size does not fit the calculated positions[23] of the confined-particle transitions. A remarkable fit exists, however, for well size $L_z' \sim 93$ Å (and the $L_z \sim 93$-Å markers of Figs.4 and 5). Note that L_B does not strongly affect the calculation of the confined-particle states.[23] All of the absorption peaks of curve (a) [77 K] in Fig.4 basically agree with the transitions n=1 (e→hh), n'=1' (e→lh), n=2 (e→hh), and n'=2' (e→lh). The small peak at $\lambda \sim 7540$ Å, which again may involve broken selection rules,[29] is ignored because at 300 K [curve (a) of Fig.5] it is hardly noticeable. The n'=1' e→lh peak of Fig.4 is somewhat lower in energy than expected, but this might be reasonable because of the smaller reduced mass of the e-lh exciton, its greater radius, and the possibly greater influence on it of GaAs (or AlAs) clustering in the alloy coupling barriers.

Just as for the large absorption sample of Fig.2, when the SL-absorption sample of Fig.4 is photoexcited at low-level [curve (c), 70 W/cm^2], the emission is located only slightly lower in energy than the n=1 e→hh and n'=1' e→lh transitions. More important, at high-level [curve (d), 10^5 W/cm^2] the emission narrows, is stimulated (with closely spaced unresolved modes), and shifts $\sim \hbar\omega_{LO}$ lower in energy than the n=1 e→hh transitions. For comparison the laser behavior of a smaller rectangular sample (23 μm x 150 μm)

is shown by curve (e) [10^5 W/cm^2]. The stimulated emission of this sample also is shifted - $\hbar\omega_{LO}$ below the lowest confined-particle transitions.

The 300 K behavior of the 121-period alloy-barrier SL wafer is shown in Fig.5 and is consistent with the 77-K (and 4.2-K) data of Fig.4. As expected the 300 K absorption curve (a) is shifted to lower energy from 77 K by $E_g(77)-E_g(300)$ - 85 meV. Otherwise all the basic absorption peaks remain the same and merely shift downward in energy. Because the absorption sample (a), as for the similar case of Fig.3, is not properly heat sunk for cw 300-K photoexcitation, two other samples are employed for this purpose. The low-level emission of a 60 μm x 270 μm sample is shown by curve (b) [90 W/cm^2] and is seen to be well centered on the n=1 e→hh and n'=1' e→lh transitions. A longer and somewhat narrower sample (50 μm x 410 μm) is used for high-level photopumping and exhibits the laser operation shown by curve (c) [7.5×10^3 W/cm^2]. The cw 300 K laser operation of curve (c) is of itself interesting because the laser threshold is the equivalent of - 3×10^3 A/cm^2, which is remarkable for a structure with 2x121 heterointerfaces. Also, clearly the laser operation is - $\hbar\omega_{LO}$ below the n=1 e→hh transitions.

V. DISCUSSION AND CONCLUSIONS

The data above make it clear that the phonon participation in the SL laser operation does not depend upon the coupling barrier composition, i.e., on whether the coupling barriers are binary or alloy crystal (clustered or not). The 121-period SL crystal with ternary coupling barriers appears, however, to exhibit larger virtual quantum-well sizes ($L_z' > L_z$) than the size L_z intended or measured. We propose, as earlier,[15,18-20] that this behavior occurs because of the compositional disorder of the coupling

barriers. As in previous work,[18-20] we introduce a simple random-number numerical procedure to simulate the formation of Al-rich and Al-depleted aggregates (clusters). The only assumption in this numerical simulation is that the coupling-barrier composition fluctuates preferentially in the direction of the crystal growth. This is not unreasonable since the epitaxial crystal growth is slow in the [100] direction, and on the low-index (100) surface, which is employed here, atoms experience considerable random walking (and smoothing of the surface) during the seeding process. Thus, in the simulation procedure the As atoms are fixed in the zinc-blende Column V sublattice; on the other hand, the Column III sublattice sites are filled with Al and Ga atoms in proportion to their ratio $x \sim 0.5$ but in a manner determined by a weighted uniform random-number generation scheme. The cluster sizes at the edges of the coupling barriers (where the clusters have a larger effect)[18-20] and their distribution are then calculated. Normalizing properly, we find in this manner the probability of a certain effective well size L_z', or

$$\langle L_z' \rangle = \{\sum L_z' \cdot P(L_z')\}/\{\sum P(L_z')\}, \tag{1}$$

where $P(L_z')$ is the probability of finding a well of size L_z' ($L_z' \geq L_z$) and, of course,

$$\sum P(L_z') = 1. \tag{2}$$

The results of these numerical calculations, which are repeated sufficiently to give convergence, are shown in Fig.6 for a SL having 121 barriers and a nominal well size of $L_z \sim 80$ Å. As is evident in Fig.6, the nominal size $L_z \sim 80$ Å occurs with lower probability than a well size one monolayer

larger (83 Å). Effective quantum-well sizes as large as L_z' ~ 90 Å occur with probability only half as great as the nominal size L_z ~ 80 Å. Based on these results (Fig.6), it is reasonable to expect the confined-particle transitions of the alloy-barrier SL to appear lower in energy than expected. We have not taken into account the fact that clusters within the barriers rather than just at the edges also play a role. In addition, it is not known whether barrier compositions near the direct-indirect transition of $Al_xGa_{1-x}As$ (x_c = 0.45) increase the tendency toward alloy clustering.[17]

Finally, it is worth mentioning that the phonon-assisted laser operation observed on the two types of SL's of this work occurs under fairly conservative operating conditions compared to earlier work on QWH's possessing small active regions [total L_z(GaAs) ≤ 1000 Å] confined by 1 μm and 0.1-0.3 μm $Al_xGa_{1-x}As$ cladding layers.[1,5-10] In this more common type of heterostructure the high-level photopumping generates carriers in the 1.1-1.3 μm ($\alpha \sim 10^4$ cm^{-1}) $Al_xGa_{1-x}As$ confining layers; the carriers then are collected, and thermalize, in a compact phonon-generating quantum-well active region. Hence, for similar excitation levels the same number of photons are generated for laser operation in both structures but spatially more spread out in the SL. In a common QWH the carriers are contained in a smaller volume with a correspondingly larger "trapped" phonon density that can more strongly influence the recombination process. In other words, for the same excitation conditions (W/cm^2) the density of phonons generated in a SL is not as great as in the usual QWH; nevertheless, phonon-assisted laser operation is observed in a SL and is even more likely in an ordinary QWH.

ACKNOWLEDGMENTS

The authors are grateful to Yuri S. Moroz, R.T. Gladin, B.L. Marshall, and B.L. Payne for technical assistance, and to G.E. Stillman for various conversations. The work of the Illinois group has been supported by NSF Grants No. DMR 79-09991 and No. DMR 77-23999, and Navy Contract No. N00014-76-C-0708. The work of the Rockwell group has been partially supported by ONR Contract No. N00014-78-C-0711.

REFERENCES

1. N. Holonyak, Jr., R.M. Kolbas, R.D. Dupuis, and P.D. Dapkus, IEEE J. Quantum Electron. QE-16, 170 (1980).
2. G.H.B. Thompson, Physics of Semiconductor Lasers (Wiley, New York, 1980), pp. 240-286.
3. R. Chin, N. Holonyak, Jr., B.A. Vojak, K. Hess, R.D. Dupuis, and P.D. Dapkus, Appl. Phys. Lett. 36, 19 (1980).
4. E.R. Anderson, B.A. Vojak, N. Holonyak, Jr., G.E. Stillman, J.J. Coleman, and P.D. Dapkus, Appl. Phys. Lett. 38, 555 (1981).
5. N. Holonyak, Jr., R.M. Kolbas, W.D. Laidig, M. Altarelli, R.D. Dupuis, and P.D. Dapkus, Appl. Phys. Lett. 34, 502 (1979).
6. R.M. Kolbas, N. Holonyak, Jr., B.A. Vojak, K. Hess, M. Altarelli, R.D. Dupuis, and P.D. Dapkus, Solid State Commun. 31, 1033 (1979).
7. N. Holonyak, Jr., R.M. Kolbas, W.D. Laidig, B.A. Vojak, K. Hess, R.D. Dupuis, and P.D. Dapkus, J. Appl. Phys. 51, 1328 (1980).
8. J.J. Coleman, P.D. Dapkus, B.A. Vojak, W.D. Laidig, N. Holonyak, Jr., and K. Hess, Appl. Phys. Lett. 37, 15 (1980).
9. N. Holonyak, Jr., B.A. Vojak, W.D. Laidig, K. Hess, J.J. Coleman, and P.D. Dapkus, Appl. Phys. Lett. 37, 136 (1980).
10. W.D. Laidig, N. Holonyak, Jr., M.D. Camras, B.A. Vojak, K. Hess, J.J. Coleman, and P.D. Dapkus, Solid State Commun. 38, 301 (1981).
11. C. Weisbuch, R.C. Miller, R. Dingle, A.C. Gossard, and W. Wiegmann, Solid State Commun. 37, 219 (1981).
12. R. Dingle, Comment to J.J. Coleman and P.D. Dapkus, First International Conference on Metalorganic Vapor Phase Epitaxy (Corsica, May 1981).

13. P.D. Dapkus, J.J. Coleman, W.D. Laidig, N. Holonyak, Jr., B.A. Vojak, and K. Hess, Appl. Phys. Lett. 38, 118 (1981).

14. J.J. Coleman, P.D. Dapkus, N. Holonyak, Jr., and W.D. Laidig, Appl. Phys. Lett. 38, 894 (1981).

15. N. Holonyak, Jr., W.D. Laidig, B.A. Vojak, K. Hess, J.J. Coleman, P.D. Dapkus, and J. Bardeen, Phys. Rev. Lett. 45, 1703 (1980).

16. R.C. Miller, C. Weisbuch, and A.C. Gossard, Phys. Rev. Lett. 46, 1042 (1981).

17. N. Holonyak, Jr., W.D. Laidig, K. Hess, J.J. Coleman, P.D. Dapkus, Phys. Rev. Lett. 46, 1043 (1981).

18. N. Holonyak, Jr., W.D. Laidig, M.D. Camras, K. Hess, M.S. Burroughs, J.J. Coleman, and P.D. Dapkus, "Size Fluctuations and High Energy Laser Operation of $Al_xGa_{1-x}As$-AlAs-GaAs Quantum-Well Heterostructures," unpublished.

19. N. Holonyak, Jr., W.D. Laidig, M.D. Camras, H. Morkoç, T.J. Drummond, and K. Hess, "Clustering and Phonon Effects in $Al_xGa_{1-x}As$-GaAs Quantum-Well Heterostructure Lasers Grown by Molecular Beam Epitaxy," Solid State Commun., to be published.

20. N. Holonyak, Jr., W.D. Laidig, M.D. Camras, H. Morkoç, T.J. Drummond, K. Hess, and M.S. Burroughs, "Clustering in MBE $Al_xGa_{1-x}As$-GaAs Quantum-Well Heterostructure Lasers," unpublished.

21. H.M. Manasevit, J. Electrochem. Soc. 118, 647 (1971).

22. R.D. Dupuis, L.A. Moudy, and P.D. Dapkus, 7th Intl. Symp. on GaAs and Related Compounds, St. Louis, 1978, ed. C.M. Wolfe (Institute of Physics, London, 1979), pp. 1-9.

23. B.A. Vojak, W.D. Laidig, N. Holonyak, Jr., M.D. Camras, J.J. Coleman, and P.D. Dapkus, J. Appl. Phys. 52, 621 (1981).

24. W.D. Laidig, N. Holonyak, Jr., M.D. Camras, K. Hess, J.J. Coleman, P.D. Dapkus, and J. Bardeen, Appl. Phys. Lett. 38, 776 (1981).

25. N. Holonyak, Jr., B.A. Vojak, R.M. Kolbas, R.D. Dupuis, and P.D. Dapkus, Solid-State Electron. 33, 431 (1979).

26. R.A. Logan and F.K. Reinhart, J. Appl. Phys. 44, 4172 (1973).

27. B.A. Vojak, N. Holonyak, Jr., W.D. Laidig, K. Hess, J.J. Coleman, and P.D. Dapkus, Solid State Commun. 35, 477 (1980).

28. E.A. Andryushin and A.P. Silin, Fiz. Tverd. Tela 22, 2676 (1980) [Sov. Phys. Solid State 22, 1562 (1980)].

29. A. Ya. Shik, Pis'ma Zh. Tekh. Fiz. 5, 869 (1979) [Sov. Tech. Phys. Lett. 5, 359 (1979)].

FIGURE CAPTIONS

Fig.1 Shallow-angle (~ 0.38°) slant cross section of a 121-period $Al_xGa_{1-x}As$-GaAs superlattice (region between arrows) grown by metalorganic chemical vapor deposition (MO-CVD). (Slant magnification ~ 150x in the vertical direction, no increased magnification in the horizontal direction.)

Fig.2 Absorption and luminescence (77 K) of an 80-period all-binary superlattice with L_B ~ 25-Å AlAs barriers and L_z ~ 75-Å GaAs wells. The absorption peaks [(a) 77 K, (b) 4.2 K] correspond closely to the n=1 e-hh transitions and the n'=1' e-lh transitions (dark and light markers on horizontal axis). Continuous [(c) 70 W/cm^2] and pulsed [(d) 10^5 W/cm^2] photoexcitation of the same large sample used for absorption measurements [(a), (b)] show that the luminescence shifts ~ $\hbar\omega_{LO}$ to lower energy at higher excitation levels, which is consistent with the laser operation of smaller samples [(e) 10^5 W/cm^2].

Fig.3 Room temperature absorption (a) and low-level photoluminescence [(b) 140 W/cm^2, cw] of the AlAs-GaAs superlattice of Fig.2. At high excitation [(c) 9.4×10^3 W/cm^2, cw 300 K] the superlattice lases ~ $\hbar\omega_{LO}$ below the n=1 e-hh transitions.

Fig.4 Absorption and emission (77 K) of the 121-period $Al_xGa_{1-x}As$-GaAs superlattice shown in Fig.1. The peaks in absorption [(a) 77 K, (b) 4.2 K] and in low-level [(c) 70 W/cm^2, cw] photoluminescence occur near the n=1 e-hh and n'=1' e-lh transitions of a superlattice with an effective well size of L_z' ~ 93 Å. High level

(pulsed) excitation [(d) 10^5 W/cm^2] of the large absorption sample of (a) and a much smaller sample [(e) 10^5 W/cm^2] leads to laser operation shifted - $\hbar\omega_{LO}$ below the lowest (n=1) transitions.

Fig.5 Room temperature absorption (a) and low-level photoluminescence [(b) 90 W/cm^2, cw] of the $Al_xGa_{1-x}As$-GaAs superlattice of Figs.1 and 4. The 121-period alloy-barrier superlattice operates [(c) 7.5×10^3 W/cm^2] as a cw 300 K laser - $\hbar\omega_{LO}$ below the n=1 e-hh transitions.

Fig.6 Probability of larger effective well size L_z' ($L_z' > L_z$ = 80 Å) as a result of alloy clustering in the 121-period superlattice of Figs.1, 4 and 5 with L_B - 80 Å $Al_xGa_{1-x}As$ (x - 0.3) barriers and L_z - 80 Å GaAs wells. The random distribution of Al and Ga in the $Al_xGa_{1-x}As$ barriers results in a relatively large probability of an effective quantum-well size of L_z' - 93 Å in agreement with the data of Figs.4 and 5.

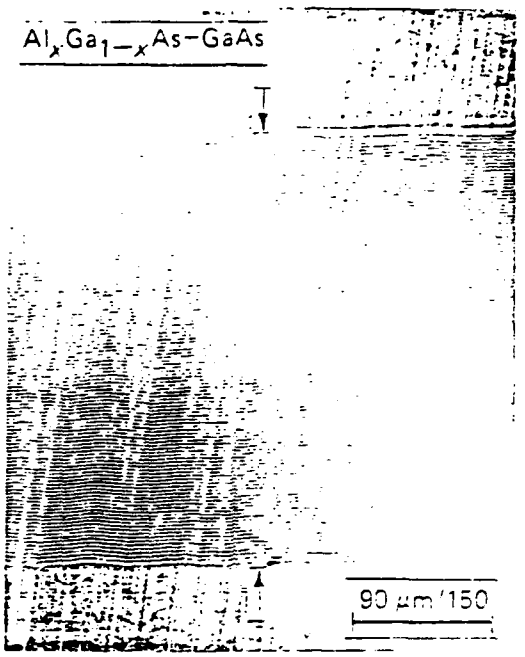

Fig. 1

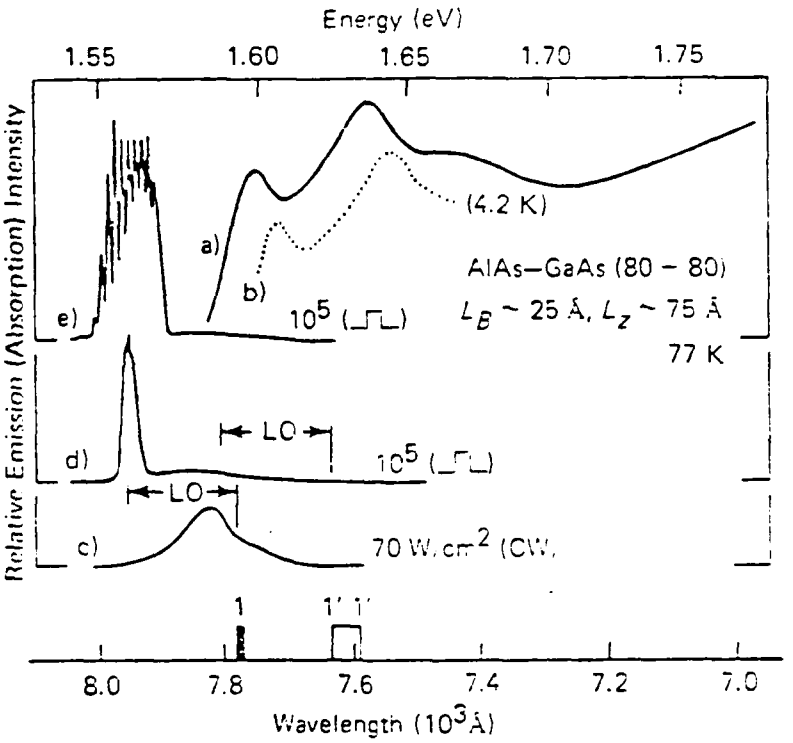
Energy (eV)
1.55
1.60
1.65
1.70
1.75
Relative Emission (Absorption) Intensity
(4.2 K)
a)
b)
AlAs–GaAs (80 – 80)
$L_B \sim 25$ Å, $L_z \sim 75$ Å
77 K
e)
10^5 (⊓⊓)
LO
d)
10^5 (⊓⊔)
LO
c)
70 W.cm^{-2} (CW)
1
1'
1''
8.0
7.8
7.6
7.4
7.2
7.0
Wavelength (10^3Å)

Fig. 2

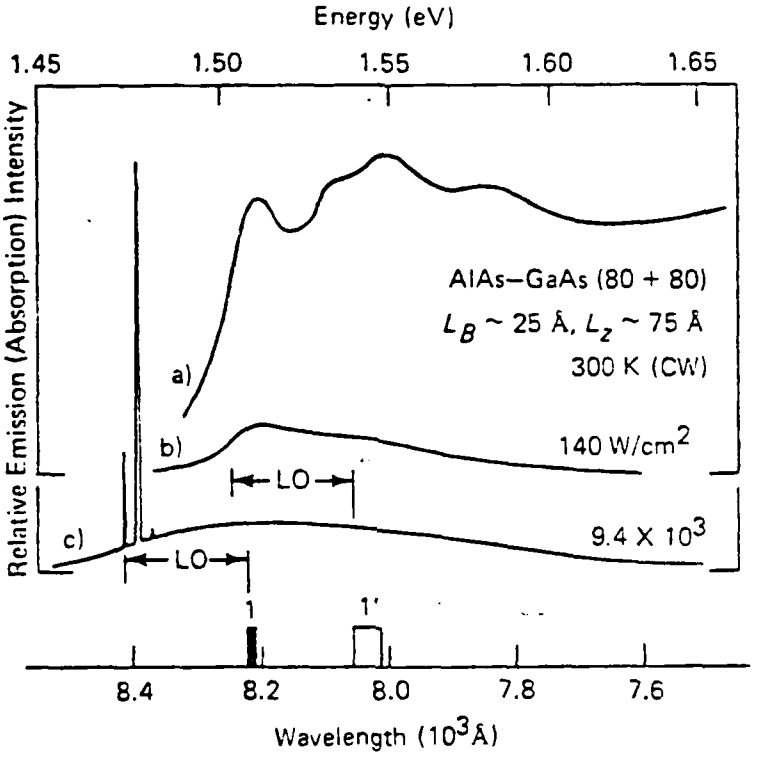
Energy (eV)
1.45
1.50
1.55
1.60
1.65
Relative Emission (Absorption) Intensity
AlAs–GaAs (80 + 80)
$L_B \sim 25$ Å, $L_z \sim 75$ Å
300 K (CW)
a)
b)
140 W/cm^2
LO
c)
9.4 X 10^3
LO
1
1'
8.4
8.2
8.0
7.8
7.6
Wavelength (10^{3}Å)

Fig. 3

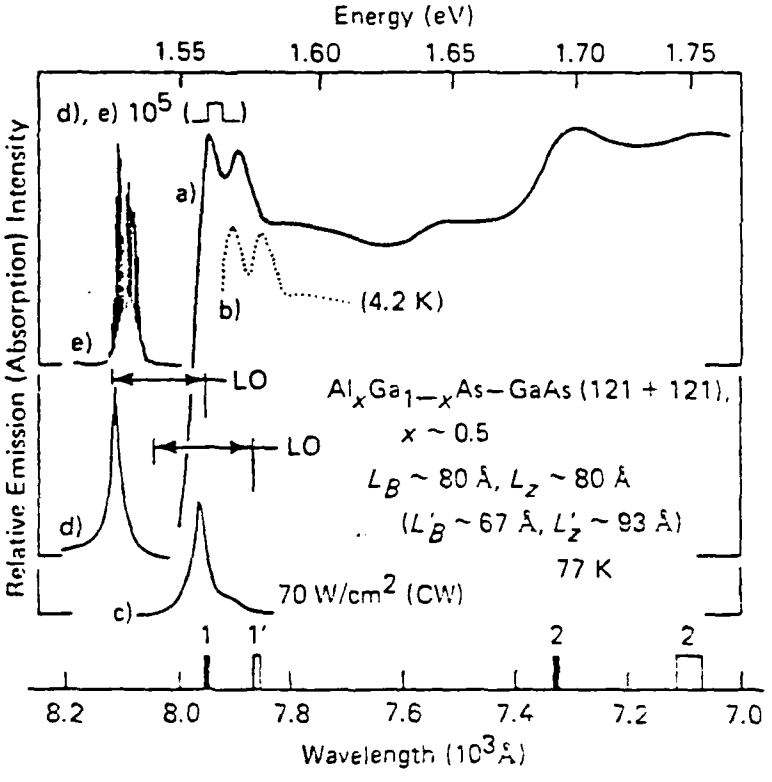
Energy (eV)
1.55
1.60
1.65
1.70
1.75
d), e) 10^5
a)
b)
(4.2 K)
e)
LO
LO
$Al_xGa_{1-x}As-GaAs$ (121 + 121),
$x \sim 0.5$
$L_B \sim 80$ Å, $L_z \sim 80$ Å
$(L'_B \sim 67$ Å, $L'_z \sim 93$ Å)
77 K
d)
c)
70 W/cm^2 (CW)
Relative Emission (Absorption) Intensity
1
1'
2
2
8.2
8.0
7.8
7.6
7.4
7.2
7.0
Wavelength (10^3Å)

Fig. 4

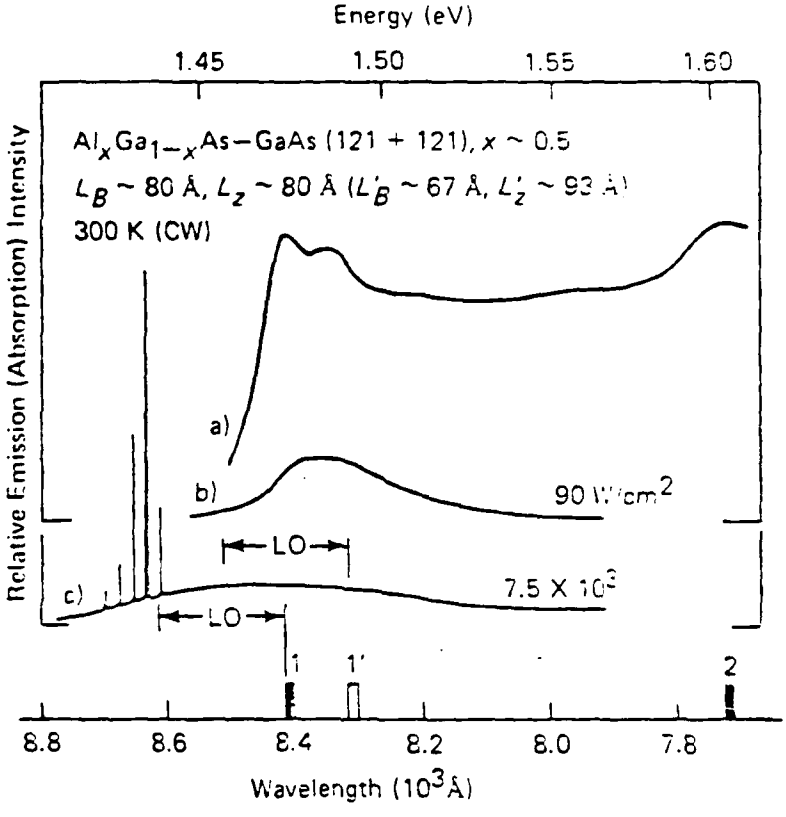
Energy (eV)
1.45
1.50
1.55
1.60
$Al_xGa_{1-x}As$–GaAs (121 + 121), $x \sim 0.5$
$L_B \sim 80$ Å, $L_z \sim 80$ Å ($L'_B \sim 67$ Å, $L'_z \sim 93$ Å)
300 K (CW)
Relative Emission (Absorption) Intensity
a)
b)
90 W/cm^2
LO
c)
7.5 X 10^3
LO
1
1'
2
8.8
8.6
8.4
8.2
8.0
7.8
Wavelength (10^3Å)

Fig. 5

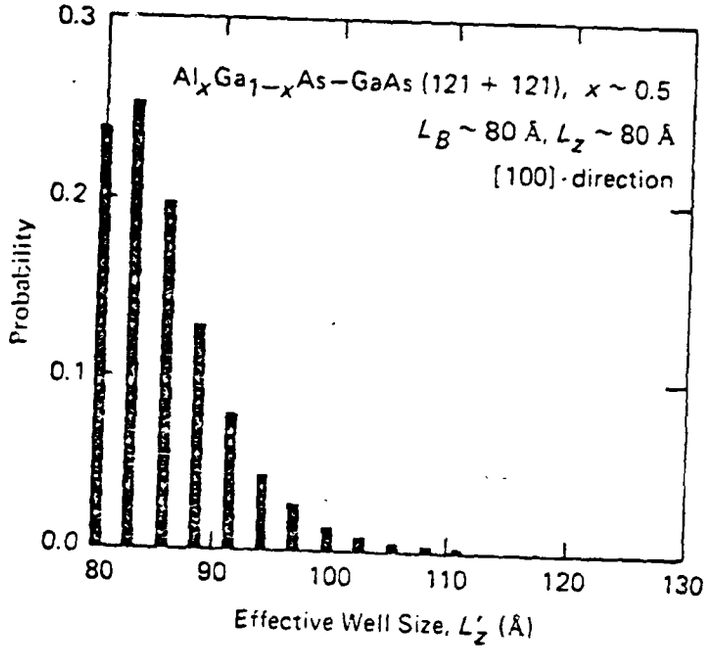
0.3
0.2
0.1
0.0
Probability
$Al_xGa_{1-x}As-GaAs$ (121 + 121), $x \sim 0.5$
$L_B \sim 80$ Å, $L_z \sim 80$ Å
[100]-direction
80
90
100
110
120
130
Effective Well Size, L_z' (Å)

Fig. 6

ABSORPTION AND STIMULATED EMISSION IN AN AlAs-GaAs SUPERLATTICE

J.J. Coleman, P.D. Dapkus, and D.R. Clarke[a)]

Rockwell International, Microelectronics Research and Development Center

Anaheim, California 92803

and

M.D. Camras and N. Holonyak, Jr.

Electrical Engineering Research Laboratory and Materials Research Laboratory

University of Illinois at Urbana-Champaign, Urbana, Illinois 61801

Absorption and stimulated-emission data (77 and 300 K) are presented on a 50-period all-binary AlAs-GaAs superlattice (SL) grown by metalorganic chemical vapor deposition (MO-CVD). Laser operation of the SL is observed $\Delta E \sim \hbar\omega_{LO}$ below the absorption, which corresponds accurately to the lowest confined-particle transitions determined from the measured (transmission electron microscope, TEM) barrier and well sizes of $L_B \sim 120$ Å and $L_z \sim 160$ Å.

a)Rockwell International Science Center, Thousand Oaks, CA 91360.

Although ample evidence exists showing that phonon assistance plays a part in the laser operation of an $Al_xGa_{1-x}As$-GaAs quantum-well heterostructure (QWH),[1-7] these observations continue to be questioned.[8] (See Ref.9 for a review of QWH laser operation). A recent criticism of laser experiments (high-excitation-level experiments) performed on QWH crystals grown by metalorganic chemical vapor deposition (MO-CVD) is that the confined-particle state identification, and hence identification of phonon participation, has not been confirmed by absorption measurements.[10] This comment is not well founded when it is recalled that absorption measurements are commonly made at low signal levels, and in the case of an $Al_xGa_{1-x}As$-GaAs QWH the active region contains usually less than 1000 Å of total GaAs quantum well region.[9] This is to be compared to a direct-gap bulk-crystal absorption coefficient of typically $\alpha \sim 10^4$ cm^{-1}, or $1/\alpha \sim 1$ μm, which is not matched by the ≤1000 Å of GaAs in an ordinary QWH.

For an absorption measurement to be convenient, a large number of GaAs quantum wells is required, for example, as occurs in a superlattice (SL). As recently shown,[11] this type of heterostructure can, in fact, be operated as a laser, and, of course, absorption measurements are possible on a SL of appreciable GaAs content. In this paper we describe absorption and stimulated emission measurements, the latter with phonon assistance, on a 50-period all-binary MO-CVD AlAs-GaAs superlattice.[12-14] We confirm the positions (energy) of the electron-to-heavy-hole (e→hh) and electron-to-light-hole (e→ℓh) confined-particle transitions via the absorption data and independently via calculations[15] based on the measured (transmission electron microscope, TEM) barrier (L_B~120 Å)and well sizes (L_z~160 Å) of the SL. (These results can be compared, of course, with luminescence measurements on narrow samples that also reveal the confined-particle transitions; e.g., see Fig.14 of Ref.9.)

The SL crystals of interest here have been grown by the basic MO-CVD process described in detail elsewhere.[16,17] Of particular interest is the recent demonstration that the MO-CVD process can be used to grow, in addition to GaAs and $Al_xGa_{1-x}As$, high quality AlAs layers,[14] and thus AlAs-GaAs SL's. In the present case an all-binary 50-period SL with L_B~120-Å AlAs coupling barriers and L_z~160-Å GaAs quantum wells is grown on a thick GaAs substrate and is capped with ~3 μm of GaAs. This configuration makes possible preparation of thin samples normal to a cleave edge for accurate TEM measurements of the ultra thin layer sizes L_B and L_z. The results of these measurements are shown in Fig.1 (L_B~120 Å, L_z~160 Å) and are used, as described in Ref.15, to calculate (simply and reliably) the locations of the various e→hh (n) and e→ℓh (n') confined-particle transitions. These are shown by dark and light markers on the horizontal axes of Figs.2 and 3.

For absorption and emission measurements the GaAs cap layer and the substrate are removed from the MO-CVD wafer, thus leaving a bare SL. A large 0.25 x 0.33 cm^2 rectangle is used for absorption measurements (made with a Cary 14 RI). For this purpose the sample is attached with grease to a sapphire, which in turn is fastened on a Cu plate over a 0.2 cm diameter hole. Because sapphire is a good low temperature heat conductor, absorption samples are used also for 77-K emission measurements (pulsed excitation). Much smaller cleaved rectangles of the bare SL are compressed under a diamond window into annealed Cu for cw 300-K (and 77-K) photopumped laser operation (Ar^+ laser photoexcitation, 5145 Å).

Figure 2 shows (a) the 300 K absorption behavior of the bare all-binary SL; (b) and (c) show the cw 300 K laser operation of a 40-μm x 95-μm and a

15-μm x 415-μm sample [J(equiv) ~ 3.9×10^3 A/cm^2]. The structure in the absorption curve and the positions of the confined-particle transitions basically agree. Other data on SL samples with smaller values of L_z(<100 Å) show that the main absorption at transitions n=1 (e→hh) and n'=1' (e→ℓh) can be resolved into two peaks,[18] but here this is not the case because of the large value of L_z and possibly because of some size variation from well to well. If alloy barriers ($Al_xGa_{1-x}As$) are employed, then the well-size variation (an increase) and shift of the absorption to lower energies, with 1 and 1' moving closer together, is greater because of alloy clustering,[18] which, of course, is not a problem in the present work. Most important, the data of Fig.2 make it clear that the SL laser operation [curves (b) and (c)] occurs $\Delta E \sim \hbar\omega_{LO}$ below the fundamental absorption [curve (a)] and the corresponding n=1 e→hh and n'=1' e→ℓh transitions.

The 77-K absorption data of Fig.3 [curve (a)] agree with the 300-K data of Fig.2, with, as expected, a spectral shift to higher energy of $E_g(77)-E_g(300) \sim 85$ meV. As already mentioned, it is possible (77 K) to photopump the large absorption sample and examine it in emission [curves (b) and (c)]. When this is done, a peak labeled A [curve (b)] is commonly observed ~10 meV below the n=1 e→hh transition. The possibility that this peak is caused by exciton effects has been raised earlier.[19] Recently the proposal has been made that at $\Delta E \sim 10$ meV other mechanisms become important in the quasi-two-dimensional case.[20] Because peak A is identifiable at lower level [curve (b)] and at higher level [curve (c)], a more remote possibility is the effect discussed in Ref.21. This (peak A) is not our main concern here, however, and in any case it is possible to observe on a much smaller sample (55 μm x 170 μm) low-level emission centered right on the n=1, n'=1' transitions [curve (d), 100 W/cm^2].

More important for present purposes is the high-level emission at 77 K of the large absorption sample [curve (c), 9×10^4 W/cm^2] and that of a much smaller sample [30 μm x 235 μm, curve (e), 1.5×10^5 W/cm^2]. In both cases laser emission is observed $\Delta E \sim \hbar\omega_{LO} \simeq 36$ meV below the n=1 e→hh and n'=1' e→ℓh transitions, not ~10 meV as in Refs.20 and 21. The two large modes of curve (e) are spaced $\Delta\lambda \sim 30$ Å apart, which agrees with the sample width of ~30 μm. The much smaller mode separation of $\Delta\lambda \sim 5$ Å (at ~8280 Å) of the large absorption sample of curve (c) is at first surprising but, in fact, agrees with the sample photopumping 150-180 μm from an edge.

The AlAs-GaAs SL absorption measurements presented here, not to mention the accurate size measurements (via TEM) of the SL coupling barriers L_B and GaAs quantum wells L_z, remove any ambiguity or doubt that stimulated emission in these SL heterostructures occurs with phonon cooperation $\Delta E \sim \hbar\omega_{LO}$ below the lowest confined-particle transitions. Note that in an ordinary QWH the excess-carrier (and phonon) "filling" of the active region is ten or more times larger (because of the more compact size of the QWH active region) and thus is more prone to exhibit phonon-assisted laser operation[1-7] than even a SL.

For various contributions to this work we wish to thank K. Hess and W.D. Laidig, and for technical assistance Yuri S. Moroz, R.T. Gladin, B.L. Marshall, and B.L. Payne. The work of the Illinois group has been supported by NSF Grants No. DMR 79-09991 and No. DMR 77-23999. The work of the Rockwell group has been partially supported by ONR Contract No. N00014-78-C-0711.

REFERENCES

1. N. Holonyak, Jr., R.M. Kolbas, W.D. Laidig, M. Altarelli, R.D. Dupuis, and P.D. Dapkus, Appl. Phys. Lett. 34, 502 (1979).

2. R.M. Kolbas, N. Holonyak, Jr., B.A. Vojak, K. Hess, M. Altarelli, R.D. Dupuis, and P.D. Dapkus, Solid State Commun. 31, 1033 (1979).

3. N. Holonyak, Jr., R.M. Kolbas, W.D. Laidig, B.A. Vojak, K. Hess, R.D. Dupuis, and P.D. Dapkus, J. Appl. Phys. 51, 1328 (1980).

4. K. Hess, N. Holonyak, Jr., W.D. Laidig, B.A. Vojak, J.J. Coleman, and P.D. Dapkus, Solid State Commun. 34, 749 (1980).

5. J.J. Coleman, P.D. Dapkus, B.A. Vojak, W.D. Laidig, N. Holonyak, Jr., and K. Hess, Appl. Phys. Lett. 37, 15 (1980).

6. N. Holonyak, Jr., B.A. Vojak, W.D. Laidig, K. Hess, J.J. Coleman, and P.D. Dapkus, Appl. Phys. Lett. 37, 136 (1980).

7. W.D. Laidig, N. Holonyak, Jr., M.D. Camras, B.A. Vojak, K. Hess, J.J. Coleman, and P.D. Dapkus, Solid State Commun. 38, 301 (1981).

8. C. Weisbuch, R.C. Miller, R. Dingle, A.C. Gossard, and W. Wiegmann, Solid State Commun. 37, 219 (1981).

9. N. Holonyak, Jr., R.M. Kolbas, R.D. Dupuis, and P.D. Dapkus, IEEE J. Quantum Electron. QE-16, 170 (1980).

10. R. Dingle, comment to J.J. Coleman and P.D. Dapkus, "MO-CVD" Crystal-Growth Conference, May, 1981, Corsica, France.

11. P.D. Dapkus, J.J. Coleman, W.D. Laidig, N. Holonyak, Jr., B.A. Vojak, and K. Hess, Appl. Phys. Lett. 38, 118 (1981).

12. J.J. Coleman, P.D. Dapkus, W.D. Laidig, B.A. Vojak, and N. Holonyak, Jr., Appl. Phys. Lett. 38, 63 (1981).

13. W.D. Laidig, N. Holonyak, Jr., M.D. Camras, K. Hess, J.J. Coleman, P.D. Dapkus, and J. Bardeen, Appl. Phys. Lett. 38, 776 (1981).

14. J.J. Coleman, P.D. Dapkus, N. Holonyak, Jr., and W.D. Laidig, Appl. Phys. Lett. 38, 894 (1981).

15. B.A. Vojak, W.D. Laidig, N. Holonyak, Jr., M.D. Camras, J.J. Coleman, and P.D. Dapkus, J. Appl. Phys. 52, 621 (1981).

16. H.M. Manasevit, J. Electrochem. Soc. 118, 647 (1971).

17. R.D. Dupuis, L.A. Moudy, and P.D. Dapkus, 7th Intl. Symp. on GaAs and Related Compounds, St. Louis, 1978, ed. C.M. Wolfe (Institute of Physics, London), pp. 1-9.

18. J.J. Coleman, P.D. Dapkus, M.D. Camras, N. Holonyak, Jr., W.D. Laidig, T.S. Low, M.S. Burroughs, and K. Hess, "Absorption, Stimulated Emission, and Clustering in AlAs-$Al_xGa_{1-x}As$-GaAs Superlattices," J. Appl. Phys., to be published (R 1868).

19. B.A. Vojak, N. Holonyak, Jr., W.D. Laidig, K. Hess, J.J. Coleman, and P.D. Dapkus, Solid State Commun. 35, 477 (1980).

20. B.K. Ridley, private communication, June , 1981, Santa Barbara, Calif.

21. C.H. Henry, R.A. Logan, and F.R. Merritt, J. Appl. Phys. 51, 3042 (1980).

FIGURE CAPTIONS

Fig.1 Transmission electron microscope (TEM) image of part of a 50-period all-binary AlAs-GaAs superlattice (SL) grown by MO-CVD. The light layers are AlAs of size $L_B \sim 120$ Å; the dark layers are GaAs of size $L_z \sim 160$ Å.

Fig.2 Room temperature absorption data (a) and the lower energy ($\Delta E \sim \hbar\omega_{LO}$) cw laser emission (b) and (c) of the 50-period all-binary MO-CVD AlAs-GaAs superlattice (SL) of Fig.1. [The sample of (b) is a 40 μm x 95 μm bare SL and that of (c) is a narrower 15 μm x 415 μm bare SL.]

Fig.3 77 K absorption data (a), spontaneous emission data (b), (d), and stimulated emission data (c), (e) of the 50-period all-binary MO-CVD AlAs-GaAs superlattice (SL) of Fig.1. The data of (a), (b), and (c) are for a large "absorption sample" of size 2500 μm x 3300 μm [same sample as (a) of Fig.2]. The data of (d) are for a sample of size 55 μm x 170 μm and for (e) 30 μm x 235 μm. Note that the laser modes of (c) and (e) are $\Delta E \sim \hbar\omega_{LO} \simeq 36$ meV below the absorption of (a), which corresponds to the n=1 e→hh and n'=1' e→ℓh transitions of the SL. (Note also that the shift in peak A is only $\Delta E_A \sim 10$ meV.)

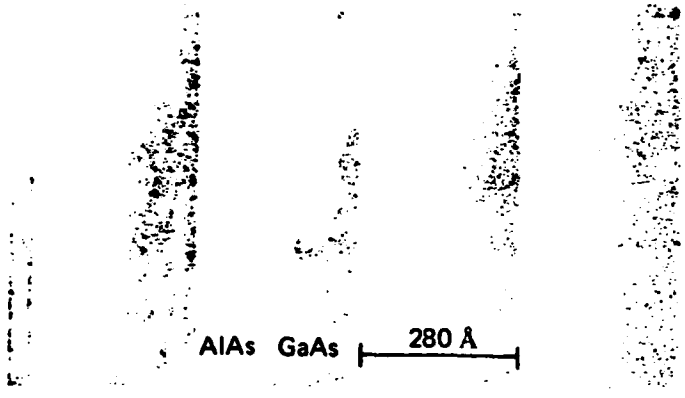

Fig. 1

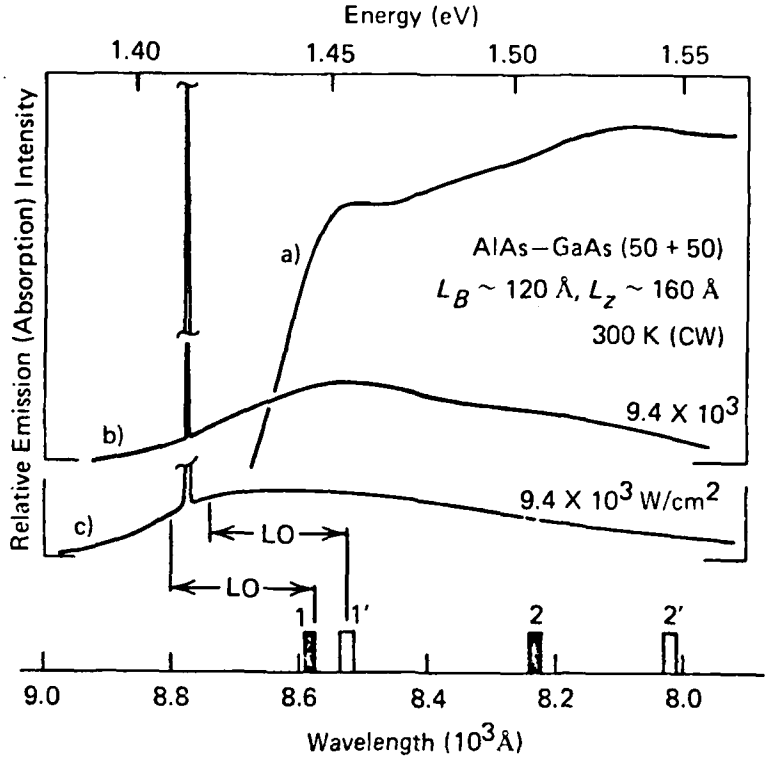
Energy (eV)
1.40
1.45
1.50
1.55
Relative Emission (Absorption) Intensity
a)
AlAs–GaAs (50 + 50)
$L_B \sim 120$ Å, $L_z \sim 160$ Å
300 K (CW)
b)
9.4×10^3
c)
9.4×10^3 W/cm^2
LO
LO
1
1'
2
2'
9.0
8.8
8.6
8.4
8.2
8.0
Wavelength (10^3Å)

Fig. 2

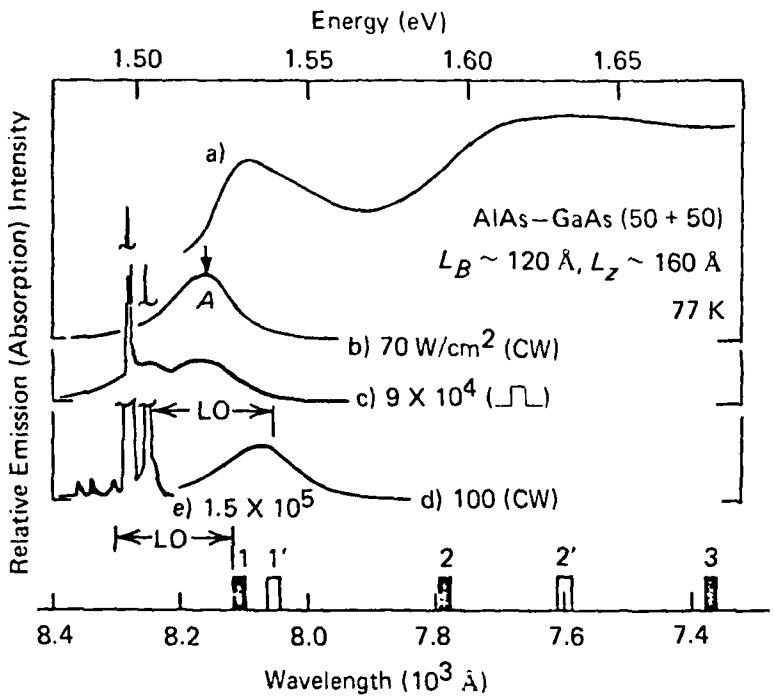
Energy (eV)
1.50
1.55
1.60
1.65
Relative Emission (Absorption) Intensity
a)
AlAs–GaAs (50 + 50)
$L_B \sim 120$ Å, $L_z \sim 160$ Å
77 K
A
b) 70 W/cm^2 (CW)
c) 9 X 10^4
LO
e) 1.5 X 10^5
d) 100 (CW)
LO
1
1'
2
2'
3
8.4
8.2
8.0
7.8
7.6
7.4
Wavelength (10^3 Å)

Fig. 3

APPENDIX IV

Laser Emission from GaAlAs/GaAs Superlattices

1. Continuous Room-Temperature Photopumped Laser Operation of Modulation-Doped $Al_xGa_{1-x}As$/GaAs Superlattices, P. D. Dapkus, J. J. Coleman, W. D. Laidig, N. Holonyak, Jr., B. A. Vojak, and K. Hess, Appl. Phys. Lett. 38, 118 (1981).

Continuous room-temperature photopumped laser operation of modulation-doped $Al_xGa_{1-x}As/GaAs$ superlattices

P. D. Dapkus and J. J. Coleman
Rockwell International, Electronics Research Center, Anaheim, California 92803

W. D. Laidig, N. Holonyak, Jr., and B. A. Vojak
Department of Electrical Engineering and Materials Research Laboratory, University of Illinois at Urbana-Champaign, Urbana, Illinois 61801

K. Hess
Department of Electrical Engineering and Coordinated Science Laboratory, University of Illinois at Urbana-Champaign, Urbana, Illinois 61801

(Received 11 August 1980; accepted for publication 22 October 1980)

The low-threshold continuous room-temperature laser operation of a photopumped metalorganic chemical vapor deposition $Al_xGa_{1-x}As$-GaAs superlattice is described. The superlattice, a bare superlattice without cladding or confining layers, consists of 25 140-Å $Al_xGa_{1-x}As$ ($x \sim 0.3$) coupling barriers doped to a level $n_d \sim 7\times10^{17}/cm^3$ and 25 alternating undoped 140-Å GaAs quantum wells. Low-temperature data (77 K) are presented indicating that the threshold for phonon-assisted recombination occurs near the excitation level at which the excess carrier density approaches the built-in carrier density $\sim 7\times10^{17}/cm^3$ of the superlattice.

PACS numbers: 42.55.Px, 72.20.Fr, 73.60.Fw, 78.55.Ds,

It has been well established that quantum-well heterostructures (QWH) can be grown by several methods and can be used to shift the laser emission of direct-gap crystals (e.g., GaAs, $Al_xGa_{1-x}As$, $In_{1-x}Ga_xP_{1-z}As_z$) well above the bulk-limit band edge. (For a review and a list of references, see Ref. 1.) It is possible in quantum well to observe laser emission from various confined-particle transitions. In addition, recombination one or two phonons below the lowest optical transitions has also been identified on photopumped $Al_xGa_{1-x}As$-GaAs QWH samples[1,2] grown by metalorganic chemical vapor deposition (MO-CVD).[3,4] Of further significance, it has been possible to operate MO-CVD $Al_xGa_{1-x}As$-GaAs QWH lasers continuously at room temperature (cw 300 K) either by photopumping or by injection.[5-7] None of these QWH lasers has employed a superlattice configuration; in addition, their active regions have been sandwiched between relatively thick ($\sim 1\ \mu m$) pairs of wide-gap confining layers that serve as low-loss waveguides and resonators. In contrast, in this letter we describe the low-threshold cw 300 K laser operation of an MO-CVD $Al_xGa_{1-x}As$-GaAs superlattice that is not enclosed between confining layers and is excited by photopumping. In other words, laser operation is described (cw 300 K) of a true artificial crystal, a bare superlattice without any form of cladding.

The MO-CVD process employed to grow the crystals of this work has been described extensively elsewhere.[3,4] In the present work the only basic difference from previous work is that the GaAs and $Al_xGa_{1-x}As$ growth rates have been reduced, to the range 2–50 Å/s for the former and 2.5–100 Å/s for the latter. This makes it practical to grow individual layers as thin as 10 Å. Also, highly accurate superlattices can be grown as shown by the slant cross section ($\sim 0.8°$ angle) of Fig. 1.

One period of the superlattice of Fig. 1 is indicated by the two closely spaced arrows in the center of the figure. The region between the two arrows labeled a represents 25 $Al_xGa_{1-x}As$ coupling barriers (light layers) of composition $x \sim 0.3$ and individual layer thickness $L_B = 140$ Å, and 25 alternating GaAs quantum wells (dark layers) of thickness

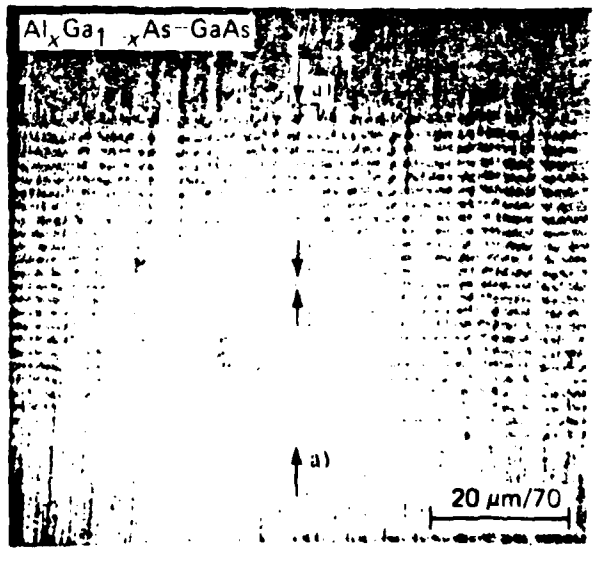

FIG. 1. Scanning electron microscope photograph of a beveled and stained cross section of a superlattice grown by MO-CVD. The shallow-angle bevel ($\sim 0.8°$) causes the layers to appear enlarged by a factor of 70. One period (shown between the center two arrows) consists of one 140-Å undoped GaAs layer and one 140-Å $Al_xGa_{1-x}As$ ($x \sim 0.30$) layer doped with Se ($n_d \sim 7\times10^{17}/cm^3$). The entire superlattice contains 25 periods and is indicated by the two arrows labeled a.

 0003-6951/81/030118-03$00.50

$L_z = 140$ Å. The edge of the topmost GaAs layer, the upper a arrow, is not visible because of the difficulty in polishing and staining a sharp corner on a $\sim 0.8°$ slant cross section. The $\sim 0.8°$ angle, however, can be measured accurately by dragging a Sloan Dektak probe across the top, flat GaAs layer and then down the slant incline.

One special feature of the superlattice shown in Fig. 1 is that the $Al_{1-x}Ga_xAs$ coupling barriers are doped with Se to a level $n_d \sim 7\times 10^{17}/cm^3$, and the GaAs layers are undoped. As a result the carriers from the donors in the GaAlAs barriers spill over into the GaAs wells where there are essentially no donors. This doping profile[8] leads to an unusually high measured mobility for the carriers in the GaAs channel layers. The detailed transport properties of such layers grown by MO-CVD will be described in a separate publication.[9] However, for the sample described here a room-temperature mobility of 5500 cm^2/V sec was measured for a concentration in the GaAs channels at $n \sim 7\times 10^{17}\ cm^{-3}$. At 77 K, the mobility was 16500 cm^2/V sec. It is expected that the coupling of these superior electronic properties with the optical properties reported here will made these materials of great interest for devices and circuits in which electronic and optical devices are integrated.

For excitation levels leading to excess carrier densities (δn) larger than the built-in carrier density of $\sim 7\times 10^{17}/cm^3$, electron relaxation into the coupled GaAs quantum wells changes and involves a noticeable shift to phonon-assisted recombination which is discussed below.

For the photopumping experiments of interest here

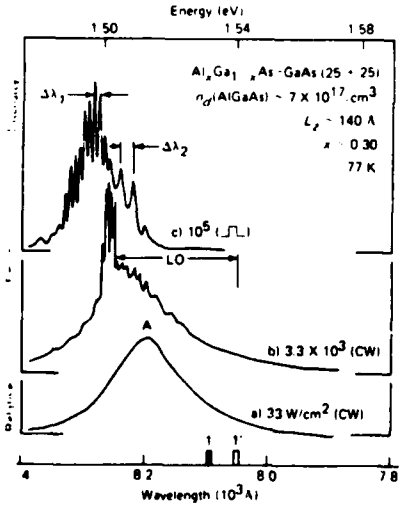

FIG. 2. Spectra (77 K) of a photopumped rectangular sample ($36\times 260\ \mu m^2$) cleaved from the superlattice shown in Fig. 1. The heavy and light markers on the horizontal axis indicate the $n = 1$ $e\rightarrow hh$ and $n' = 1'$ $e\rightarrow lh$ confined-particle transitions, respectively. Low-level cw emission (a, 33 W/cm^2) peaks (A) ~ 20 meV below the $n = 1$ transition and corresponds to the expected recombination energy of a two-dimensional electron-heavy-hole exciton. At higher excitation (b, 3.3×10^3 W/cm^2) narrowly spaced end-to-end modes ($\Delta\lambda_1$) turn on abruptly one phonon (LO label) below the $n' = 1'$ transition. Pulsed operation (c, 10^5 W/cm^2) shows clearly the $\Delta\lambda_1$ modes one phonon below the lowest transitions and the higher-energy, more widely spaced, edge-to-edge modes $\Delta\lambda_2$.

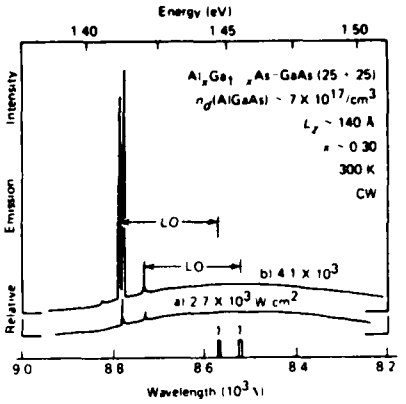

FIG. 3. Continuous room-temperature laser operation of a rectangular sample ($20\times 70\ \mu m^2$) cleaved from the superlattice wafer of Fig. 1 (substrate removed). Low-threshold laser operation (a, 2.7×10^3 W/cm^2) occurs one phonon below the $n = 1$ $e\rightarrow hh$ transition, with spontaneous background peaking in the range of the $n = 1$ and $n' = 1'$ transitions. At slightly higher excitation (b, 4×10^3 W/cm^2), closely spaced end-to-end ($\sim 70\ \mu m$) modes are clearly visible near 8780 Å.

samples are prepared by polishing and selectively etching off the GaAs substrate,[10] which, for the wafer of Fig. 1, is the region under the bottom a arrow. Rectangular samples (30–100×100–$300\ \mu m^2$) are cleaved from the remaining thin wafer (0.7 μm), i.e., the region between the a arrows of Fig. 1, and for heat sinking are imbedded into In under sapphire windows for 77-K experiments and in Cu under diamond windows for 300-K experiments. The samples are photopumped with an argon laser (5145 Å) that can be operated pulsed (cavity dumped) or continuously (cw), and can be conveniently focused at various positions on the samples (for any advantage in excitation geometry).

The laser operation at 77 K of a $36\times 260\ \mu m^2$ rectangular superlattice sample cleaved from the wafer of Fig. 1 is shown in Fig. 2. At low level (a, 33 W/cm^2), the recombination radiation peaks (A) in the region ~20 meV below the $n - 1$ $e\rightarrow hh$ transition. The peak A lies in the region expected of the two-dimensional exciton,[11] and with increased pumping broadens and tends to exhibit stimulated emission on the widely spaced edge-to-edge modes labeled $\Delta\lambda_2$ corresponding to $l = 36\ \mu m$ in the mode-spacing expression

$$\Delta\lambda = \lambda^2\left[2l\left(\frac{n-\lambda dn}{d\lambda}\right)\right]^{-1}. \tag{1}$$

Near the pumping level of $\sim 3.3\times 10^3$ W/cm^2 (b), however, end-to-end laser modes ($\Delta\lambda_1, l = 260\ \mu m$) appear abruptly in the range $\hbar\omega_{LO}$ below the $n' = 1'$ $e\rightarrow 1h$ transition (E_1') and with increased pumping level ($b\rightarrow c$) extend to still lower energy, to $\hbar\omega \lesssim E_1' - \hbar\omega_{LO}$. We suggest, by considering a simple charge analysis or

$$\delta n = \tau J/(\tfrac{1}{2}qL) \sim 2.4\times 10^{26}\,\tau/cm^3, \tag{2}$$

that the end-to-end modes $\Delta\lambda_1$ of curve (b) appear abruptly, at $J \sim 3.3\times 10^3 (2.41)^{-1}$ A/cm^2, when the excess carriers δn approach (and exhaust) the built-in carrier supply of $\sim 7\times 10^{17}/cm^3$. In Eq. (2), L is the thickness of the sample ($L = 0.7\ \mu m$), q is the elementary charge, and τ is the excess-carrier lifetime, which these data indicate is $\tau \sim 3\times 10^{-9}$ sec

near the threshold (curve b) for end-to-end phonon-assisted laser operation.[2] (We mention that in the case of a narrower sample, 11-μm, it is possible to observe stimulated emission [77 K, data not shown] distinctly on peak A, $\sim$8200 Å, and also on the $n = 1$ $e \rightarrow hh$ transition, $\sim$8095 Å.)

Perhaps of greater practical interest, the bare superlattice of Fig. 1 easily operates as a cw 300-K photopumped laser. This laser operation is shown in Fig. 3, with threshold occurring at an equivalent current density of $J_{equiv} \sim 10^3$ A/cm^2. The spontaneous background emission peaks in the range of the $n = 1$ $e \rightarrow hh$ and $n' = 1'$ $e \rightarrow 1h$ transitions as expected, while laser operation occurs one phonon ($\hbar\omega_{LO}$) below these transitions. As in Fig. 2, the sample of Fig. 3 is a rectangle, and two different sets of modes and two different mode spacings occur. The more widely spaced edge-to-edge modes are seen to modulate the narrow end-to-end modes. This behavior is characteristic of phonon-assisted recombination in a thin rectangle.[2] The sample length in the end-to-end direction is 70 μm, which corresponds to a resonator end loss of $\alpha \sim 170$ cm^{-1}. A typical stripe-configuration diode has a resonator length of $l \sim 250$ μm and an end loss $\alpha \sim 47$ cm^{-1}. Thus it is reasonable to speculate that stripe-configuration superlattice laser diodes will operate as lasers well below the equivalent threshold current-density $J_{equiv} \sim 10^3$ A/cm^2 of Fig. 3, or well below the photopumping input power of 25 mW ($I_{equiv} \sim 10$ mA) that has been easily realized in this work in spite of surface losses.

The authors are grateful to Y. S. Moroz, R. T. Gladin, B. L. Marshall, and M. Suits (Urbana) for techanical assistance and to G. E. Stillman for various discussions. The work of the Rockwell group has been partially supported by the Office of Naval Research, Contract No. N00014-78-C-0711; the work of the Illinois group has been supported by NSF, Grant No. DMR 77-23999 and DMR 79-09991 and Navy Contract No. N00014-79-C-0768.

[1] N. Holonyak, Jr., R. M. Kolbas, R. D. Dupuis, and P. D. Dapkus, IEEE J. Quantum Electron. QE-16, 170 (1980).
[2] N. Holonyak, Jr., R. M. Kolbas, W. D. Laidig, B. A. Vojak, K. Hess, R. D. Dupuis, and P. D. Dapkus, J. Appl. Phys. 51, 1328 (1980).
[3] H. M. Manasevit, J. Electrochem. Soc. 118, 647 (1971).
[4] R. D. Dupuis and P. D. Dapkus, in *7th International Symposium on GaAs and Related Compounds, St. Louis*, 1978, edited by C. M. Wolfe (Institute of Physics, London, 1979), pp. 1–9.
[5] R. D. Dupuis, P. D. Dapkus, R. Chin, N. Holonyak, Jr., and S. W. Kirchoefer, Appl. Phys. Lett. 34, 265 (1974).
[6] R. D. Dupuis, P. D. Dapkus, N. Holonyak, Jr., and R. M. Kolbas, Appl. Phys. Lett. 35, 487 (1979).
[7] B. A. Vojak, N. Holonyak, Jr., W. D. Laidig, K. Hess, J. J. Coleman, and P. D. Dapkus, J. Appl. Phys. (to be published).
[8] R. Dingle, H. L. Stormer, A. C. Gossard, and W. Wiegmann, Appl. Phys. Lett. 33, 665 (1978).
[9] P. D. Dapkus and J. J. Coleman (unpublished).
[10] R. A. Logan and F. K. Reinhart, J. Appl. Phys. 44, 4172 (1973).
[11] B. A. Vojak, N. Holonyak, Jr., W. D. Laidig, K. Hess, J. J. Coleman, and P. Dapkus, Solid State Commun. 35, 477 (1980).

APPENDIX V

Diffusion-Enhanced Disorder of Superlattices

1. Disorder of an AlAs-GaAs Superlattice by Impurity Diffusion, W. D. Laidig, N. Holonyak, Jr., M. D. Camras, K. Hess, J. J. Coleman, P. D. Dapkus, and J. Bardeen, Appl. Phys. Lett. 38, 776 (1981).
2. IR-red GaAs-AlAs Superlattice Laser Monolithically Integrated in a Yellow-gap Cavity, N. Holonyak, Jr., W. D. Laidig, M. D. Camras, J. J. Coleman, and P. D. Dapkus, Appl. Phys. Lett. 39, 102 (1981).

Disorder of an AlAs-GaAs superlattice by impurity diffusion

W. D. Laidig, N. Holonyak, Jr., and M. D. Camras
Electrical Engineering Research Laboratory[a] and Materials Research Laboratory, University of Illinois at Urbana-Champaign, Urbana, Illinois 61801

K. Hess
Electrical Engineering Research Laboratory[a] and Coordinated Science Laboratory, University of Illinois at Urbana-Champaign, Urbana, Illinois 61801

J. J. Coleman and P. D. Dapkus
Rockwell International, Electronics Research Center, Anaheim, California 92803

J. Bardeen
Department of Physics, University of Illinois at Urbana-Champaign, Urbana, Illinois 61801

(Received 20 January 1981; accepted for publication 24 February 1981)

Data are presented showing that Zn diffusion into an AlAs-GaAs superlattice (41 $L_z \sim 45$-Å GaAs layers, 40 $L_B \sim 150$-Å AlAs layers), or into $Al_xGa_{1-x}As$-GaAs quantum-well heterostructures, increases the Al-Ga interdiffusion at the heterointerfaces and creates, even at low temperature (< 600 °C), uniform compositionally disordered $Al_xGa_{1-x}As$. For the case of the superlattice, the diffusion-induced disordering causes a change from direct-gap AlAs-GaAs ($E_g \sim 1.61$ eV) to indirect-gap $Al_xGa_{1-x}As$ ($x \sim 0.77$, $E_{gX} \sim 2.08$ eV).

PACS numbers: 61.70.Bv, 78.45. + h, 64.70.Kb, 81.40.-z

Because the AlAs-$Al_xGa_{1-x}As$-GaAs system is effectively lattice-matched at all compositions ($0 \leq x \leq 1$) and can be grown by a variety of methods, it has been extensively developed and has served as the practical and prototype system for various forms of heterostructures. Essentially abrupt heterojunctions or heterointerfaces can be formed in this III-V system and apparently are stable to quite high temperatures. For example, Chang and Koma[1] have shown that appreciable Al-Ga interdiffusion, or cross diffusion, at initially an AlAs-GaAs interface requires a high temperature. The activation energy for Al and Ga interdiffusion is high (> 3.6 eV) and the diffusion constants small.[1] These earlier results have recently been confirmed by thermal annealing experiments (875–925 °C, excess As in the diffusion ampoule)[2,3] performed on a number of $Al_xGa_{1-x}As$-GaAs quantum-well heterostructures (QWH) grown by metalorganic chemical vapor deposition (MO-CVD).[4,5] In contrast to the results of impurity-free thermal annealing experiments,[1-3] we show in this letter that Zn diffusion into an $Al_xGa_{1-x}As$-GaAs QWH causes, at much lower temperatures (more than 300 °C lower), Al-Ga interdiffusion. We show, by diffusing Zn into an AlAs-GaAs superlattice (500–600 °C), that an AlAs-GaAs or $Al_xGa_{1-x}As$-GaAs heterointerface becomes unstable and disorders (Al-Ga disorders) at temperatures as low as $\lesssim 500$ °C when a large hole population accumulates in the GaAs.

Various QWH's grown (750 °C) by MO-CVD (Refs. 4 and 5) have been employed in the present work. Data are shown here, however, on only an AlAs-GaAs superlattice, initially undoped, that consists of 41 $L_z \sim 45$-Å GaAs layers alternating with 40 $L_B \sim 150$-Å AlAs coupling layers. With the substrate removed the bare superlattice (heat sunk under diamond)[6] operates as a low-threshold cw, 300-K photopumped laser as shown in Fig. 1. This superlattice crystal and data are unique, showing that the 80 interfaces of the 0.8-μm thick superlattice are essentially ideal. Otherwise the low-threshold laser operation ($J \sim 1.5 \times 10^3$ A/cm^2, cw, 300 K) of Fig. 1 would be impossible.

When this MO-CVD wafer is converted to p type by conventional Zn (+ As) diffusion ($ZnAs_2$, 575 °C, 4 h) in an evacuated silica ampoule,[7-9] the superlattice (substrate removed) appears yellow in color and not dull red as initially, remains single crystalline as determined by x-ray analysis, cleaves into {100} rectangles, but yields little photoluminescence output because it has become disordered into indirect-gap $x \sim 0.77$ $Al_xGa_{1-x}As$ ($E_{gX} \sim 2.08$ eV). Note that this "phase" transition from order to disorder, from direct to indirect gap, occurs far below the thermal-annealing tem-

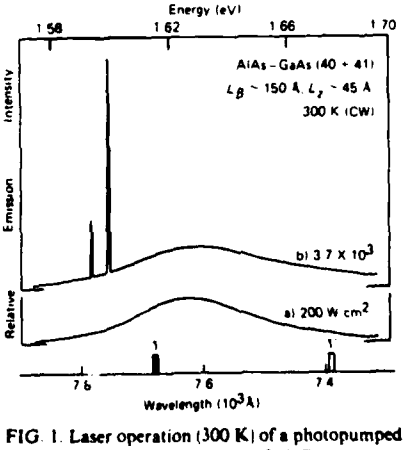

FIG. 1. Laser operation (300 K) of a photopumped MO-CVD superlattice sample (15 μm wide) consisting of 41 GaAs quantum wells ($L_z \sim 45$ Å) alternating with 40 AlAs coupling barriers ($L_B \sim 150$ Å). At relatively low excitation power density [(*a*) 200 W/cm^2] the emission peaks near the lowest-energy electron-to-heavy-hole transition ($n = 1, e \rightarrow hh$) calculated using the Kronig-Penney approximation (Ref. 13). With higher excitation [(*b*) 3.7×10^3 W/cm^2 or $\sim 1.5 \times 10^3$ A/cm^2] cw, 300-K laser operation is observed (~ 7750 Å) in spite of the 80 heterointerfaces.

[a]In the Department of Electrical Engineering, University of Illinois at Urbana-Champaign.

 0003-6951/81/100776-03$00.50

peratures employed in Ref. 1. For comparison we show in Fig. 2 the photoluminescence behavior (laser operation, 77 K) of (a) an as-grown bare-superlattice sample and (b) a similar sample but first annealed for 4 h at 575 °C without Zn but with excess As in the evacuated silica ampoule.[1] The laser operation does not change. It is clear that it is the Zn introduced by diffusion into the AlAs-GaAs superlattice that changes the crystal to compositionally disordered indirect-gap $x \sim 0.77$ $Al_xGa_{1-x}As$.

For a Zn diffusion time of 4 h at 575 °C in bulk GaAs, $(D_{Zn}t)^{1/2} \sim 1\ \mu m$ ($N_{Zn} \sim 4\times10^{19}/cm^3$).[9] In contrast, Zn diffusion at 575 °C as outlined above penetrates 80% of the thickness of the superlattice of this work in 10 min, which, because of the ampoule thermal inertia, corresponds to an actual diffusion time of 5–7 min.[8,10] These results, shown in Fig. 3 as Zn-diffused stripes through 10-μm-wide openings in a Si_3N_4 surface mask, indicate that the diffusion through the AlAs layers is much faster than through the GaAs layers. In fact, $[D_{Zn}(GaAs)t]^{1/2} \sim 41\times45$ Å at 575 °C ($D_{Zn} \sim 8.3\times10^{-13}$ cm²/s)[9] leads to $t \sim 6.5$ min. These results suggest that it is the GaAs in $Al_xGa_{1-x}As$ that controls the diffusion and that the Zn diffusion depth data of others[11] can be fit if a factor of $(1-x)^{-1}$, $0 \leqslant x \leqslant 0.7$, is applied.

The main point of Fig. 3, however, is to show that where Zn is diffused into the superlattice, the crystal becomes compositionally disordered $Al_xGa_{1-x}As$, and where the Zn does not penetrate by diffusion or is blocked by the Si_3N_4 mask, the superlattice remains intact. This is particularly clear in the magnified slant cross section (~0.4 °, 145× in vertical direction, not aligned with the stripe) of Fig. 3(b),[12] which shows that the Zn in the stripe region did not diffuse beyond the last seven or eight periods of the superlattice (actually the first seven or eight periods grown on the substrate). In fact, where the Zn concentration decreases appreciably, i.e., in the region of the 8–12 periods above the substrate, the Zn-induced disordering is not complete.

The fact that diffusion of Zn greatly enhances the interdiffusion of Ga and Al in the superlattice heterostructures indicates that a modification of the interstitial-substitutional mechanism for Zn diffusion[7,8] is required. It is suggested that a closely associated Zn-vacancy pair formed by substitutional Zn moving into a neighboring interstitial site forms an intermediate link between purely interstitial and substitutional Zn according to the reactions

$$Zn_i^+ + V^0 \rightleftarrows (Zn_i, V)^+ \rightleftarrows Zn_s^- + 2h^+. \quad (1)$$

Here V^0 indicates a neutral vacancy and h a hole. Neighboring Ga and Al atoms could move into the vacancy of the (Zn_i, V) pair, but the Zn_i would remain attached. In this way, interdiffusion of Ga and Al would be promoted as well as provide an additional mechanism for Zn diffusion.

The total Zn concentration is $c = c_i + c_p + c_s$, where c_i is that of isolated Zn interstitials, c_p that of (Zn_i, V) pairs and c_s that of substantial Zn. It is assumed that $c_i \ll c_p \ll c_s$, so that $c_s \cong c$. According to the laws of mass action,

$$c_p = K_1(T)c_ip^2 = K_2(T)cc_v, \quad (2)$$

where c_v is the concentration of isolated neutral vacancies. If the motion of pairs dominates the Zn diffusion, the diffusion rate should be proportional to the square root of the As_2 vapor pressure, $p_{As_2}^{1/2}$. Data[8] on the Zn diffusion in GaAs at higher temperature (here extended to $Al_xGa_{1-x}As$) indicate that D_{eff} varies inversely with $p_{As_2}^{1/2}$, which shows that interstitial diffusion of Zn in GaAs-bearing III-V alloys dominates over pair diffusion. However, pairs are required to account for the observed enhancement of interdiffusion of Ga and Al.

Diffusion by (Zn_i, V) pairs has the same Zn concentration dependence as that by the interstitial Zn mechanism. In

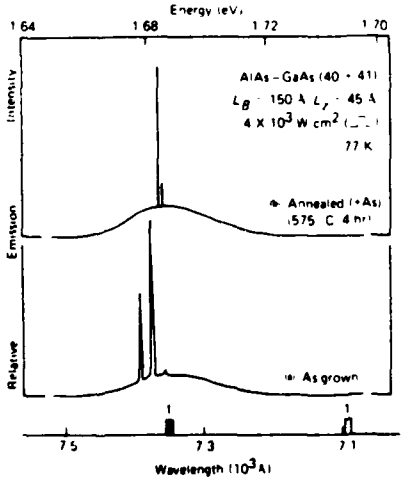

FIG. 2. Laser spectra (77 K) of (a) an as-grown AlAs-GaAs superlattice sample (same crystals as Fig. 1) and (b) a thermally annealed comparison sample (575 °C, 4 h, excess As in ampoule). The emission spectra (a) and (b) are nearly identical. The emission line shape is broadened only slightly because of small size fluctuations (on the order of a monolayer) in the layer thicknesses. The emission is peaked at the expected $n = 1$, $e \rightarrow hh$ transition.

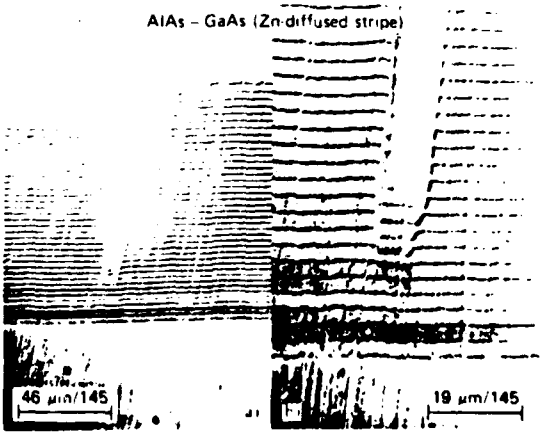

FIG. 3. Shallow-angle (~0.4 °) cross section of a portion of the superlattice wafer of Figs. 1 and 2 that, except for a ~10-μm stripe, has been masked with Si_3N_4 and has been Zn diffused ($ZnAs_2$) for 10 min at 575 °C. The shallow-angle magnification is ~145× in the vertical direction (no horizontal magnification) and is skewed somewhat relative to the orientation of the Zn-diffused stripe. In the region of the Zn diffusion the 40-period superlattice ($L_z \sim 45$ Å, $L_B \sim 150$ Å) has become compositionally disordered indirect-gap $x \sim 0.77$ $Al_xGa_{1-x}As$ that changes color from dull red to yellow (7680–5960 Å).

this case it follows from electrical neutrality that $p = c_1$, so that D_{Zn} varies as p^2 or c_1^2. While this must be true on the average in the superlattice structures, the concentration of holes will be enhanced in the GaAs quantum wells and decreased in the adjacent AlAs layers. The band-edge discontinuity for holes is $\sim 0.15\Delta E_\Gamma \sim 0.24$ eV at the start of the diffusion process and, depending upon the AlAs-GaAs layer widths, the enhancement may be as large as $\lesssim 10$ (superlattice above). This enhancement of the hole concentration will in turn tend to greatly increase the diffusion rate in the GaAs layers and decrease it in the AlAs layers. Since Zn diffusion is normally much more rapid in AlAs than in GaAs, the enhanced hole concentration in the GaAs layers will increase the overall Zn diffusion rate in the superlattice structures.

The accumulation of holes near the GaAs-AlAs boundaries also will enhance the interdiffusion of Ga and Al and account for the observed rapid formation of homogeneous $Al_xGa_{1-x}As$. This could not occur by the interstitial-substitutional mechanism because interstitials diffusing at the advancing impurity front would tend to move into vacant sites and reduce rather than increase their number. The vacancy concentration in the absence of Zn can be enhanced by increasing the As_2 vapor pressure at the diffusion temperatures. This increase gives only a modest increase in the rate of interdiffusion of Ga and Al at much higher temperatures. The rapid interdiffusion is observed only in the presence of Zn. We believe that these are strong arguments for the formation of (Zn_i, V) pairs and for their participation in Al-Ga interdiffusion, at least in the temperature range of 500–600 °C, where the present experiments have been done.

The effects described above occur at AlAs-GaAs or $Al_xGa_{1-x}As$-GaAs heterointerfaces and, just as shown in Fig. 3, have been observed in the present work at all Zn-diffusion temperatures employed, including at temperatures as low as 500 °C (9 h to disorder the superlattice). These results indicate that the doping in AlAs-$Al_xGa_{1-x}As$-GaAs heterostructure active regions should be kept $< 10^{19}/cm^3$.

We are grateful to Y. S. Moroz, R. T. Gladin, B. L. Marshall, and B. L. Payne (Urbana) for technical assistance, and B. A. Vojak for helpful discussions. The work of the Illinois group has been supported by NSF Grants No. DMR 79-09991 and No. DMR 77-23999 and Navy Contract No. N00014-76-C-0708. The work of the Rockwell group has been partially supported by ONR, Contract No. N00014-78-C-0711.

[1] L. L. Chang and A. Koma, Appl. Phys. Lett. **29**, 138 (1976). See also R. M. Fleming, D. B. McWhan, A. C. Gossard, W. Wiegmann, and R. A. Logan, J. Appl. Phys. **51**, 357 (1980).
[2] W. D. Laidig, N. Holonyak, Jr., M. D. Camras, B. A. Vojak, K. Hess, J. J. Coleman, and P. D. Dapkus, Solid State Commun. (to be published).
[3] W. D. Laidig, N. Holonyak, Jr., M. D. Camras, J. J. Coleman, and P. D. Dapkus (unpublished).
[4] H. M. Manasevit, J. Electrochem. Soc. **118**, 647 (1971).
[5] R. D. Dupuis and P. D. Dapkus, *7th International Symposium on GaAs and Related Compounds, St. Louis, 1978*, edited by C. M. Wolfe (Institute of Physics, London, 1979), pp. 1–9.
[6] N. Holonyak, Jr., R. M. Kolbas, R. D. Dupius, and P. D. Dapkus, IEEE J. Quantum Electron. **QE-16**, 170 (1980).
[7] D. L. Kendall, in *Semiconductors and Semimetals*, Vol. 4, edited by R. K. Willardson and A. C. Beer (Academic, New York, 1968), pp. 163–259.
[8] H. C. Casey, in *Atomic Diffusion in Semiconductors*, edited by D. Shaw (Plenum, New York, 1973), pp. 351–430.
[9] Y. Yamamoto and H. Kanabe, Jpn. J. Appl. Phys. **19**, 121 (1980).
[10] E. A. Rezek, P. D. Wright, and N. Holonyak, Jr., Solid-State Electron. **21**, 325 (1978).
[11] C. P. Lee, S. Margalit, and A. Yariv, Solid-State Electron. **21**, 905 (1978).
[12] N. Holonyak, Jr., B. A. Vojak, R. M. Kolbas, R. D. Dupuis, and P. D. Dapkus, Solid-State Electron. **22**, 431 (1979).
[13] B. A. Vojak, W. D. Laidig, N. Holonyak, Jr., M. D. Camras, J. J. Coleman, and P. D. Dapkus, J. Appl. Phys. **52**, 621 (1981).

IR-red GaAs-AlAs superlattice laser monolithically integrated in a yellow-gap cavity

N. Holonyak, Jr., W. D. Laidig, and M. D. Camras
Electrical Engineering Research Laboratory and Materials Research Laboratory, University of Illinois at Urbana-Champaign, Urbana, Illinois 61801

J. J. Coleman and P. D. Dapkus
Rockwell International, Electronics Research Center, Anaheim, California 92803

(Received 5 March 1981; accepted for publication 9 April 1981)

Disk-shaped IR-red ($E_g \sim 1.61$ eV) GaAs-AlAs superlattice lasers (41 $L_z \sim 45$-Å GaAs layers, 40 $L_B \sim 150$-Å AlAs layers) are demonstrated (cw 300 K) that are monolithically integrated into rectangular yellow-gap $Al_xGa_{1-x}As$ [$x \sim L_B/(L_z + L_B)$, $E_{gx} \sim 2.08$ eV] cavities. The yellow-gap $Al_xGa_{1-x}As$ ($x \sim 0.77$) is generated by low-temperature Zn diffusion (575 °C, 30 min), which disorders selected portions of the superlattice [portions complementary to regions (disks) masked by Si_3N_4]

PACS numbers: 81.40.−z, 78.20.−e, 78.45.+h, 77.40.+k

Various forms of double-heterostructure[1] (DH) and quantum-well heterostructure (QWH) lasers[2] are capable of room-temperature continuous (cw 300 K) operation. Recently we have shown that bare superlattices of metalorganic chemical vapor deposited (MO-CVD) GaAs-$Al_xGa_{1-x}As$[3] or GaAs-AlAs[4] are capable of cw 300-K laser operation. The latter, taken with the fact that a superlattice (SL), or QWH, can be selectively disordered by low-temperature (500–600 °C) impurity diffusion,[4] leads to a special capability. A wide variety of infrared (IR) or red lasers, and potentially other lower-gap device elements, can be imbedded (monolithically integrated) into a higher-gap red, orange, or even yellow cavity, thus establishing a basis for an optoelectronic "chip." In this paper we demonstrate IR-red (1.61 eV) disk-shaped GaAs-AlAs SL lasers imbedded in rectangular single-crystal yellow-gap $Al_xGa_{1-x}As$ ($x \sim 0.77$, $E_{gx} \sim 2.08$ eV) cavities, the yellow-gap $Al_xGa_{1-x}As$ is the compositionally disordered form of the as-grown SL crystal.

The superlattice, or quantum-well heterostructure (QWH), crystals of interest here have been grown by the basic MO-CVD process described extensively elsewhere.[5,6] This system of crystal growth proves to be advantageous also for the growth of high-quality GaAs-AlAs QWH's[7] and superlattices (SL's).[4] For the present work a SL with 41 $L_z \sim 45$-Å GaAs layers coupled by 40 $L_B \sim 150$-Å AlAs layers is employed. This MO-CVD SL crystal is special in two respects: (i) Although it is an ordered structure, a SL, with a coupled quantum-well direct-gap of $E_g \sim 1.61$ eV, as disordered $Al_xGa_{1-x}As$ its average composition is $x \sim 0.77$ [$x \sim L_B/(L_z + L_B)$], and (ii) it can be disordered, in any desired geometrical pattern, by relatively low-temperature impurity diffusion.[4] Then the SL becomes compositionally disordered $Al_xGa_{1-x}As$ with its energy gap changed from $E_g \sim 1.61$ to $E_{gx} \sim 2.08$ eV, or from dull red to yellow.

Ordinarily Al-Ga interdiffusion in the temperature range 500–600 °C is negligible,[8] but not when Zn is diffused, even at a low temperature, into an AlAs-GaAs SL or QWH.[4] The Zn, which diffuses by an interstitial-substitutional process,[9,10] establishes an acceptor concentration $\gtrsim 10^{19}/cm^3$. If the Zn, occupying a column III vacancy site, is viewed as a closely associated Zn-vacancy molecule, then at 500–600 °C there is sufficient thermal energy for the Zn to spend part time in an interstitial site.[4] This makes available an unusually large vacancy concentration to take part in, *and enhance*, Al-Ga interdiffusion.[4] Thus, at low temperature (in any pattern desired), a GaAs-AlAs or GaAs-$Al_xGa_{1-x}As$ SL or QWH can be fully disordered and, depending upon the GaAs layer thickness L_z and the L_z/L_B ratio, can be increased in energy gap or even be shifted, as here, from direct gap to indirect gap.

Typical results obtained on the 40 period GaAs-AlAs SL are shown in Fig. 1. This wafer, with red "polka-dot" SL disks in/on a yellow $Al_xGa_{1-x}As$ background, has been prepared by a 30-min $ZnAs_2$ diffusion (at 575 °C) on the MO-CVD SL[4] after it is first masked (via KPR) with 38-μm Si_3N_4 disks located on 76-μm centers. After the Zn diffusion, the SL wafer is stripped of the Si_3N_4, the substrate is thinned by polishing and finally removed by selective etching, and the wafer is then cleaved and a sample compressed into In to make possible the colored photograph of Fig. 1. Any one of the disks can be photopumped (Ar$^+$ laser, 5145 Å) and be operated as a red laser. For a SL disk near the wafer edge (Fig. 1), the edge acts as one Fabry–Perot reflector, and an inner disk can act as a second reflector. A large part of the cavity is nonabsorbing yellow-gap $Al_xGa_{1-x}As$. Clearly the active region geometry can be designed independent of that of the cavity.

Figure 2 shows, also in color, rectangular samples cleaved from the masked and diffused 40-period SL wafer of this work; the samples are compressed under a diamond window into an annealed Cu heat sink. Scratches in the metal and room dust are evident in the figure. In Fig. 3 we show cw 300-K laser data for the SL full-disk labeled (1) in Fig. 2 and the partial disk labeled (2) that, unlike (1), lies at one end of a cleaved rectangle. Superlattice disk (1) is surrounded by yellow-gap $Al_xGa_{1-x}As$ and operates as a laser as shown in Fig. 3 by curves (a) and (b). The low-level emission (*a*, 95 W/cm^2 excitation level) is rather well centered at the expect-

 0003-6951/81/130102-03$00.50

AD-A108 390 ROCKWELL INTERNATIONAL THOUSAND OAKS CA MICROELECTR--ETC F/G 20/7
ELECTRONIC TRANSPORT IN ULTRATHIN HETEROSTRUCTURES,(U)
OCT 81 P D DAPKUS N00014-78-C-0711
UNCLASSIFIED MRDC40129 NL

END
DATE FILMED
1 82
DTIC

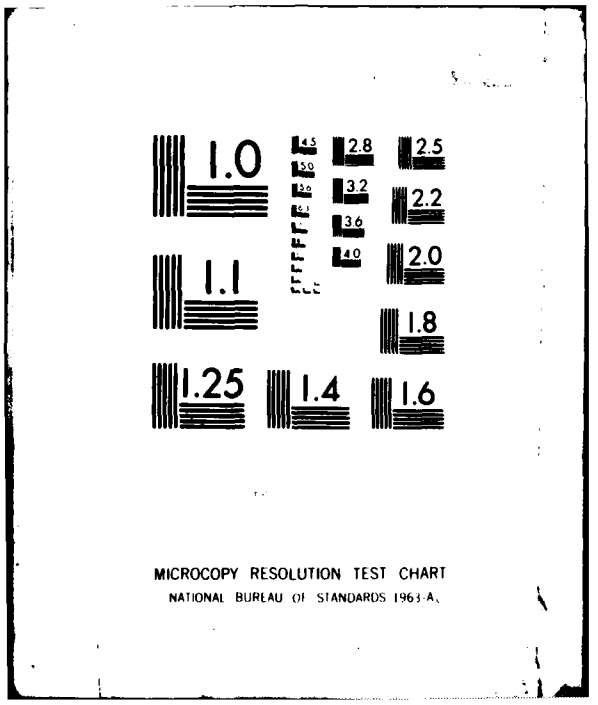
1.0
1.1
1.25
1.4
1.6
1.8
2.0
2.2
2.5
2.8
3.2
3.6
4.0
MICROCOPY RESOLUTION TEST CHART
NATIONAL BUREAU OF STANDARDS 1963-A

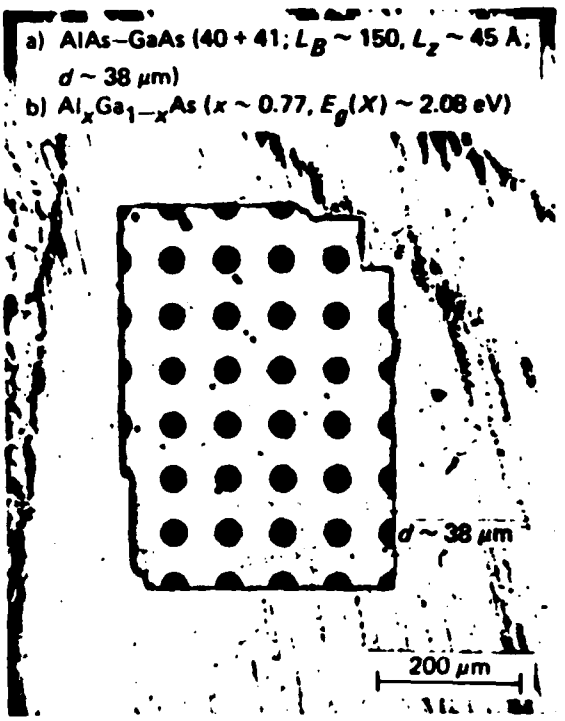

FIG. 1. "Polka-dot" pattern of (a) GaAs-AlAs superlattice (41 $L_z \sim 45$-Å GaAs layers, 40 $L_B \sim 150$-Å AlAs layers) disks (38 μm diameter on 76 μm centers) surrounded by (b) yellow-gap $Al_xGa_{1-x}As$ [$x \sim L_B/(L_z + L_B) \sim 0.77$, $E_{gx} \sim 2.08$ eV] that is formed by disordering, via low-temperature Zn diffusion (575 °C, 30 min), a portion of the original as-grown 40-period (40 × 195 Å) superlattice.

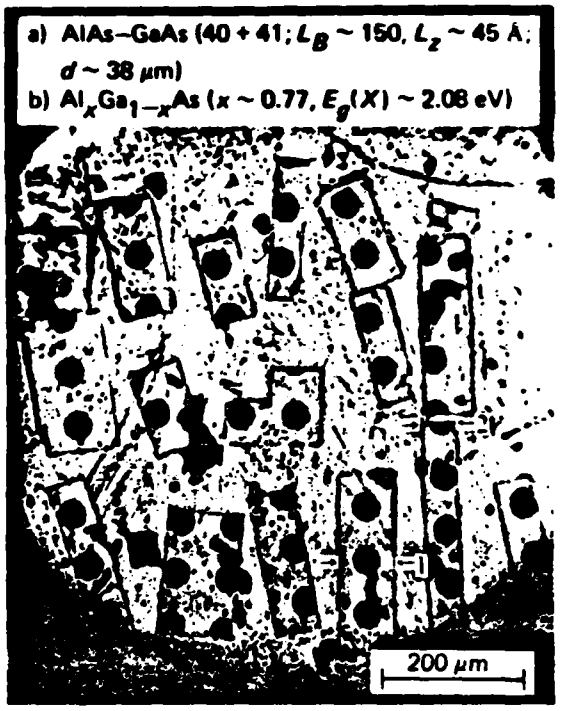

FIG. 2. Cleaved (100) samples of (a) IR-red GaAs-AlAs superlattice disks ($E_g \sim 1.61$ eV) "monolithically integrated" into (b) yellow-gap $Al_xGa_{1-x}As$ ($E_{gx} \approx 2.08$ eV) rectangular cavities (see Fig. 1). The single-crystal samples are compressed under a diamond window into annealed copper for cw 300-K photopumping (Ar^+ laser, 5145 Å).

ed $n = 1$ electron-to-heavy-hole ($e \rightarrow hh$) confined-particle transition (dark marker). At 7.5×10^3 W/cm^2 (or $J \sim 3.1 \times 10^1$ A/cm^2) cw 300-K laser operation is observed $\sim \hbar\omega_{LO}$ below the $n = 1$ $e \rightarrow hh$ transition. The mode spacing $\Delta\lambda_1 \approx 10.5$ Å corresponds quite accurately to the cavity length of 80 μm between the arrows (38 μm of SL disk and 23 + 19 μm of yellow $Al_xGa_{1-x}As$).

Perhaps more interesting is the laser operation (Fig. 3, curve c, 7.5×10^1 W/cm^2) of the SL half-disk (2) of Fig. 2 that is only partly surrounded by yellow-gap $Al_xGa_{1-x}As$. The ten uniformly spaced cavity modes $\Delta\lambda_2 \approx 16$ Å correspond to the cavity length of 52 μm between the arrows. These modes are modulated or grouped with a spacing $\Delta\lambda_1 \sim 60$ Å, which corresponds to a cavity reflection occurring over a length ~ 14 μm. This agrees with the measured width of the partial SL disk (2). It is evident that reflection exists at the red-yellow interfaces and can be detected if enough modes are excited. The problem of the red-yellow index change Δn is unsolved. We estimate this change, however, as the difference between the refractive index for $Al_xGa_{1-x}As$,[11]

$$n(x) = 3.590 - 0.710x + 0.091x^2, \quad (1)$$

corresponding to an energy gap of $E_g \approx 1.61$ eV, or simulated

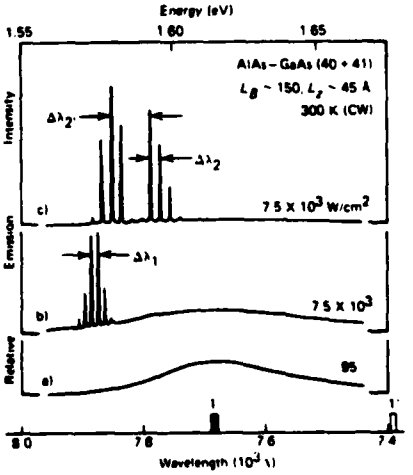

FIG. 3. Continuous 300-K laser spectra of superlattice disk (1) in Fig. 2 (curves a and b) and superlattice partial disk (2) (curve c). The mode spacing $\Delta\lambda_1 \sim 10.5$ Å of curve (b) corresponds to the yellow cavity edge-to-edge width of ~ 80 μm marked by the arrows in Fig. 2. The $\Delta\lambda_2 \sim 16$-Å mode spacing of curve c corresponds to an edge-to-edge width of ~ 52 μm (two arrows of Fig. 2). The $\Delta\lambda_2' \sim 60$-Å spacing agrees with the 14-μm transverse width of the partial disk labeled (2).

composition $x \sim 0.15$, and $E_{gX} \sim 2.08$ eV ($x \sim 0.77$), giving $\Delta n = 0.39$. We do not take this estimate too seriously except to suggest, in agreement with experimental observations (300 and 77 K), that the red-yellow reflection (or Δn) is significant.

The laser data presented here are of the same quality as the data obtained on the as-grown, unmodified SL crystal.[4] Thus there is no question that the conversion of a GaAs-AlAs SL, or of a QWH, to $Al_x Ga_{1-x}As$ can be accomplished without modifying or damaging protected or masked regions of the as-grown crystal. The results presented here make it clear that it is possible to integrate into a wider gap optoelectronic "chip" a large variety of narrower-gap elements, and that these can be also current-driven elements and not just the photopumped disks utilized (for convenience) in this work.

We wish to thank Y. S. Moroz, R. T. Gladin, B. L. Marshall, and B. L. Payne (Urbana) for technical assistance, J. Bardeen, T. A. DeTemple, K. Hess, and G. E. Stillman for helpful discussions, and D. E. Hill and D. L. Keune for various photomasks. The work of the Illinois group has been supported by NSF under Grant Nos. DMR 79-09991 and DMR 77-23999 and under Navy Contract No. N00014-76-C-0708. The work of the Rockwell group has been partially supported by ONR, Contract No. N00014-78-C-0711.

[1] G. H. B Thompson, *Physics of semiconductor lasers* (Wiley, New York, 1980), pp. 287–304.
[2] N. Holonyak, Jr., R. M. Kolbas, and R. D. Dupuis, and P. D Dapkus, IEEE J. Quantum Electron QE-16, 170 (1980). See also E. R. Anderson, B. A. Vojak, N. Holonyak, Jr., G. E. Stillman, J. J. Coleman, and P. D Dapkus, Appl. Phys. Lett. **38**, 585 (1981).
[3] P. D. Dapkus, J. J. Coleman, W. D. Laidig, N. Holonyak, Jr., B. A. Vojak, and K. Hess, Appl. Phys. Lett. **38**, 118 (1981).
[4] W. D. Laidig, N. Holonyak, Jr., M. D. Camras, K. Hess, J. J. Coleman, P. D. Dapkus, and J. Bardeen, Appl. Phys. Lett. **38**, 776 (1981).
[5] H. M. Manasevit, J. Electrochem. Soc. **118**, 647 (1971).
[6] R. D. Dupuis, L. J. Moudy, and P. D. Dapkus, *7th International Symposium on GaAs and Related Compounds*, St. Louis, 1978, edited by C. M Wolfe (Institute of Physics, London, 1979), pp. 1–9.
[7] J. J. Coleman, P. D. Dapkus, W. D. Laidig, B. A. Vojak, and N. Holonyak, Jr., Appl. Phys. Lett. **38**, 63 (1981).
[8] L. L. Chang and A. Koma, Appl. Phys. Lett. **29**, 138 (1976).
[9] D. L. Kendall, in *Semiconductors and semimetals*, Vol. 4, edited by R. K. Willardson and A. C. Beer (Academic, New York, 1968), pp. 163–259.
[10] H. C. Casey, Jr., in *Atomic diffusion in semiconductors*, edited by D. Shaw (Plenum, New York, 1973), pp. 351–430.
[11] H. C. Casey, Jr. and M. B. Panish, *Heterostructure lasers: Part A* (Academic, New York, 1978), p. 45.

APPENDIX VI

Transport Properties of MOCVD MQW Structures

1. Single-Interface Enhanced Mobility Structures by Metalorganic Chemical Vapour Deposition, J. J. Coleman, P. D. Dapkus, and J. J. J. Yang, Electron. Lett. 17, 606 (1981).
2. The Growth and Characterization of Metalorganic Chemical Vapor Deposition (MO-CVD) Quantum Well Transport Structures, J. J. Coleman, P. D. Dapkus, D. E. Thompson, and D. R. Clarke, J. Crys. Growth 55, 207, 1981.

SINGLE-INTERFACE ENHANCED MOBILITY STRUCTURES BY METALORGANIC CHEMICAL VAPOUR DEPOSITION

Indexing terms: Semiconductor devices and materials, Doping, III-V semiconductors

Enhanced mobility effects in single-interface 2-dimensional electron gas heterostructures grown by metalorganic chemical vapour deposition (MOCVD) are reported. The mobility-temperature characteristics of single-interface structures, with and without an undoped spacer to reduce coulomb scattering at the interface, are described.

Recently there have been several reports of enhanced electron mobility effects in modulation-doped multiple-layer[1] and single-layer[2-5] GaAs-GaAlAs heterostructures. In all of these reports the epitaxial layers of interest were grown by molecular beam epitaxy (MBE). In this letter we describe measurements of enhanced mobility in 2-dimensional electron gas single-interface structures grown by metalorganic chemical vapour deposition (MOCVD). We relate the mobilities measured in single-interface structures to the background mobility of undoped bulk MOCVD GaAs and detail the growth conditions which particularly affect bulk and heterostructure electron mobilities.

In earlier work[6] we showed that enhanced electron mobility effects are observed in multiple-layer modulation-doped quantum well heterostructures (QWH) grown by MOCVD. These structures showed mobilities (20 000 cm^2/Vs, 77 K) more than five times greater than comparably doped bulk GaAs but much lower, however, than predicted[7] for pure undoped GaAs. The explanation for these reduced 77 K electron mobilities is

...at the mobility of the QWH is limited by the background mobility of the MOCVD GaAs, and further reduced[8] by coulomb scattering at the heterostructure interfaces.

The background mobility of MOCVD undoped bulk GaAs depends on a number of factors,[9] particularly the type and amount of impurities in the source materials (trimethylgallium and arsine) and the growth temperature which affects the extent to which these impurities are incorporated into the epitaxial layers. Shown in Fig. 1 is the dependence of the 77 K electron mobility on growth temperature for undoped epitaxial layers of MOCVD GaAs (8–15 μm thickness). The measurements are made using an etched van der Pauw geometry in a magnetic field of 5 kG. The data of Fig. 1 are for the source materials used in this work, and indicate that the optimum growth temperature for high-mobility GaAs is ~ 615°C. The multiple-layer QWH transport structures of Reference 6, however, were grown entirely at 750°C, which is the optimum temperature for the growth of $Ga_{1-x}Al_xAs$ by MOCVD, based on other work in our laboratory.[10,11] From the data of Fig. 1 it is apparent that a factor-of-four increase in the 77 K electron mobilities of multiple-layer QWH samples can be obtained by merely lowering the GaAs growth temperature to ~ 615°C. In addition the careful selection or repurification of starting source materials[9] would allow atmospheric growth of MOCVD GaAs with 77 K mobilities in excess of 100 000 cm^2 Vs.

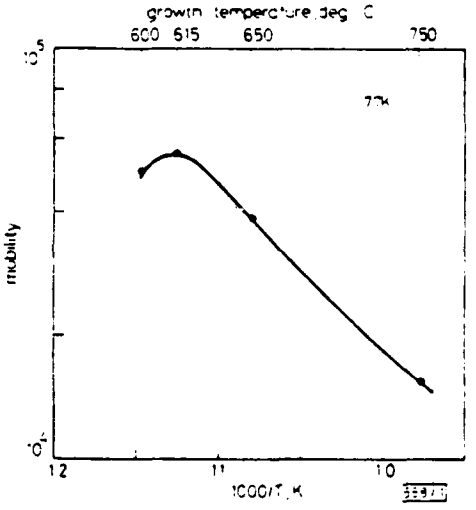

Fig. 1 *Liquid nitrogen temperature mobility against growth temperature for bulk undoped MOCVD GaAs*

It is not particularly convenient to cycle the growth temperature for multiple-layer QWH transport samples, and so we are concerned here only with single-interface 2-dimensional electron gas structures. These structures consist of a single undoped GaAs layer (1–4 μm thickness) grown at 615°C on a Cr-doped semi-insulating substrate. Ga_0-$Al_{0.3}As$ (200–1000 Å thickness) doped with Se ($5–8 \times 10^{17}$ cm^{-3}) is then grown at 750°C on the undoped GaAs. The heterojunction discontinuity between the GaAs and the GaAlAs results in the schematic conduction-band structure shown in Fig. 2. The band bending at the interface results in a local energy minimum near the interface which contains carriers contributed by the doped GaAlAs. It is the mobility of these carriers parallel to the interface which is measured by use of the Hall effect. The background carrier concentration of the undoped GaAs is $\sim 1.2 \times 10^{14}$ cm^{-3} and the average electron concentration obtained from Hall measurements gives an effective interface concentration of $\sim 10^{12}$ cm^{-2} for the heterostructures. Samples have been prepared with and without undoped Ga_0-$Al_{0.3}As$ spacer layers[3] to determine the effect of coulomb scattering at the interface.[8]

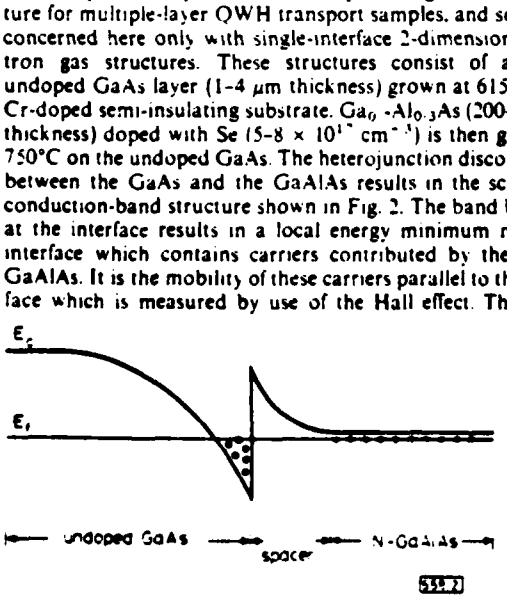

Fig. 2 *Schematic conduction-band diagram for a single-interface 2-*

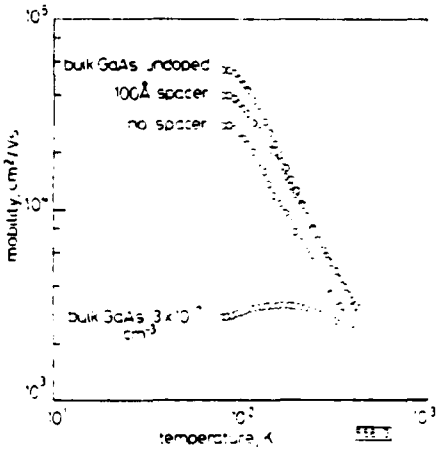

Fig. 3 *Hall mobility against temperature for single-interface 2-dimensional electron gas heterostructures with and without spacers*

Shown also for reference are data on doped and undoped bulk MOCVD GaAs epitaxial layers

Hall mobility data as a function of temperature in the range 77 to 400 K are shown in Fig. 3. Data from a bulk GaAs sample doped with Se to 3×10^{17} cm^{-3} are shown for reference. Also, data from a bulk GaAs sample that is not intentionally doped is shown, to indicate the limit to electron mobility resulting from the background impurities in the source materials. The remaining two sets of data in Fig. 3 are for enhanced mobility single-interface MOCVD heterostructures. The structure without an undoped spacer shows a 77 K mobility (~ 35 000 cm^2 Vs) that is more than one order of magnitude greater than comparably doped GaAs. Further enhancement in the 77 K mobility is obtained with the insertion of an undoped Ga_0-$Al_{0.3}As$ spacer layer (100 Å thickness). Presumably, coulomb scattering does contribute significantly to the overall scattering process[8] and can be reduced by increasing the spatial separation of the free carriers and the ionised impurities.[3]

In conclusion, we have shown that 2-dimensional electron gas enhanced mobility effects can be observed in single-interface, modulation-doped heterostructures grown by MOCVD. The optimum growth temperature for high-mobility GaAs is ~ 615°C, and coulomb scattering at the interface of the heterostructure can be reduced by the insertion of an undoped GaAlAs spacer layer. Single-interface 77 K electron mobilities greater than 45 000 cm^2 Vs at an effective interface carrier concentration of 10^{12} cm^{-2} are reported.

Acknowledgment This work was supported in part by the US Office of Naval Research, contract N00014-78-C-0711.

J. J. COLEMAN
P. D. DAPKUS
J. J. J. YANG

Rockwell International
Microelectronics Research and Development Center
3370 Miraloma Avenue
Anaheim, CA 92803, USA

15th July 1981

References

1 DINGLE, R., STORMER, H. L., GOSSARD, A. C., and WIEGMANN, W.: 'Electron mobilities in modulation doped semiconductor heterojunction superlattices', *Appl. Phys. Lett.*, 1978, 33, pp. 665–667

2 HIYAMIZU, S., MIMURA, T., FUJII, T., and NANBU, K.: 'High mobility of two-dimensional electrons at the GaAs n-AlGaAs heterojunction interface', *ibid.*, 1980, 37, pp. 805–807

3 WITKOWSKI, L. C., DRUMMOND, T. J., STANCHEK, C. M., and MORKOÇ, H.: 'High mobilities in AlGaAs-GaAs heterojunctions', *J. Appl. Phys.*

Journal of Crystal Growth 55 (1981) JCG 17
North-Holland Publishing Company

THE GROWTH AND CHARACTERIZATION OF METALORGANIC CHEMICAL VAPOR DEPOSITION (MO-CVD) QUANTUM WELL TRANSPORT STRUCTURES

J.J. COLEMAN, P.D. DAPKUS, D.E. THOMPSON and D.R. CLARKE *
Rockwell International, Microelectronics Research and Development Center, Anaheim, California 92803, USA

Data are presented which describe the general growth of $Ga_{1-x}Al_xAs$ by metalorganic chemical vapor deposition (MO-CVD) with specific application to quantum well heterostructure (QWH) transport structures. These data, including preliminary TEM data, Hall mobility data and carrier concentration profile data, show that alternating-layer, modulation-doped, $Ga_{1-x}Al_xAs$–GaAs QWH samples exhibit 77 K mobilities several times greater than the observed or predicted upper limit for comparably doped bulk GaAs. The carrier concentration profile data reflect the periodic nature of the multiple layer samples but indicate an asymmetrical peak in the carrier concentration of each GaAs well.

1. Introduction

Quantum well heterostructures (QWH) of alternating thin layers of GaAs and $Ga_{1-x}Al_xAs$ have attracted much attention in recent years. Since the first reports [1,2] of absorption measurements on QWH structures there have been reports of various optical and electrical phenomena associated with these quasi-two dimensional materials. These include laser operation above the bulk GaAs band edge [3–7] and the demonstration of unusually high electron mobilities [7–11]. In this paper we describe the details of the growth of QWH structures by metalorganic chemical vapor deposition (MO-CVD) [7,12,13]. The MO-CVD process allows the growth of uniform QWH structures having a large number of thin epitaxial layers [7,14] with the necessary abrupt interfaces between the layers [15,16]. We describe here briefly the general conditions for the MO-CVD growth of GaAs and $Ga_{1-x}Al_xAs$ and the specific conditions for the growth of a large number of thin alternating layers. Data are presented, including preliminary TEM data, temperature dependent Hall mobility data and carrier concentration profile data, on selected QWH samples grown by MO-CVD. These samples demonstrate 77 K mobilities several times greater than the theoretical predicted upper limit for comparable bulk GaAs. The carrier concentration profile data indicate an asymmetrical carrier density with a carrier concentration peak in each GaAs well.

* Rockwell International, Science Center, Thousand Oaks, California 91360, USA.

2. Quantum well heterostructure growth

The growth of $Ga_{1-x}Al_xAs$ by MO-CVD is the result of a pyrolysis reaction of the metal alkyl sources trimethylgallium (TMGa) and trimethylaluminum (TMAl) with gaseous arsine. This process, which can be described by the reaction equation:

$$AsH_3 + x\,(CH_3)_3Al + (1-x)(CH_3)_3Ga \xrightarrow[\Delta]{H_2} Ga_{1-x}Al_xAs + 3\,CH_4\,, \quad (1)$$

is entirely a deposition process without any competing dissolution reactions. Thus, abrupt heterostructure interfaces in the absence of diffusion are expected. Experimentally, the growth of $Ga_{1-x}Al_xAs$ takes place under conditions of excess As. The metal alkyls, which are liquids with reasonable vapor pressure near room temperature, are transported to the reactor by bubbled hydrogen gas. The composition of the epitaxial layer is determined by the relative flow rates (controlled electronically) of the hydrogen gas through the TMAl (23c) and TMGa (0C) source bubblers. A meaningful expression for this flow rate relationship is given by the dimensionless flow ratio ρ:

$$\rho = F(Al)/[F(Al) + F(Ga)]\,, \quad (2)$$

0022-0248/81/0000–0000/$02.50

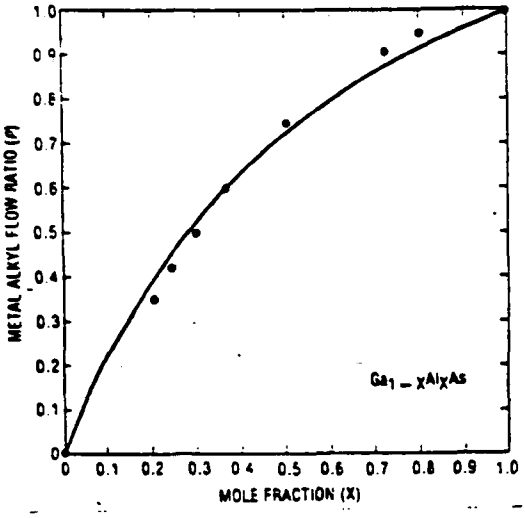

Fig. 1. $Ga_{1-x}Al_xAs$ alloy composition versus dimensionless metal alkyl flow ratio ρ.

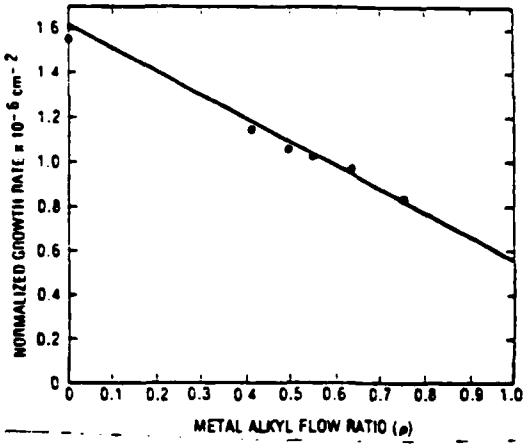

Fig. 2. Growth rate (normalized to total alkyl flow) versus metal alkyl flow ratio ρ.

where $F(Al)$ and $F(Ga)$ are the flow rates of the bubbler hydrogen for TMAl and TMGa respectively. The growth rate g, is a function of composition and therefore a function of ρ. The growth rate is also limited by the total metal alkyl flow rate $[F(Al) + F(Ga)]$, so a more general expression is the normalization growth rate g' given by

$$g' = \frac{g[\rho, F(Al) + F(Ga)]}{F(Al) + F(Ga)} . \quad (3)$$

Shown in fig. 1 are data on the composition of grown epitaxial layers of $Ga_{1-x}Al_xAs$ on GaAs substrates as a function of the flow ratio ρ. These data are obtained by a combination of X-ray lattice parameter measurements and photoluminescence measurements (where practical). Shown in fig. 2 are corresponding data on the normalized growth rate g', as a function of ρ. These data are obtained from SEM measurements of thick layers.

It is possible to develop analytical expressions for x versus ρ and g' versus ρ using the gas law with the vapor pressures of the sources and the geometry of the zinc blende lattice. Using a single data point to account for the geometry of the reactor, we have arrived at an expression for ρ versus x which is

$$\rho = x/(0.347 + 0.653x) . \quad (4)$$

This expression is shown as a solid line in fig. 1. A corresponding expression for the normalized growth rate g', is given by

$$g' = 1.62 \times 10^{-6}(1 - 0.653\rho)\ \text{cm}^{-2} , \quad (5)$$

and is shown as a solid line in fig. 2. There is a slight systematic discrepancy between the analytical expression (eq. (4)) and the experimental data of fig. 1 indicating that a small second order effect has been perhaps neglected.

Several additional considerations are required to reduce the general information above to the specific case of multiple layer structures of alternating thin layers of GaAs and $Ga_{1-x}Al_xAs$. We are able, with commonly available electronic mass flow controllers, to obtain growth rates as low as 2.5 Å/s at 750°C. A microprocessor controller is used to allow the sequencing of automatic valves with precise timing. The combination of this precise timing and accurately controlled flow rates allows the reproducible growth of layers less than 20 Å thick. The total number of such layers is virtually unlimited; we have grown as many as 500. In this work on such layers is virtually unlimited; we have grown as many as 500. In this work on QWH transport structures we have been concerned only with layers in the thickness range 80 to 500 Å.

Under the conditions described here, high quality QWH samples with abrupt interfaces can be grown by

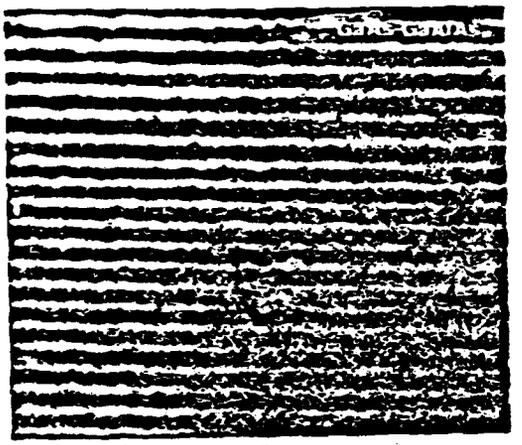

Fig. 3. TEM photograph of alternating GaAs (80 Å) and $Ga_{1-x}Al_xAs$ ($x \approx 0.40$, 70 Å). MO-CVD QWH sample.

MO-CVD. Shown in fig. 3 is a TEM photograph of part of an MO-CVD QWH structure containing 250 alternating layers of GaAs (80 Å) and $Ga_{1-x}Al_xAs$ ($x \approx 0.40$, 70 Å). Preliminary studies [16] indicate that the layers are uniform in thickness, the interfaces are abrupt and no defect structure is evident in the samples. These data corroborate earlier Auger data [15] which indicate that the MO-CVD growth process produces high-quality, atomically-abrupt $Ga_{1-x}Al_xAs$–GaAs interfaces.

3. Quantum well heterostructure mobility

The $Ga_{1-x}Al_xAs$–GaAs QWH samples of interest here are alternating layers of equal thickness in which only the wide-gap $Ga_{1-x}Al_xAs$ is intentionally doped [7–11]. The n-type dopant source is gaseous H_2Se diluted in hydrogen and controlled with an electronic mass flow controller. The undoped GaAs has a background doping level (n-type) of $<10^{14}$ cm^{-3} and mobilities of 5000–6000 cm^2/V · s at room temperature and 12,000–16,000 cm^2/V · s at 77 K. In other work under different growth conditions, however, 77 K mobilities greater than 100,000 cm^2/V · s have been observed in MO-CVD GaAs [17]. Hall mobilities in a magnetic field of 5000 Gauss are measured using an etched van der Pauw geometry on QWH samples grown on semi-insulating GaAs : Cr.

The basic physics of a modulation-doped QWH [8] is shown in fig. 4. This figure shows a schematic energy band diagram for an alternating layer $Ga_{1-x}Al_xAs$–GaAs heterostructure in which the wide-gap $Ga_{1-x}Al_xAs$ is intentionally doped with shallow donors. Except at very low temperatures these donors supply free electrons to the conduction band of the $Ga_{1-x}Al_xAs$ and from there they diffuse to the bottom of the GaAs well (or to the $n = 1$ quantum state in the well). The electron concentration in the well is that of the doped $Ga_{1-x}Al_xAs$ and can be high ($>10^{18}$ cm^{-3}). At the same time the mobility of these carriers is that of undoped GaAs and will be higher than bulk GaAs doped to the same

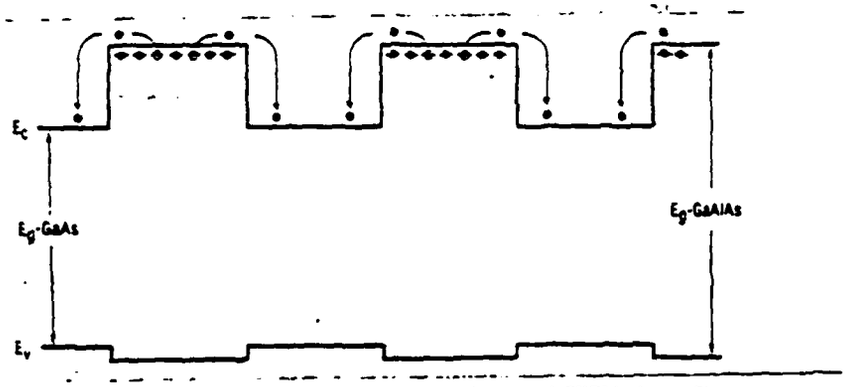

Fig. 4. Schematic energy band diagram for a modulation doped QWH high mobility structure.

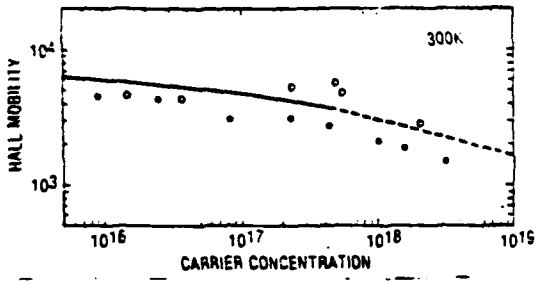

Fig. 5. Hall mobility versus carrier concentration. The solid line is the extended theoretical upper limit predicted for bulk GaAs. Data points represent bulk MO-CVD GaAs (•) and QWH MO-CVD samples (○).

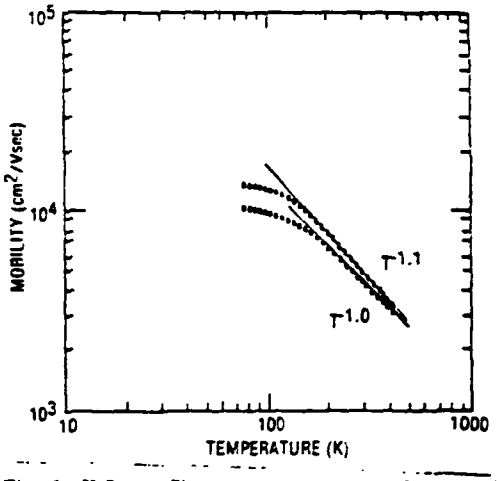

Fig. 6. Hall mobility versus temperature for two QWH MO-CVD transport samples. The lower curve corresponds to a QWH with 200 Å wells doped 5×10^{17} cm^{-3} and the upper curve corresponds to a QWH with 240 Å wells doped 2.4×10^{17} cm^{-3}.

carrier concentration. This is, of course, because the mobility of bulk GaAs at a given temperature decreases with increasing impurity concentration owing to increased impurity scattering [18]. Detailed consideration [19,20] of the scattering mechanisms (Coulomb and electron-phonon) in QWH structures has given a theoretical basis for the expectation of greatly increased electron mobilities in these structures.

Shown in fig. 5 is the dependence of the Hall mobility on the carrier concentration at room temperature. The solid line represents an extension of the upper limit to the mobility of bulk GaAs expected from a Brooks-Herring analysis [21]. The solid data points are representative samples of bulk MO-CVD GaAs and the open circles are selected data from MO-CVD QWH samples. The mobilities of the QWH samples are essentially independent of carrier concentration and for concentrations greater than 10^{17} cm^{-3} the measured mobilities are considerably greater than both the experimental and theoretical values for similarly doped bulk GaAs. It is not clear whether the data point at 2×10^{18} cm^{-3} is anomalous or if there is an effect on the mobility resulting from a higher concentration of free electrons. The MO-CVD QWH data of fig. 5 are comparable to earlier experimental data [8–11] on single and multiple layer QWH structures prepared by other epitaxial growth techniques.

The temperature dependence of the Hall mobility for two typical MO-CVD QWH samples is shown in fig. 6. The samples are alternating layers of GaAs and $Ga_{0.7}Al_{0.3}As$ with the alloy layers doped with Se to 5×10^{17} cm^{-3} (lower curve) and 2.4×10^{17} cm^{-3} (upper curve). The thickness of the wells are 200 Å (lower curve) and 240 Å (upper curve). The 77 K mobilities are greater than 12,000 $cm^2/V \cdot s$ which is several times greater than the theoretical upper limit for comparably doped bulk GaAs [21]. These temperature data on MO-CVD QWH samples are comparable to earlier reported data [8,11] on samples prepared by other techniques. The 77 K mobilities are not as high as more recent reports [22,23] of $Ga_{1-x}Al_xAs$–GaAs heterostructure mobilities for the reason that the 77 K mobilities of this work are limited by ~~(and the same as)~~ the background impurity level of bulk GaAs grown in this reactor with these particular sources. With appropriate high-purity sources and optimized growth parameters (such as growth at temperatures lower than 750°C), the 77 K mobilities should be considerably higher [17]. The Hall mobility data of figs. 5 and 6 indicate that MO-CVD QWH structures are of sufficiently high quality to be suitable for various mobility electronic device structure [22,24].

4. Quantum well heterostructure carrier profiles

Carrier concentration profile measurements have been made on these high mobility MO-CVD QWH samples. These measurements are made using a Lehighton–Miller capacitance profiler on evaporated dot Schottky barrier diodes made from samples grown on conducting GaAs. The measurement accuracy is inherently limited by the Debye length of carriers in GaAs. For reference the Debye lengths at room temperature in GaAs are ~43 and ~135 Å for doping levels of 10^{18} and 10^{17} cm^{-3}, respectively.

Profiles of several samples of a 51 layer $Ga_{0.7}Al_{0.3}As$–GaAs QWH having alternating 200 Å layers is shown in fig. 7. The alloy layers are doped with Se to (7–8) $\times 10^{17}$ cm^{-3} and the figure is drawn with distance away from the Schottky barrier (depletion width) increasing to the right. Several features of fig. 7 are noteworthy. Since only a single layer (or interface is apparently sampled, the high concentration region on the left is the possible result of conduction near zero bias of the Schottky diode. The concentration peak on the right near 3×10^{18} cm^{-3} clearly occurs before the diode breaks down. Similar high concentration spikes have been seen in single interface profile measurements and have been attributed to a two-dimensional gas [22] or to a combination of interface states and heterojunction discontinuity [25]. In any case, the deviation from the expected step-like change in the profile cannot be completely explained by Debye length smearing since the shape of the profiles does not change greatly with increased thickness or reduced measurement temperature.

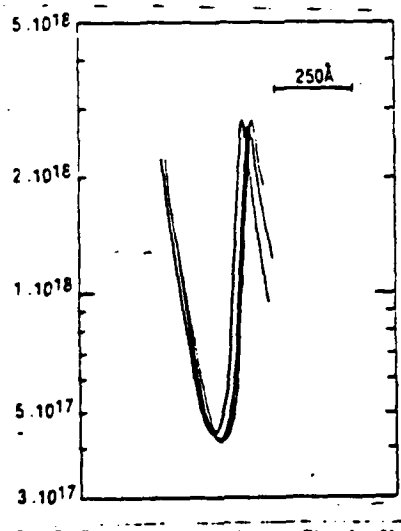

Fig. 7. Carrier concentration profile of a 51 layer QWH with 200 Å wells and doped to 7-8 x 10^{17} cm^{-3}.

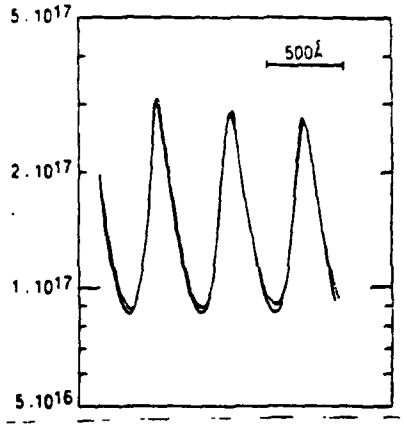

Fig. 8. Carrier concentration profile of a 51 layer QWH with 240 Å wells and doped to 2.4 x 10^{17} cm^{-3}.

The profiles shown in fig. 8 show more detail. This sample is 51 layers of alternating GaAs (240 Å) and $Ga_{0.7}Al_{0.3}As$ (225 Å) in which the alloy is doped ~2×10^{17} cm^{-3}. More than three full periods have been sampled in these profiles and three peaks which, as in fig. 7, are greater than the $Ga_{1-x}Al_xAs$ doping level, are evident. Based on the thicknesses of the wells and the barriers, the data of fig. 7 suggest that there is only a single peak in the electron concentration in each GaAs well. The location of this peak, within the well is not clear. If the peak is associated with an interface [25], then there is no evidence in the carrier concentration profile for a similar peak (or a minimum) at the other interface of the well. As in fig. 7, Debye length smearing cannot completely account for the features evident. An expanded portion of the middle period of fig. 8 is shown in fig. 9. For reference, The carrier concentration spikes are separated by 470 Å. Careful measurements of this curve indicate that, if the carrier concentration peaks can be presumed to occur at an interface (of the well) nearest the Schottky contact, the concen-

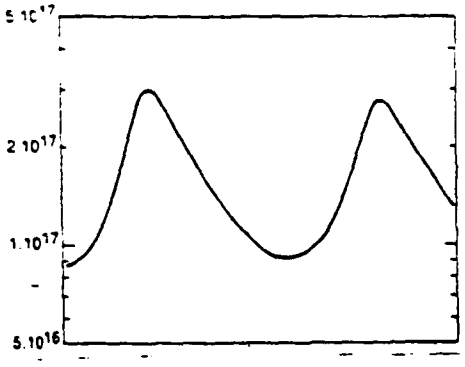

Fig. 9. Expanded portion of the middle period of the profile of fig. 8. For reference the separation between the peaks is 470 Å.

tration minima occur well beyond the next interface and some distance into the $Ga_{1-x}Al_xAs$ barrier layer.

5. Conclusion

In this work we have described the general conditions for the growth of high quality $Ga_{1-x}Al_xAs$ by metalorganic chemical vapor deposition and the specific requirements for the growth of thin layer quantum well heterostructure transport structures. We have mentioned preliminary TEM data which indicate that the MO-CVD layers are uniform and without defects and have abrupt interfaces. We have described Hall mobility data showing unusually high electron mobilities at room temperature and below. These mobilities for QWH samples doped 10^{17} cm^{-3} and greater, are higher than the theoretical upper limit of corresponding bulk GaAs. Carrier concentration profiles indicate concentration peaks which occur only once in each GaAs well. These peaks, which exceed the intentionally doped level, are possibly a two-dimensional electron gas effect.

Acknowledgements

The authors would like to thank J.J.J. Yang for technical assistance and acknowledge the support of the office of Naval Research Contract N000-14-78-C-0711.

References

[1] R. Dingle, in: Festkorperprobleme XV, Advances in Solid State Physics (Pergamon–Vieweg, Braunschweig, 1975) p. 21.
[2] R. Dingle, A.C. Gossard and W. Wiegmann, Phys. Rev. Letters 34 (1975) 1327.
[3] J.P. van der Ziel, R. Dingle, R.C. Miller, W. Wiegmann and W.A. Nordland, Jr., Appl. Phys. Letters 26 (1975) 462.
[4] E.A. Rezek, H. Shichijo, B.A. Vojak and N. Holonyak, Jr. Appl. Phys. Letters 31 (1977) 534.
[5] R.D. Dupuis, P.D. Dapkus, N. Holonyak, Jr., E.A. Rezek and R. Chin, Appl. Phys. Letters 32 (1978) 295.
[6] N. Holonyak, Jr. R.M. Kolbas, R.D. Dupuis and P.D. Dapkus, IEEE J. Quantum Electron. QE-16 (1980) 170, and references cited.
[7] P.D. Dapkus, J.J. Coleman, W.D. Laidig, N. Holonyak, Jr., B.A. Vojak and K. Hess, Appl. Phys. Letters 38 (1981) 118.
[8] R. Dingle, H.L. Stormer, A.C. Gossard and W. Wiegmann, Appl. Phys. Letters 33 (1978) 665.
[9] H.L. Stormer, R. Dingle, A.C. Gossard, W. Wiegmann and M.D. Sturge, Solid State Commun. 29 (1979) 705.
[10] D.C. Tsui and R.A. Logan, Appl. Phys. Letters 35 (1979) 99.
[11] S. Himyamuru, T. Mimura, T. Fujii and K. Nanbu, Appl. Phys. Letters 37 (1980) 805.
[12] H.M. Manasevit, J. Electrochem. Soc. 118 (1971) 647.
[13] R.D. Dupuis, L.A. Moudy and P.D. Dapkus, in: Proc. 7th Intern. Symp. on GaAs and Related Compounds, St. Louis, 1978, Inst. Phys. Conf. Ser. 45 (Inst. Phys., London, 1979) p. 1.
[14] B.A. Vojak, W.D. Laidig, N. Holonyak, Jr., J.J. Coleman and P.D. Dapkus, J. Appl. Phys. 52 (1981) 621.
[15] R.D. Dupuis, P.D. Dapkus, A.M. Garner, C.Y. Su and W.E. Spicer, Appl. Phys. Letters 34 (1979) 335.
[16] D.R. Clarke, J.J. Coleman and P.D. Dapkus, unpublished data.
[17] P.D. Dapkus, H.M. Manasevit, K.L. Hess, T.S. Low and G.E. Stillman, J. Crystal Growth 55 (1981) •••.
[18] E. Cornwell and V.F. Weisskopf, Phys. Rev. 77 (1950) 388.
[19] K. Hess, Appl. Phys. Letters 35 (1979) 484.

END

DATE
FILMED

1-82

DTIC